Computational modeling approaches to multifactorial aspects of atopic dermatitis

Eléa Greugny

INSTITUT POLYTECHNIQUE DE PARIS

NTT : 2022IPPAX083

Thèse de doctorat

Computational modeling approaches to multifactorial aspects of atopic dermatitis

Thèse de doctorat de l'Institut Polytechnique de Paris
préparée à École Polytechnique

École doctorale n°626 Ecole Doctorale de l'Institut Polytechnique de Paris (ED IP Paris)
Spécialité de doctorat: Mathématiques et Informatique

Thèse présentée et soutenue à Palaiseau, le 4 Octobre 2022, par

Eléa Thibault Greugny

Composition du Jury :

Thao Dang Directrice de Recherche, CNRS, Verimag	Présidente
Reiko Tanaka Reader, Biological Control Systems Lab, Department of Bioengineering, Imperial College London	Rapportrice
Romain Yvinec Chargé de Recherche, Biology & Bioinformatics of Signalling Systems, INRAE	Rapporteur
Laurence Calzone Ingénieure de Recherche, Biologie des Systèmes du Cancer, Institut Curie	Examinatrice
Ina Koch Professor, Goethe University Frankfurt	Examinatrice
Ovidiu Radulescu Professor, Theoretical Biophysics and Systems Biology, LPHI	Examinateur
François Fages Directeur de Recherche, EP Lifeware, Inria de Scalay	Directeur de thèse
Georgios Stamatas PhD, Johnson&Johnson Santé Beauté France	Co-Directeur de thèse
Jalil Bensaci PhD, Reacteev	Co-Encadrant (Invité)

Abstract

Atopic dermatitis (AD) is a common chronic disease affecting up to 20% of young children, depending on countries, and around 10% of adults globally. It manifests as dry, itchy and sometimes cracked skin lesions on the face and body. Despite efficient immunotherapy treatments for the most severe forms of the disease, the complex mechanisms involved are still incompletely understood and improvements can be made regarding management strategies for milder forms. AD involves diverse interacting factors such as impaired skin barrier function, exacerbated inflammation, and microbiome dysbiosis, making it challenging to develop adequate *in vitro* models.

A computational approach allows the aggregation of current pathophysiology knowledge, facilitates the visualization of the phenomena involved, and enables the prediction of certain behaviors of the system under specific conditions. First, we introduce an agent-based model of the epidermis, able to represent aspects of atopic skin such as skin barrier dysfunction and microbiome dysbiosis. By integrating enzymatic reactions contributing to the desquamation process, into an existing agent-based model of the epidermis at the cellular level, we can study the impact of skin surface pH on the epidermal structure and function. The model predicts that an elevation of skin surface pH above physiologic levels accelerates the desquamation process through its action on serine proteases. This results in a significant reduction of the skin's capacity to retain water, and increases its permeability to external penetration, including irritants. This skin barrier impairment further leads to a more intense inflammatory reaction under conditions of high skin surface pH, compared to physiologic pH levels.

Next, we introduce a mathematical model of the microbiome, based on ordinary differential equations, with 2 types of bacteria populations (skin commensals and opportunistic pathogens) to study the mechanisms driving the dominance of one population over the other. On the time scale of the experiments, the model predicts that certain changes of the environment, like the elevation of skin surface pH from physiologic levels, create favorable conditions for the emergence and colonization of the skin by opportunistic pathogens. Interestingly, for certain parameter values, a meta-stable state settled at around 2 days following the introduction of bacteria in the model, is followed by a reversed stable state after 300 hours.

Finally, we integrate the mathematical model of the microbiome into the agent-based model. Special consideration is taken regarding the timescales of the processes described and their location in the epidermis. The resulting model is used to study how the constant surface cells renewal impacts the microbiome kinetics. This work provides additional evidence that skin surface pH, serine proteases and skin microbiome could be interesting therapeutic targets for AD maintenance therapy.

Résumé

La dermatite atopique (DA) est une maladie chronique affectant jusqu'à 20% des jeunes enfants, en fonction des pays, et environ 10% des adultes dans le monde. Elle se traduit par une sécheresse cutanée, d'intenses démangeaisons et la formation de lésions. Malgré des traitements efficaces à base d'anticorps monoclonaux pour les formes les plus sévères, les mécanismes complexes impliqués sont encore mal compris et des progrès restent à faire pour soulager les formes plus légères de cette maladie. Divers facteurs contribuent à la DA tels qu'une fonction barrière réduite, une inflammation cutanée exacerbée et un déséquilibre du microbiome. Cette multiplicité de facteurs et leur lien étroit rendent difficile le développement des malades in vitro. L'approche computationnelle permet de rassembler les connaissances actuelles sur la maladie et de prédire le comportement du système sous certaines conditions, tout en facilitant la visualisation des phénomènes impliqués.

L'objectif de cette thèse est de développer un modèle computationnel de l'épiderme, intégrant plusieurs éléments clés de la pathophysiologie de la DA : le disfonctionnement de la barrière cutanée, l'inflammation et le déséquilibre du microbiome. Nous nous concentrons sur la peau non lésionnelle et cherchons à répondre aux questions suivantes :

1) Peut-on mettre en évidence, grâce à un modèle computationnel, l'impact de l'élévation du pH cutané sur la fonction barrière de la peau, via son action sur les kallicréines ?
2) Peut-on identifier des facteurs contribuant à l'équilibre ou au déséquilibre du microbiome en utilisant la modélisation ?
3) Est-il possible d'étudier l'impact de la nature dynamique de la peau sur l'évolution du microbiome grâce à un modèle à agent ?

Pour répondre à la première question, nous introduisons un modèle multi-échelles combinant deux modèles préexistants. Le premier est un modèle multi-agents récapitulant la structure dynamique de l'épiderme et intégrant la fonction barrière de la peau ainsi que la perméation d'une substance à travers l'épiderme. Le second modèle décrit les interactions moléculaires des kallicréines et de leur inhibiteur LEKTI (Lympho-Epithelial Kazal-Type related Inhibitor) grâce à un système d'équations différentielles ordinaires (EDO). Dans la peau saine, les kallicréines contribuent au renouvellement des cellules de la peau en dégradant les protéines assurant la cohésion entre les cellules de la strate carnée. Leur activité est fortement dépendante du pH et augmente avec celui-ci. Or, une augmentation du pH cutané a été

observé chez le personnes atteintes de dermatite atopique. Combiner ces deux modèles nous permet donc de mieux comprendre les conséquences de l'augmentation du pH sur la barrière cutanée.

Le modèle multi-échelles obtenu prédit que l'élévation du pH accélère le processus de desquamation à travers son action sur les kallicréines. Ceci conduit à un affaiblissement significatif de la capacité de la peau à retenir l'eau ainsi qu'à une perméabilité accrue aux substances irritantes provenant de l'extérieur. Le modèle prédit également une inflammation plus intense lorsque le pH cutané est plus élevé que son niveau physiologique.

Dans un deuxième temps, nous introduisons un modèle mathématique du microbiome cutané pour répondre à notre deuxième question de recherche. Ce modèle, basé sur des EDO, considère 2 types de populations bactériennes (les espèces commensales et les pathogènes opportunistes) afin d'étudier les mécanismes responsables de la prédominance d'une population sur l'autre. Certaines maladies de peau, telles que la DA, ont en effet été associées à une perte de diversité du microbiome, au profit de la surcroissance d'une espèce pathogène (Staphylococcus aureus dans le cas de la DA). Notre modèle prend en compte un des mécanismes de défense de la peau contre les pathogènes : les peptides antimicrobiens (PAM). Nous considérons également, sur la base d'observations expérimentales, la production de PAM par les bactéries commensales.

Notre modèle se compose initialement de 3 variables et 13 paramètres. En utilisant des données expérimentales, que l'on suppose correspondre aux états stables de notre modèle, nous parvenons à identifier la valeur de certains paramètres et à établir des relations mathématiques permettant de calculer la valeur d'autres paramètres en fonction de ceux restants. Cette méthode nous permet de réduire l'espace paramétrique de 13 à 5, facilitant l'analyse du modèle. Sur une échelle de temps similaire à celle des expériences, le modèle prédit que certaines modifications de l'environnement, telles que l'augmentation du pH, créent des conditions favorables pour l'émergence et la colonisation de la peau par des pathogènes opportunistes.

De façon surprenante, pour certaines valeurs de paramètres, un état qui apparaissait stable sur l'échelle de temps des expériences (50 heures), se réveille être métastable et glisser

progressivement jusqu'à basculer vers un état inverse après environ 13 jours. Cette observation nous conduit à s'interroger sur l'hypothèse communément utilisée en biomathématiques selon laquelle les observations et mesures expérimentales correspondent aux états stables des modèles.

Pour finir, nous intégrons notre modèle EDO du microbiome dans le modèle multi-agents de l'épiderme pour répondre à notre dernière question de recherche. L'organisation en couches successives de l'épiderme est le résultat d'un équilibre dynamique. Les cellules basales prolifèrent et créent de nouvelles cellules qui montent progressivement vers la surface, les cellules perdent petit à petit leur adhésion aux cellules voisines et sont desquamées. Le microbiome étant situé à la surface de l'épiderme, il est donc confronté au renouvellement et à la disparition constante de son environnement. L'intégration de notre modèle EDO du microbiome dans le modèle multi-agents permet d'étudier l'impact de la structure dynamique de la peau sur la croissance bactérienne.

Notre modèle prédit que la desquamation est une limitation forte pour les populations bactériennes, les empêchant d'atteindre les concentrations observées précédemment dans le modèle EDO. De plus, le basculement métastable est absent ou fortement retardé dans notre nouveau modèle hybride EDO/multi-agents. Ceci souligne la valeur ajoutée de ce type de modèle hybride, permettant d'étudier les dynamiques de populations exposées à un environnement changeant.

Pour conclure, le travail présenté dans cette thèse constitue une bonne base de départ pour l'implémentation d'un modèle de la DA dynamique et intégratif. Notre modèle a permis de faire des prédictions pertinentes tout en soulevant des questions intéressantes d'un point de vue biologique ainsi que pour la modélisation.

Acknowledgments

My first thoughts and thank you go to my amazing supervising team François FAGES, Georgios STAMATAS and Jalil BENSACI.

Georgios, the first who saw in me the potential for being a PhD student and planted the idea in my head. I have learnt a lot by your side on the wonderful research subject that is skin and on how to be a great researcher in R&D. Thank you for your guidance during these past 3 years and the internship before that, the careful paper and poster reviews and your benevolent advice.

Jalil, the one who fought for months to make this doctorate happen and went through all the struggles and paperwork to make sure I could do this doctorate under the best conditions. Thank you for being a wonderful mentor, consistently pushing me out of my comfort zone to help me grow. You have helped me learn a lot about myself and find my way. Thank you for the intense and detailed presentation rehearsals, the philosophical discussions, and the continuous support, even after you left J&J.

François qui m'a fait découvrir le monde de la recherche académique et le logiciel du vivant. Merci pour ton enthousiasme éternel et pour avoir cru en ce projet dès le début. Grâce à toi j'ai découvert la puissance de la logique temporelle et le parallèle entre cellule et ordinateur. Tu futs d'une aide précieuse tout au long de cette thèse et particulièrement ces derniers mois, de la rédaction à la soutenance.

I am grateful to Reiko TANAKA and Romain YVINEC for agreeing to review my thesis manuscript and for their insightful comments on my work. I also want to thank all the jury members, Laurence CALZONE, Thao DANG, Ina KOCH and Ovidiu RADULESCU, for attending to my thesis defence (in person or virtually) and for the interesting discussions that followed.

This thesis would not have been possible without founding. I am glad that a program such as the CIFRE exists and enables innovative collaborations between academia and industry. Speaking of which, I owe a deep thank you to Johnson&Johnson Santé Beauté France for welcoming me as an employee during the past 3 years.

Je tenais également à remercier mes collègues que j'ai côtoyés pendant ces 3 ans. Tout d'abord, merci aux membres de l'équipe Lifeware, Sylvain SOLIMAN, Mathieu HEMERY, Aurélien NALDI, pour m'avoir conseillée sur l'utilisation de Biocham et m'avoir débloquée plusieurs fois en résolvant des bugs parfois mystérieux. Un merci tout particulier aux doctorants qui ont montré la voie, Julien MARTINELLI et Jérémy GRIGNARD, et beaucoup d'encouragements pour celles qui, je n'en doute pas, termineront brillamment leur thèse, Sahar AGHAKHANI et Marine COLLERY.

Du côté de J&J, je voudrais d'abord remercier mes chères collègues Imane LBOUKILI et Fanny ALSAMAD, avec qui j'aurais passé le plus de temps en présentiel. Merci pour tous ces moments partagés, les discussions, les conseils avisés, et les gâteaux. J'ai hâte de suivre la suite de vos aventures ! Une pensée pour ma première équipe, les Computational Solutions : Sandra, Manon, Maxime, Sushank, Patrice et Lucie. Je garde en tête les problématiques passionnantes sur lesquelles nous travaillions autour de la data et du digital, mais surtout, la bonne humeur et les rires, même en plein confinement à travers nos écrans. Un grand merci à l'équipe Essential Health Translational Science Skin Strategic Science: Thierry, Cécilia, Aurélie, Ayla, José, Hélène, Claire. Je suis fière d'avoir fait partie d'une telle équipe, toujours en quête de nouvelles connaissances et d'innovation.

Cette thèse fût une aventure humaine presque autant qu'une aventure scientifique. Elle fût pleine de rebondissements, de joie et de déception, de fierté et de doute. Et cette partie de l'aventure n'aurait pas été la même sans le soutien sans faille de mon entourage. Un grand merci à tous mes amis et à ma famille pour avoir été à mes côtés dans les moments difficiles et m'avoir portée jusqu'au bout de cette thèse. Un merci tout particulier à mes parents et à ma sœur pour leurs encouragements et leur confiance inébranlable en mes capacités. Enfin, un immense merci à celui qui a été aux premières loges de toutes ces aventures, mon époux Théo. Ton soutien psychologique et logistique a fait toute la différence et a grandement contribué au succès de cette thèse.

Table of Contents

List of Figures

List of Tables

List of Annexes

Acronyms

AA: Amino-acids

AD: Atopic dermatitis

AMPs: Anti-microbial peptides

ASU: Arbitrary surface unit

AU: Arbitrary unit

CFU: Colony forming unit

IL: Interleukin

KLK: Kallikrein

KLK*: active kallikrein

LEKTI: Lympho-epithelial Kazal-type related inhibitor

NMF: Natural moisturizing factor

OD: Optical density

ODE: Ordinary differential equations

PAR2: Proteinase-activated receptor-2

QSP: Quantitative system pharmacology

S. aureus: *Staphylococcus aureus*

SBML: Systems Biology Markup Language

SC: *Stratum corneum*

SLS: Sodium lauryl sulphate

VE: Viable epidermis

Chapter I - Introduction

I.1. Atopic dermatitis: a complex skin disease

I.1.1. The epidermis dynamic structure and function

Skin is one of the largest organs of the human body. It is located at the interface with the environment, and its main function is to protect us from external aggressions such as irritant substances, pollution or UV-light, and dehydration. As expected, the outer layer, the epidermis, plays the most significant role in this barrier function (Proksch, Brandner, and Jensen 2008). The epidermis can be divided into 4 layers: *stratum basale*, *stratum spinosum*, *stratum granulosum* and *stratum corneum* (SC). The overall epidermal structure is the result of dynamic homeostasis. The epidermal cells, called keratinocytes, are constantly moving towards the surface, the top cells being desquamated and replaced by inner cells. Therefore, the different epidermal layers correspond to the successive cellular differentiation states, from basal to corneal (Moreci and Lechler 2020).

The upper layer differs from the others because it is composed of flattened, dead cells, the corneocytes. These cells lose their nucleus when differentiating from the granular to the corneal state, meaning that they cannot have any synthetic activity. However, there is enzymatic activity in this layer, enabling the breakdown of proteins, control of pH, control of microbial growth, *etc*. The corneocytes are surrounded by a lipid matrix and linked together through crosslinked protein structures named corneodesmosomes (Pouillot et al. 2008; Matsui and Amagai 2015).

Desquamation is regulated by kallikreins (KLKs), which are serine protease enzymes responsible for cleaving corneodesmosomes to ensure proper corneocyte desquamation (Eissa and Diamandis 2008). They are secreted at the interface between *stratum granulosum* and *stratum corneum* as inactive precursors and are activated by irreversible proteolysis. The activity of KLKs is further regulated by Lympho-epithelial Kazal-type related inhibitor (LEKTI), by direct interaction. LEKTI is a protease inhibitor (the protein encoded by the *SPINK5* gene)

that binds directly to activated KLK, ensuing its inhibition (Meyer-Hoffert, Wu, and Schröder 2009).

I.1.2. Atopic Dermatitis pathophysiology

Atopic dermatitis (AD) is a very common skin disease affecting a significant proportion of the population, ranging from 2.5 to 20% of children depending on countries and around 10% of adults globally (Bylund et al. 2020). The typical onset of atopic dermatitis usually occurs in early childhood, around the age of three to six months. Although in some cases the disease clears up at adolescence, it can also persist until or even appear during adulthood (Abuabara et al. 2018). AD is characterized by itchy, red, swollen and cracked skin, which can cause sleep disturbance and therefore affect the patient's quality of life (Drucker et al. 2017). The exact cause of the disease remains incompletely understood but seems to be a combination of an unfavorable genetic predisposition and aggravating environmental factors. The importance of the genetic aspect has been underlined by the fact that the strongest risk factor for AD is parent history of atopy (Apfelbacher, Diepgen, and Schmitt 2011). The genetic factors can be divided into two groups: the first one related to skin barrier function and the second one linked to an exacerbated inflammation.

The most important genetic mutation relating to AD identified so far is the mutation on the *FLG* gene, involved in the production of the filaggrin, an essential protein for the barrier function (Palmer et al. 2006; Morar et al. 2007). The resulting loss of function of filaggrin leads to a reduced capacity of the skin to retain water (Kezic et al. 2008). It is also thought to contribute to the elevation of pH observed in AD skin (Jungersted et al. 2010; Eberlein-König et al. 2000). The skin pH is an important regulator of the epidermal homeostasis through its action on the enzymatic activity at a molecular scale. The activity of KLK on corneocyte adhesion is increased following pH elevation, which might lead to barrier impairment (Brattsand et al. 2005).

The other category of genetic factors predisposing to AD concerns an exacerbated inflammation. Inflammatory molecules such as cytokines, are overly expressed in AD skin,

especially on lesions (Mu and Zhang 2020). The action of these inflammatory molecules is triple: i) down regulation of filaggrin, further damaging the barrier (Howell et al. 2007), ii) increased sensitivity to allergens via the stimulation of specific antibodies (immunoglobulin E) (Weidinger et al. 2018), iii) down regulation of antimicrobial peptides (AMPs) (Mu and Zhang 2020; Nomura et al. 2003). AMPs constitute the innate immunity of the epidermis and its first line of defense against invading pathogens. A significant decrease in expression of certain AMPs has been observed in AD skin (McGirt and Beck 2006). Overall, the genetic alterations linked to AD seem to create an increased vulnerability to external aggressions.

The impaired barrier function characteristic of AD allows an easier permeation of external irritants and allergens into the skin (Halling-Overgaard et al. 2017), leading to further inflammation. Moreover, the combination of an elevated skin surface pH and a reduced production of AMPs may explain the susceptibility of AD patients for bacterial infections, as both acidic pH and AMPs significantly limit bacterial growth (Fluhr and Elias 2002; Malik et al. 2016; Pazgier et al. 2006). AD skin has long been correlated with an alteration of the cutaneous microbiome composition, also called dysbiosis, due to its colonization by *Staphylococcus aureus* (*S. aureus*), especially on lesions, correlated with disease severity (Leyden, Marples, and Kligman 1974; Kong et al. 2012; Geoghegan, Irvine, and Foster 2018; Totté et al. 2016). The toxins produced by *S. aureus* act as superantigens, stimulating the already exacerbated inflammation and further damaging the barrier (Geoghegan, Irvine, and Foster 2018). In addition to the AMPs produced by the keratinocytes, some of the commensal bacteria of the microbiome also contribute to the defense against opportunistic pathogens like *S. aureus*. For instance, it has been shown that several members of the *Staphylococcus* genus, such as *S. hominis* or *S. lugdunensis*, produce l-antibiotics or bacterial AMPs targeted against *S. aureus* (Zipperer et al. 2016; Nakatsuji et al. 2017). Therefore, there is a necessity to investigate the community dynamics within the microbiome and its interactions with the skin to design treatment strategies for AD.

Altogether, the current knowledge of AD pathophysiology reveals a very complex disease, with several interconnected factors, both genetic and environmental. It includes molecular and cellular mechanisms having repercussion at the tissue scale, as well as changes at tissue scale impacting the cellular and molecular behaviors.

I.2. Research questions

The aim of this thesis is to develop a computational model of the epidermis, integrating several key elements of AD pathophysiology: skin barrier integrity, inflammation, and microbiome dysbiosis. The focus will be on non-lesional skin, and the following research questions will be investigated:

1) Can we demonstrate the impact of pH elevation on the skin barrier function, through its action on KLK activity, using a computational model?

2) Can we identify factors contributing to microbiome balance or dysbiosis through modelling?

3) Can we investigate the impact of the epidermis dynamic nature on microbiome kinetics, using an agent-based model?

I.3. Multiscale mathematical modelling approaches of AD

To answer these questions, multifactorial mechanisms involving different scales need to be considered, ranging from molecular interactions to cellular interactions, tissue formation and microbiome population dynamics. The pH acts on molecular interactions that have consequences at the tissue scale. The microbiome kinetics can be studied at the population scale first to identify factors of interest. However, it is also important to consider how the constant renewal of surface cells might impact the microbiome balance. Therefore, a hybrid

modelling approach based on both ordinary differential equations (ODE) and multi-agent modelling formalisms seems particularly well-suited to investigate AD pathophysiology.

I.3.1. Computational mechanistic model based on ordinary differential equations

ODE have long been used to model the dynamics of biological processes or population dynamics (Malthus 1798). This type of model can be called mechanistic when they are based on causal relations and concrete interactions responsible for the observed system behavior. The main assumption of ODE based models is that the interacting entities are homogeneously distributed in the environment of interest. To overcome this constraint, it is common to divide an heterogenous environment into several homogeneous compartments with defined boundary conditions (transitions) between them. ODE based models are usually focused on one scale (at the molecular, cellular or tissue level), and can be associated to build multiscale models. Once provided with kinetic parameter values, the ODE-based mechanistic models define the continuous dynamics of the system and can be used to simulate the dynamic behavior of system over time.

Over the years, several research groups worked towards the development of computational or mathematical models of AD-related mechanisms, using different methodologies. The most common is the one based on ODE. Nakaoka *et al.* (Nakaoka et al. 2016) introduced two models combining ODE and delay differential equations. The first one described the interplay between barrier, immune response, and bacterial infection, in the absence of competition with other species. The second one focused on the interactions of one harmful and one beneficial population of bacteria exposed to cytokines.

A group from the Imperial College London started from an ODE model of KLK activity and regulation (Tanaka, Ono, and Harrington 2011), progressively updated to integrate more mechanisms, such as the skin barrier integrity, environmental stress, and immune dysregulation (Domínguez-Hüttinger et al. 2013; 2017). This model was used to predict the

optimal treatment strategy, combining corticosteroid and emollient, on individual virtual patient cohorts (Christodoulides et al. 2017). More recently, quantitative system pharmacology (QSP) modelling was implemented to investigate the relationship between cytokines and AD pathogenesis and reproduced reported clinical efficacies of 9 drugs (Miyano, Irvine, and Tanaka 2021). In 2022, the same group published another QSP model including *S. aureus* interactions with other *Staphylococcus* to optimize *S. aureus*-targeted therapies (Miyano, Irvine, and Tanaka 2022) and introduced EzcemaPred, a computational framework for personalized prediction of AD severity dynamics (Hurault et al. 2022). AD has also been studied using a PetriNet model (Polak et al. 2017), with a focus on Langerhans cells, and pathway enrichment analysis (Subramanian, Singh, and Jere 2018).

While providing useful insights and predictions, the mathematical model cited above fail to account for the dynamic nature of the self-regenerating and continuously differentiating epidermal tissue, the structural alterations that can occur, and the spatial localization of the reactions involved.

I.3.2. Multi-agent systems

The agent-based approach allows the explicit consideration of the spatial localization of mechanisms, as well as the dynamic self-structuration of the system, with a continuous flow of cells from the epidermal base to the skin surface. In this type of model, the agent, usually the cell, is given a set of behavior rules on how to interact with the environment and its neighbors. An interesting aspect of agent-based model is to observe, during a simulation, properties at the tissue level resulting from the behavior rules encoded at the cellular level. ODE-based models can be integrated to such agent-based models to account for phenomena at varying special and temporal scales (*e.g.* to describe molecular interactions happening within an agent-cell).

The capacity of agent-based model to recapitulate the self-assembly of the epidermis and its dynamic renewal and differentiation make it a particularly relevant tool to study the epidermal physiology. Several agent-based models of the epidermis have been published. Due

to the dynamic and self-structuring nature of this type of models, they have been used in the study of wound healing (Sun et al. 2009; Adra et al. 2010; Wang et al. 2019). A Japanese group from Hokkaido University developed a 3D agent-based model of the epidermis integrating the calcium dynamics involved in cellular differentiation and a desquamation process based on KLK activity on corneodesmosomes (Y. Kobayashi et al. 2016; 2018; Ohno et al. 2021). Recently, they investigated how the deformability of the dermis affects the overall epidermal structure (Ohno et al. 2021).

For this thesis, we build on an existing 2D agent-based model of adult epidermis described by Stamatas *et al*. (Stamatas et al. 2021). This model was itself based on the 3D agent-based model of Sütterlin *et al.* (Sütterlin et al. 2017). The choice to go from 3D to 2D was made mainly to facilitate simulations, as simulating the 3D model is more time-consuming and requires more computing power. The model from Stamatas *et al.* recapitulates the dynamic epidermis structure, with proliferation, differentiation and desquamation of the keratinocytes, and the permeation of a topically applied substance as measured *in vivo*. It also includes a barrier to water exchange between neighboring cells and to water loss at the surface depending on the water gradient and the amount of lipids and tight junctions (Sütterlin et al. 2017). It is developed using the modelling and simulation platform EPISIM (Sütterlin et al. 2013). To answer our research questions, new modules will be added to the existing agent-based model by (Sütterlin et al. 2017; Stamatas et al. 2021).

I.4. Thesis outline

In Chapter II, the pH influence on epidermis structure and function is investigated through the integration of the pH-dependent KLK-LEKTI interactions in an existing agent-based model of the epidermis. This model enables to study how changes on the molecular scale impact global tissue properties, such as the thickness of the different layers or the skin capacity to retain water.

In Chapter III an ODE model describing the interactions of 2 types of bacterial populations, one commensal and one opportunistic pathogen, and the skin, is introduced. This population model is used to study how certain changes in the environmental conditions, such as an elevation of pH, can facilitate the skin colonization by the pathogenic population. The commonly used steady-state assumption is also questioned in this chapter, following the observation of a quasi-stability phenomenon.

In Chapter IV the ODE model of the microbiome introduced in Chapter III is integrated into the agent-based model described in Chapter II. The resulting hybrid model enables the study of the impact of surface cells constant renewal on the microbiome kinetics. It highlights both the added value of combining an ODE population model with an agent-based one, and the necessity to have a good understanding of the ODE system's behavior to dissect the complex dynamics observed during the agent-based simulations.

Finally, we conclude on the results achieved so far and perspectives for future work.

Chapter II reproduces content from a paper submitted to Experimental Dermatology and Chapter III corresponds to a conference paper for the International Conference on Computational Methods in Systems Biology 2022, to be presented in September.

Chapter II - Modeling pH elevation and its impact on skin barrier function and inflammation

II.1. Introduction

The acidic pH at the surface of healthy skin contributes to its protection against invading pathogens (Proksch 2018). Above all, skin surface pH is a central regulator of SC homeostasis through its action on enzymatic activity (Proksch 2018). Under physiologic conditions, the serine protease enzymes, like KLK, ensure epidermal renewal via the degradation of corneodesmosomes that link together the corneocytes, eventually leading to desquamation (Évora et al. 2021). The activity of the several types of KLK present in the SC (KLK5, KLK7, KLK14), is highly sensitive to pH, increasing in less acidic environments (Brattsand et al. 2005).

Skin surface pH is thought to play an important role in the compromised skin barrier related to AD. Indeed, an elevation of skin surface pH has been observed in patients with AD (Eberlein-König et al. 2000). In certain cases this increase can be partly explained by a mutation of the *FLG* gene coding for filaggrin, eventually leading to a faulty production of natural moisturizing factors (NMF), some of which act as pH buffers (Kezic et al. 2008). Although *FLG* mutation has been identified as a major risk factor for AD, it is not the only factor influencing skin surface pH, keeping in mind that the proportion of *FLG* mutation carriers among AD patients varies between 14.2 and 56% depending on the study (Irvine 2007).

The role of elevated pH in the pathogenesis of AD has been investigated with a murine model (Jang et al. 2016), and skin surface pH was identified as a key therapeutic target to improve the skin condition and control AD symptoms. Nevertheless, the mechanisms and effects of a change in pH remain incompletely understood. The role of pH and more broadly,

the interaction between skin barrier and inflammation has been previously studied with several ODE models (Tanaka, Ono, and Harrington 2011; Domínguez-Hüttinger et al. 2013; Nakaoka et al. 2016). While providing interesting insights, these approaches overlook the dynamic nature of skin structure and heterogeneous distribution of the different reactions throughout the epidermis.

In the present work we introduce a dynamic agent-based computational model of the epidermis, integrating the interaction of KLK with LEKTI, to demonstrate that an increase in skin surface pH alone, through the LEKTI-KLK mechanism, is sufficient to compromise the skin barrier, facilitating external irritant penetration and triggering skin inflammation.

II.2. Agent-based model extension

For this work, we build on the agent-based model of adult epidermis described by Stamatas *et al.* (Stamatas et al. 2021). This model is developed using the modeling and simulation platform EPISIM (Sütterlin et al. 2013). It recapitulates the epidermis structure and the permeation of a topically applied substance as measured *in vivo*. The substance is exchanged between neighboring agents according to the concentration gradient, weighted by a coefficient, called inter-agent exchange rate, taking values between 0 and 1, combining partition between aqueous and lipidic phase, and diffusion. One agent represents the cell and its lipid surroundings. The different compositions of the SC and the viable epidermis (VE) are translated into two different inter-agent exchange rates. Using depth profiles measured *in vivo* with Raman spectroscopy, the model has been calibrated to reproduce the observed behavior of specific compounds, by adjusting the values of the inter agent exchange rates.

The model proposed by Stamatas *et al.* (Stamatas et al. 2021) also includes a barrier to water exchange between neighboring cells and to water loss at the surface depending on the water gradient and the amount of lipids and tight junctions (Sütterlin et al. 2017). Tight junctions are produced in the *stratum granulosum* (SG) and retained upon differentiation to SC cells. Lipids are released at the interface of SG and SC.

In this model, the role of KLK is only considered indirectly through the decay of corneocyte-corneocyte adhesion forces. In order to study the impact of a change in pH, the KLK activity has to be added in the agent-based model more directly.

II.2.1. KLK-LEKTI module

The ODE model described by Tanaka et al. (Tanaka, Ono, and Harrington 2011) is adapted to focus only on the interactions of KLK with its inhibitor LEKTI. This model is then translated into an SBML (Systems Biology Markup Language) model (Finney et al. 2004) using the BIOCHAM software (Calzone, Fages, and Soliman 2006) to handle the differences in timescales (Table II.2.1). BIOCHAM also allows to check for the well-formedness and strictness conditions of the model, as defined by Fages *et al.* (Fages, Gay, and Soliman 2015). These conditions guarantee, among other things, the positivity of the system. The EPISIM platform then provides a method to integrate SBML models into the agent-based one, mapping the timescales (Sütterlin et al. 2013). In our case, the mapping is done so that the SBML model describing KLK activity has reached steady state over the course of one simulation step of the agent-based model.

The pH influence on KLK activity is translated into two sets of parameters as described by Tanaka *et al.* (Tanaka, Ono, and Harrington 2011), representing healthy skin with an acidic pH (around 4.5) and compromised skin with a less acidic pH (around 6.5) (Table II.2.2). We selected one pH value in the physiological range according to Proksch (Proksch 2018) and one above to represent a compromised skin barrier condition. To facilitate comparisons we followed the choice of pH values used by Tanaka *et al.*(Tanaka, Ono, and Harrington 2011).

When integrating the KLK-LEKTI module into the agent-based model, the location of the reactions has to be taken into account. Biologically KLK and LEKTI are released at the interface of SG and SC, together with the lamellar bodies, a process that we call corneocytes maturation. Consequently, in the agent-based model, the LEKTI-KLK module is only active in the mature corneocytes, meaning those which have released all their lamellar bodies.

The cleaving action of active KLK (KLK*) on corneodesmosomes is modeled as a decay of adhesion forces, proportional to the amount of KLK*. When the corneocyte-corneocyte adhesion goes below a certain threshold, the cell is desquamated and removed from the

simulation. The action of KLK* on adhesion forces is normalized to the quantity of KLK* at steady state produced with the set of parameter values corresponding to physiological pH. This ensures that the resulting adhesion decay, with the physiological pH parameter values, is equal to the adhesion decay rate of the original agent-based model of the epidermis, therefore preserving the previously validated epidermal structure (Stamatas et al. 2021; Sütterlin et al. 2017). In other words, if the amount of KLK* in an agent is superior to the quantity of KLK* at steady state with the physiological pH set of parameter values, the adhesion decay will be faster than the original decay rate, and inversely.

Table II.2.1: ODEs adapted from Tanaka et al. *(Tanaka, Ono, and Harrington 2011)* ***and the corresponding reactions defined using BIOCHAM.*** *MA=Mass action law kinetics; KLKa=active KLK*

ODE	**Reactions**
$\frac{d\,KLK}{dt} = -k\frac{KLK^*\,KLK}{KLK^* + C_K} - \delta_K\,KLK + m_K$ $\frac{d\,KLK^*}{dt} = k\frac{KLK^*\,KLK}{KLK^* + C_K} - k_a\,KLK^*\,LEKTI + k_d\,LEKTI.KLK - \delta_{K*}\,KLK^*$ $\frac{d\,LEKTI}{dt} = -k_a\,KLK^*\,LEKTI + k_d LEKTI.KLK - \delta_L\,LEKTI + m_L$ $\frac{d\,LEKTI.KLK}{dt} = k_a\,KLK^*\,LEKTI - k_d\,LEKTI.KLK - \delta_{LK}\,LEKTI.KLK$	MA(mk) for _ => KLK MA(ml) for _ => LEKTI MA(dk) for KLK => _ MA(dka) for KLKa => _ MA(dl) for LEKTI => _ MA(dlk) for LEKTI.KLK => _ MA(ka) for KLKa + LEKTI => LEKTI.KLK MA(kd) for LEKTI.KLK => LEKTI + KLKa k KLKa KLK/(Ck + KLKa) for KLK + KLKa => 2 KLKa

Table II.2.2 : KLK-LEKTI module: Parameter descriptions and values from Tanaka et al. (Tanaka, Ono, and Harrington 2011)

Parameter	Description	Value
k	KLK activation rate	10 (pH 4.5) 50 (pH 6.5)
k_a	LEKTI-KLK* association rate	1 (pH 4.5) 3 (pH 6.5)
k_d	LEKTI-KLK* dissociation rate	1 (pH 4.5) 0.0025 (pH 6.5)
δ_K	KLK degradation rate	1
δ_{K*}	KLK* degradation rate	1
δ_L	LEKTI degradation rate	0.5
δ_{LK}	LEKTI-KLK* degradation rate	1
C_K	Half-saturation of KLK activation	50
m_K	Basal production rate for KLK	10
m_L	Basal production rate for LEKTI	1

II.2.2. Inflammation Module

The inflammation module developed in this work represents the release of inflammatory molecules, such as cytokines, subsequently to the penetration of an irritant through the epidermis. The inflammatory reaction only begins when the irritant crosses the SC, as the corneocytes lost their nucleus when differentiating and cannot have any synthetic activity. Once the concentration of irritant around a cell of the VE rises above a certain threshold *irritation_threshold* the cell starts producing inflammatory molecules ([*IM*]) according to:

$$\frac{d[IM]}{dt} = p_i + d_i\,[IM]$$

When the irritant concentration is lower than *irritation_threshold*, the cell no longer produces inflammatory cytokines ($p_i = 0$) but their degradation persists. The value for the *irritation_threshold* is set to 0.1 so that a release of cytokines would be observed for both pH conditions, given the concentration of irritant applied at the surface equal to 1, selected for demonstration purpose. A threshold value set too high, results in no cytokine release in both pH conditions. On the contrary, lowering the threshold leads to a higher response for both skin conditions, even though the comparison will remain qualitatively the same. The parameters p_i and d_i control the kinetics and magnitude of the inflammation. For inflammatory molecules to be produced, the value of p_i needs to be higher than the one of d_i. To allow the ability to examine the dynamic changes in *IM* concentration within the time frame defined by the model, the values of p_i and d_i are set to 2 and 0.005 respectively. The model robustness to variations of these parameter values is discussed in the Results section of this Chapter. Finally, the inflammatory cytokines are exchanged between neighboring cells according to the concentration gradient.

II.3. Simulations

The simulations are done on a fully built and stable epidermis starting after 5000 simulation steps. Then the SBML model of KLK activity is switched on, and we let the model accommodate for another 500 steps to get stable thickness of the SC. The irritant is applied topically with a surface concentration of 1, inter-agent exchange rate equal to 0.58 in SC, and 0.29 in the VE.

Depending on the scenario tested, the irritant is either removed after 50 simulation steps (corresponding to 25 hours in real time) to simulate the application of a patch of irritant substance, or continuously applied until the end of the simulation. In both cases during the application, the surface concentration of the irritant is constant, simulating the application of a patch on the skin.

Simulations of the two models (physiological and less acidic pH) are compared in terms of model emerging properties, that is properties resulting from the agents' interactions, not directly encoded in the model. More specifically, we look at the thicknesses of different skin

layers, the total amount of irritant permeated in the SC and VE, the resistance to water transport, water loss at skin surface and total amount of inflammatory cytokines produced.

II.3.1. Simulated water loss at the surface and resistance to water transport

The simulated water loss at the skin surface is computed as the average of the *waterflow_surface* parameter over all surface cells. This parameter value is proportional the intracellular water content, the ratio of exposed cell surface area, the barrier properties of the cell depending on tight junctions and lipids, and evaporation rate. The resulting value for water loss at the skin surface and the simulated water depth profile are then used to compute the depth-dependent resistance to waterflow according to the method described by MDA van Logtestijn *et al*. (Logtestijn et al. 2015).

II.4. Results

II.4.1. Model overview

To study the impact of skin surface pH on skin barrier and inflammation, we introduce an agent-based model of the epidermis (Figure II.4-1). This model builds on a previously presented model that considers explicitly keratinocyte proliferation, differentiation, and desquamation processes and can recapitulate skin structure, water barrier function, and penetration kinetics of an external substance introduced at the skin surface at a given time of the simulation (Stamatas et al. 2021). This model is modified here by the introduction of KLK production, auto-activation (KLK*), and inhibition by LEKTI, processes which affect the rate of corneocyte desquamation at the skin surface (Deraison et al. 2007; Eissa and Diamandis 2008). The mathematical model first described by Tanaka *et al*. (Tanaka, Ono, and Harrington 2011) is adapted and integrated at the agent-level programming of the corneocytes, present only in the SC. This modification of the original agent-based model does not disturb the stability of the system and preserves the epidermal structure at skin surface pH of 4.5 (Figure II.4-2).

The computational model highlights two coexisting mechanisms, both of which are able to lead to increased desquamation. Figure II.4-3 shows that an increase in pH, affects the values of several parameters, resulting in higher KLK* concentration at steady-state and eventually leading to increased corneodesmosomes degradation and faster desquamation. This process is inhibited by LEKTI. A threshold effect can be observed in the presence of LEKTI concentration sufficient to form a complex with all available KLK*, completely preventing corneodesmosomes degradation. The model can be used to simulate the effect of impaired LEKTI production due to genetic mutations on *SPINK5* (the gene encoding for the LEKTI protein). Such mutations are sometimes present on AD patients (Nishio et al. 2003) . *SPINK5* mutations result in loss of function of LEKTI and can be simulated in the model as a decrease of the m_L parameter, representing the basal production of LEKTI by keratinocytes. Figure II.4-3 illustrates that at a given skin pH, the decrease of LEKTI production results in an increase of KLK* concentration at steady-state, again leading to higher rate of corneocyte desquamation.

The agent-based model also allows for the simulation of permeation of a topically applied substance, as described by Stamatas *et al*. (Stamatas et al. 2021). Here, we consider that the externally applied substance is an irritant, which can trigger skin inflammation depending on its concentration. The irritant is introduced in the model at the skin surface at a given time. It then diffuses through the epidermis following its concentration gradient. At the junction between the SC and the VE the inter-agent exchange rate is adjusted to reflect the compositional difference of the two layers (lipophilic SC compared to hydrophilic VE). Finally, the release of inflammatory molecules by keratinocytes in the VE is introduced in the model. This release is triggered when the irritant concentration inside the agent rises above a pre-defined threshold, simulating the release of inflammatory cytokines from cellular stores, which is the case for interleukin (IL)-1α for example.

This quantitative model aims at providing qualitative predictions about the impact of skin pH elevation, considering that all other influencing factors remain equal. We do not pretend to make precise quantitative predictions because this would require calibrating our model accurately using *in vivo* data that we do not have. The values of inflammation parameters were chosen only as example demonstrating the dynamics of the inflammatory

reaction at two skin surface pH conditions (physiological and less acidic pH). A more precise simulation would require experimental data of irritant-induced inflammatory reaction. Unfortunately, there is a lack of available *in vivo* studies involving molecules that act as irritants without interfering with other skin functions. Overall, the agent-based model provided here integrates a refined desquamation process, permeation of an irritant substance and acute inflammation, in a dynamic and spatially discrete way. It enables to investigate the impact of a change in skin pH at tissue level through the study of the system's emerging properties. These are properties that were not directly coded but rather emerge from the interactions of agents.

To study the robustness of these emerging properties to variations of the pH-dependent parameter values, a sensitivity analysis is conducted with simultaneous variations of 20% of the parameters k, k_a and k_d around their nominal values, which corresponds to the variability usually observed in skin clinical measurements (Figure II.4-4). The variation of lower values of k is limited to 7%, since lower values lead to $KLK^* = 0$ and infinite growth of the SC. This highlights the crucial role played by KLK in epidermis structure homeostasis.

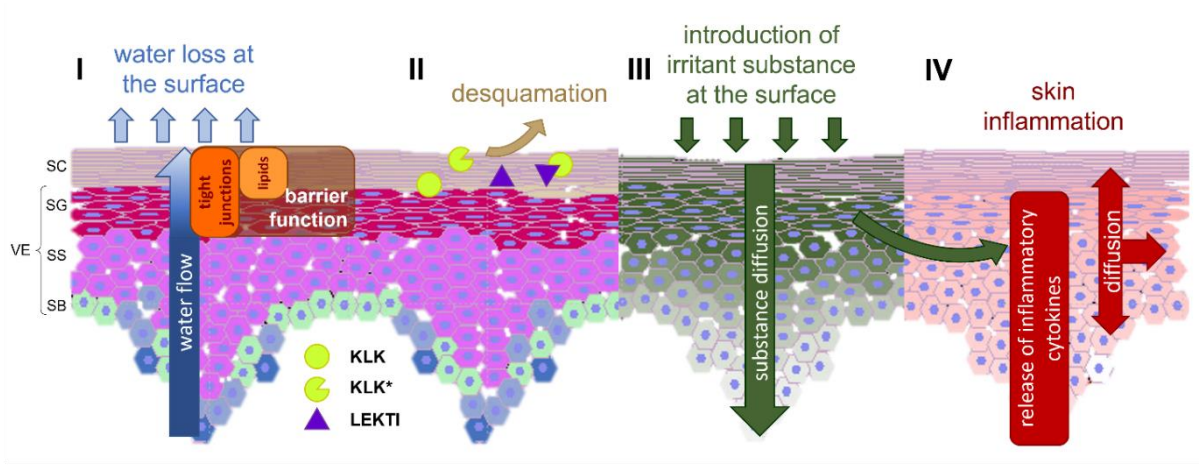

Figure II.4-1: Graphical representation of the agent-based model and spatial distribution of the modules: barrier function, LEKTI-KLK interactions and desquamation process, irritant permeation, and acute inflammation. *(I) The water flows from the bottom of the epidermis to the surface according to its gradient. It is restrained towards the surface by the skin barrier, composed of tight junctions (in the SG and SC) and lipids (in the SC) (Sütterlin et al. 2017). (II) KLK and its inhibitor, LEKTI are released at the interface of SG and SC and interact in the SC. KLK self-activates into KLK*, which can then either form a complex with LEKTI or contribute to the desquamation process by degrading corneocyte-corneocyte adhesion. (III) The irritant substance is introduced at the surface and diffuses through the epidermis according to its concentration gradient and the inter-agent exchange rates specific to the SC or the VE, reflecting the compositional difference of the two layers (lipophilic SC compared to hydrophilic VE) (Stamatas et al. 2021). (IV) When the intra-cellular irritant concentration of VE cells rises above a pre-defined threshold, it triggers the release of inflammatory cytokines. The cells are colored according to their differentiation status on the left part (dark blue for stem cells, light blue for transient amplifying cells, light green for basal cells, light pink for spinous cells, dark pink for granular cells, and tan for corneocytes), the intra-cellular irritant concentration in the middle (the greener, the higher the irritant concentration), and the intra-cellular inflammatory cytokines concentration on the right (the redder, the higher the inflammatory cytokines concentration). VE: viable epidermis, SC: stratum corneum, SG: stratum granulosum, SS: stratum spinosum, SB: stratum basale, KLK: kallikreins, KLK*: active kallikreins, LEKTI: Lympho-Epithelial Kazal-Type-related Inhibitor.*

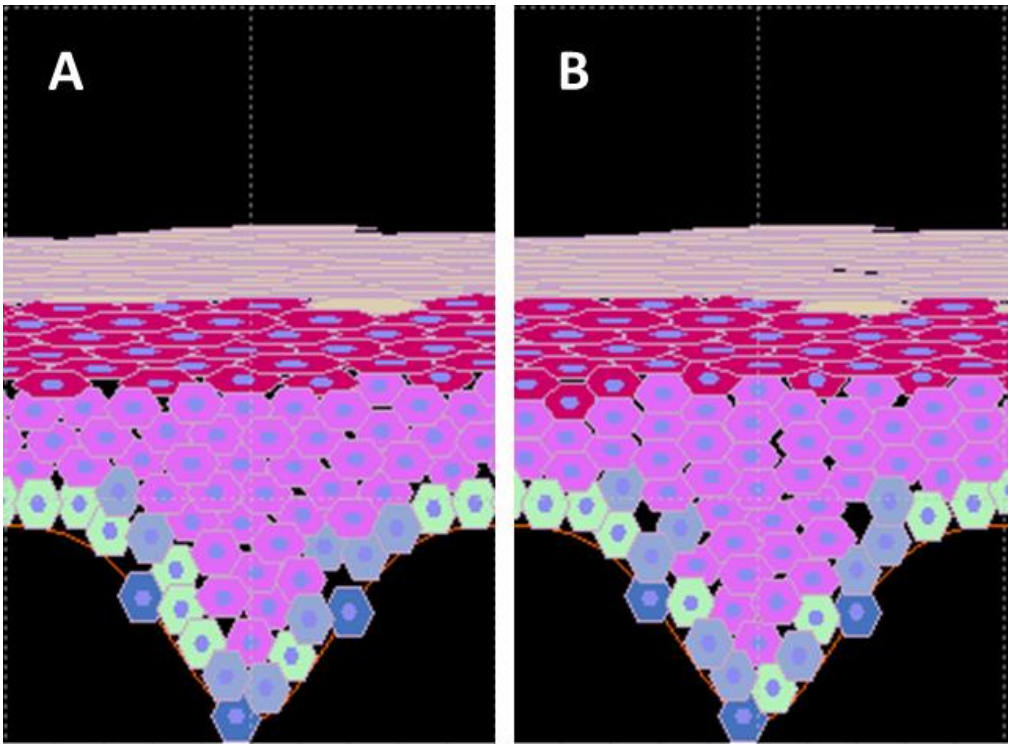

Figure II.4-2: The addition of the KLK-LEKTI module preserves the overall structure. *Simulated epidermal structure with (A) the validated agent-based model of adult epidermis described by Stamatas et al. (Stamatas et al. 2021) and (B) the new agent-based model with the addition of the KLK-LEKTI module, at skin surface pH of 4.5.*

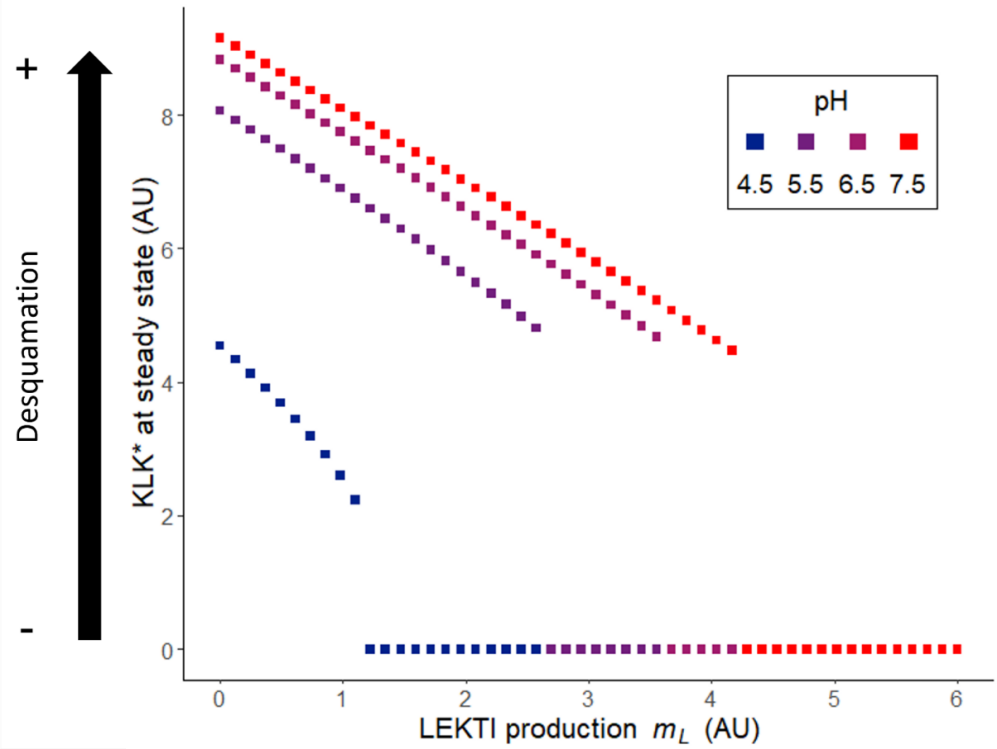

Figure II.4-3: Effect of pH and LEKTI inhibition on desquamation. *The amount of KLK* at steady state increases with pH, represented by different colors according to the legend, for a given basal production of LEKTI by keratinocytes, m_L. The model also predicts the complete inhibition of KLK* by LEKTI when m_L gets above a certain value, that increases together with pH. The steady state amount of KLK* directly affects the loss of corneocyte-corneocyte adhesion and thus desquamation. The dots correspond to the steady-state quantity of KLK* predicted by the model for each value of m_L and with four sets of parameter values reflecting four values of pH (Table II.4.1). KLK*: active kallikreins, LEKTI: Lympho-Epithelial Kazal-Type-related Inhibitor, AU: arbitrary units.*

Table II.4.1: Sets of parameter values reflecting pH variation, obtained with linear interpolation based on the two sets of parameters described by *(Tanaka, Ono, and Harrington 2011)*

pH	**4.5**	**5.5**	**6.5**	**7.5**
k	10	30	50	70
k_a	1	2	3	4
k_d	1	0.04	0.0025	0.0001

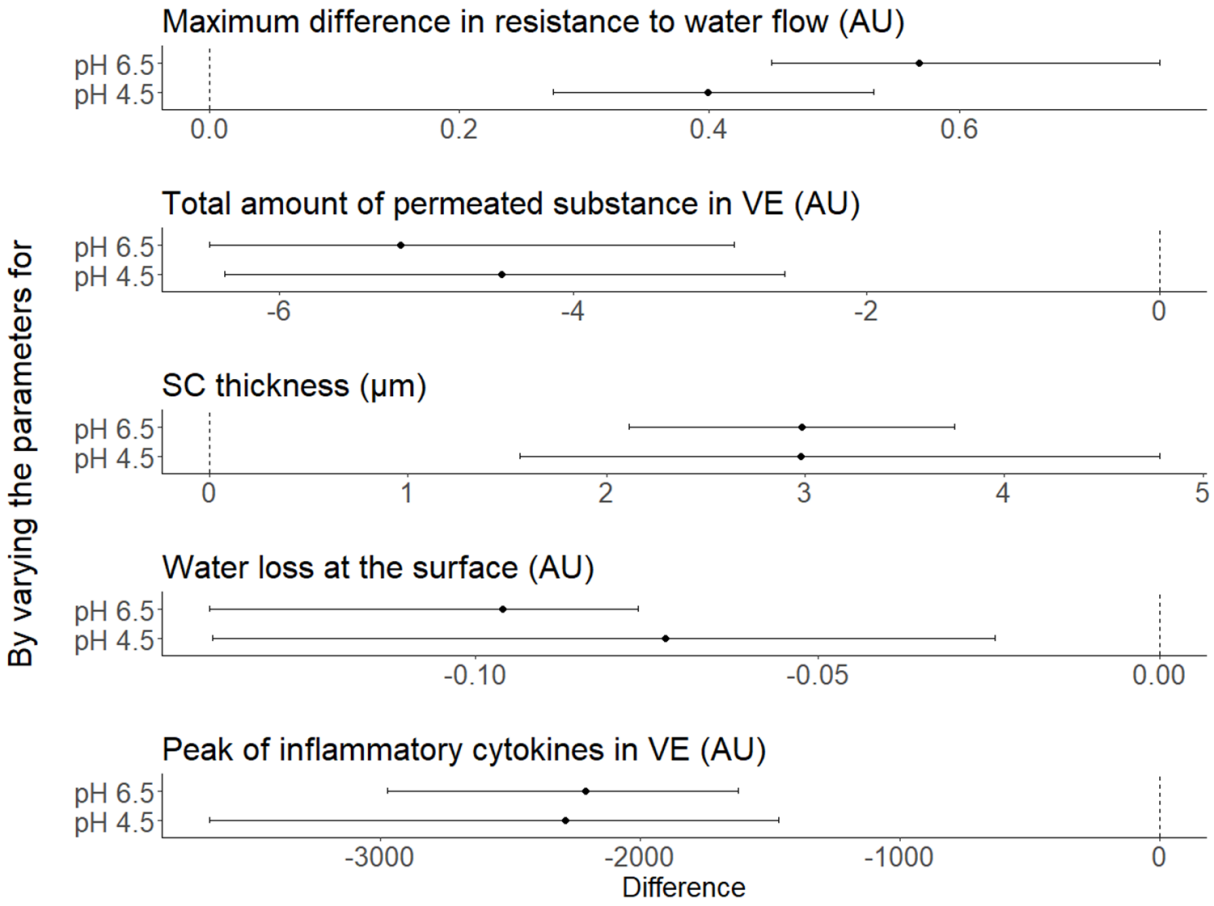

Figure II.4-4: Difference diagram for parameter value changes. *We studied the model robustness to small variations of pH-dependent parameter values of the LEKTI-KLK module: k, k_a and k_d. All the other parameter values were kept unchanged. The model was simulated using variations of 20% around the standard parameter values (Table II.2.2), except for the lowest value of k, which was limited to 7% since higher changes were leading to KLK*=0 at steady state. We then looked at how these parameter values variations impacted the model behavior through several properties of interest: resistance to water flow, total amount of permeated substance in the viable epidermis (VE), stratum corneum (SC) thickness, water loss at the surface and peak of inflammatory cytokines in VE. We compared simulations with variations of the parameter values to the model behavior with the original set of parameter values (either pH 4.5 or pH 6.5). For all the properties of interest, the difference between their values at pH 4.5 and 6.5 was robustly positive or negative (i.e their distribution is not crossing the zero line). It indicates that the two pH conditions are well separated and that the model is robust to pH-dependent parameter values variations.*

II.4.2. Impact on epidermal structure

Increased skin surface pH (and subsequent increase in KLK activity) has an immediate effect on the SC thickness (Figure II.4-5). KLK*, through its action of degrading corneodesmosomes, directly affects corneocyte adhesion and therefore the desquamation rate. The simulations demonstrate that increased KLK activity results in thinner SC by about 18% (Table II.4.**2**). The model also predicts a thinning of the VE by about 6% (Table II.4.**2**). This observation can be explained by the alteration of the calcium gradient controlling the differentiation process, consequently to SC thinning. This in turn results in weakening of the skin barrier function in both directions: outside-in (irritant permeation) and inside-out (water loss).

Table II.4.2 : Predicted properties of the system for the two conditions: physiologic pH (4.5) and less acidic pH (6.5). *VE: viable epidermis, SC: stratum corneum, AU: arbitrary unit*

	SC thickness (µm)	VE thickness (µm)	water loss at skin surface (AU)	total substance in VE / thickness (AU)	total substance in SC / thickness (AU)	total cytokines at inflammation peak in VE (AU)
Physiologic pH (4.5)	17	85	1.1	0.54	9.1	5.5 E3
Less acidic pH (6.5)	14	80	1.2	0.64	7.9	7.9 E3
% difference	**-18%**	**-6%**	**+9%**	**+19%**	**-13%**	**+44%**

II.4.3. Weakening on the skin barrier function

The skin's capacity to retain water is assessed in the model by two parameters: water loss at skin surface and resistance to water flow. At skin surface pH of 6.5, the water loss at the skin surface measured *in silico* is about 9% higher compared to a more physiologic condition of pH 4.5 (Table II.4.**2**). Moreover, Figure II.4-5 shows a decrease in resistance to water flow, particularly in the lower part of the SC. In the deeper section of the SC (depth 0.5-1), the 2 resistance profiles are similar since the water content at the interface between SC

and VE remains the same in both pH conditions. These observations are in agreement with clinically reported results concerning changes in water transport through the SC following lipid removal, tape stripping or comparing AD to healthy skin (Logtestijn et al. 2016).

To evaluate the strength of the outside-in barrier, topical application of an external substance is simulated. Figure II.4-5 shows the kinetics of the total substance amount that permeated in the VE. At a less acidic pH, the simulation predicts faster substance penetration and higher total permeated quantity at steady state compared to the physiological pH condition.

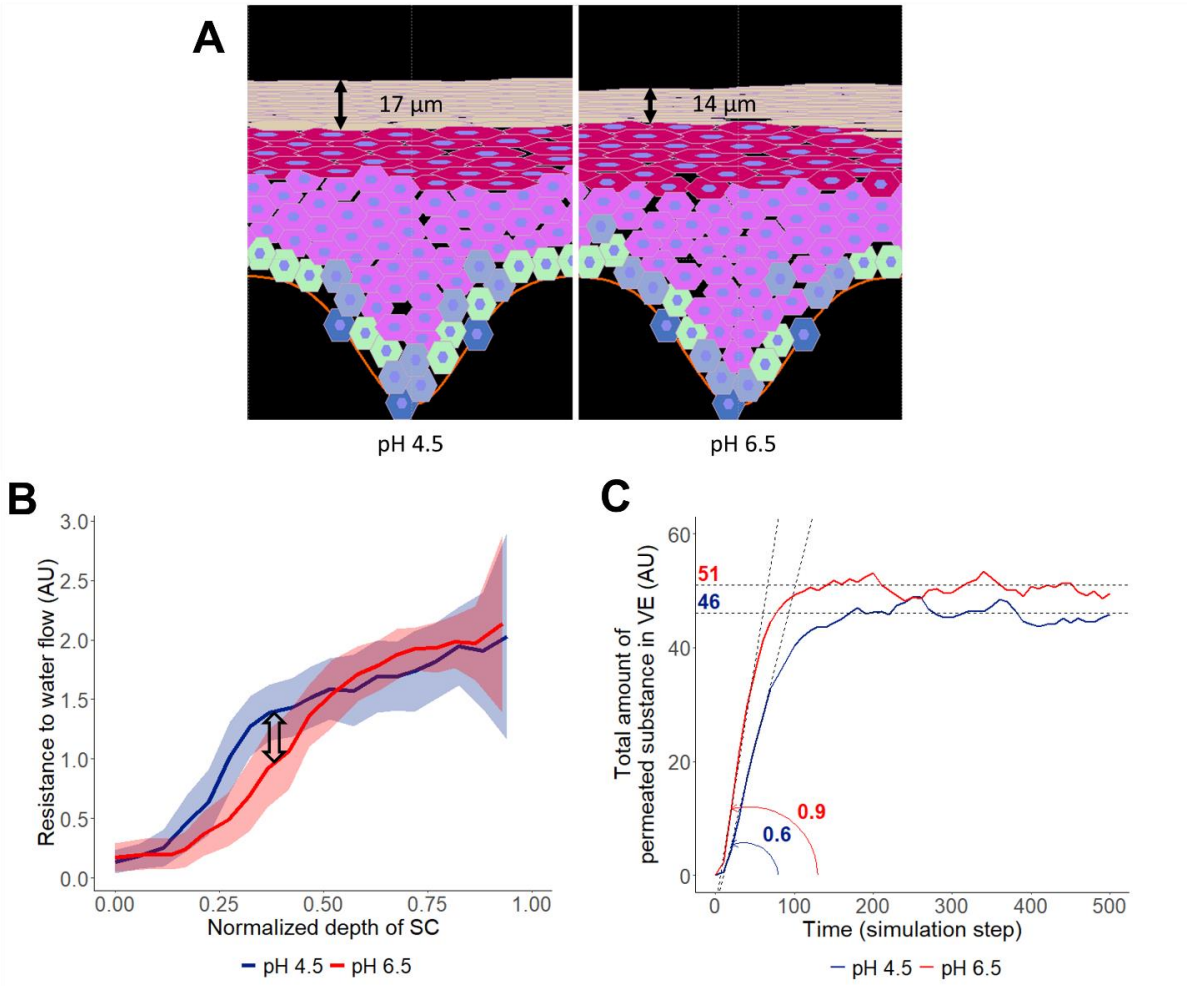

Figure II.4-5: The increase of skin surface pH results in the thinning of SC, with subsequent weakening of skin barrier function in both directions, inside-out and outside-in. *(A) The graphical output of the model for the two pH conditions (4.5 on the left and 6.5 on the right) show that the overall layered structure of the epidermis is preserved in both cases, while the SC is thinner for the less acidic pH condition. The cells are colored according to their differentiation status: dark blue for stem cells, light blue for transient amplifying cells, light green for basal cells, light pink for spinous cells, dark pink for granular cells, and tan for corneocytes. (B) The decrease in resistance to water flow (indicated with the black arrow) predicted for the less acidic pH condition (red) indicates a reduced capacity to retain water compared to the more physiologic pH condition (blue). The profiles are averaged over depth and time, and the x-axis is shown as the depth normalized to the SC thickness for easier comparison between the two pH conditions. The ribbon represents the SD of the resistance profile over time. (C) The model predicts both faster permeation (indicated by a steeper slope) and higher amount of irritant substance permeating in the VE with a less acidic pH (red), indicating a higher permeability of the epidermis to irritants, compared to the pH condition of 4.5 (blue). VE: viable epidermis, SC: stratum corneum*

II.4.4. Resulting skin inflammation

The impaired outside-in barrier function can have direct consequences on the release of inflammatory cytokines. Figure II.4-6 shows the simulated production of inflammatory cytokines resulting from the permeation of an irritant into the epidermis, following continuous irritant exposure at the skin surface for 24 hours. At the peak of inflammation, the same amount of irritant applied at the surface induces a significant increase in the concentration of inflammatory cytokines when skin pH is set at 6.5 compared to 4.5. Note that the production of inflammatory cytokines also starts earlier in the compromised skin model compared to healthy skin.

The robustness of the inflammation-related predictions of the model was assessed by simulating the model with variations of p_i, d_i and *irritation_threshold* values. The influence of each of these parameters was tested independently by simulating the model for healthy and compromised skin, with variations of 20% around the parameter nominal value ($p_i = 2$, $d_i = 0.005$, *irritation_threshold* $= 0.1$), while the other two parameters remained unchanged. For each set of parameter values, the difference in the peak of inflammatory molecules in the VE between the compromised and the healthy conditions ($\Delta_{IM}(pH\ 6.5 - pH\ 4.5)$) was computed. Table II.4.***3*** recapitulates the average, standard-deviation, and coefficient of variation of $\Delta_{IM}(pH\ 6.5 - pH\ 4.5)$ for each parameter. $\Delta_{IM}(pH\ 6.5 - pH\ 4.5)$ is positive for all parameters and the coefficient of variations are relatively small, meaning that the model robustly predicts an increased production of cytokines with a less acidic pH.

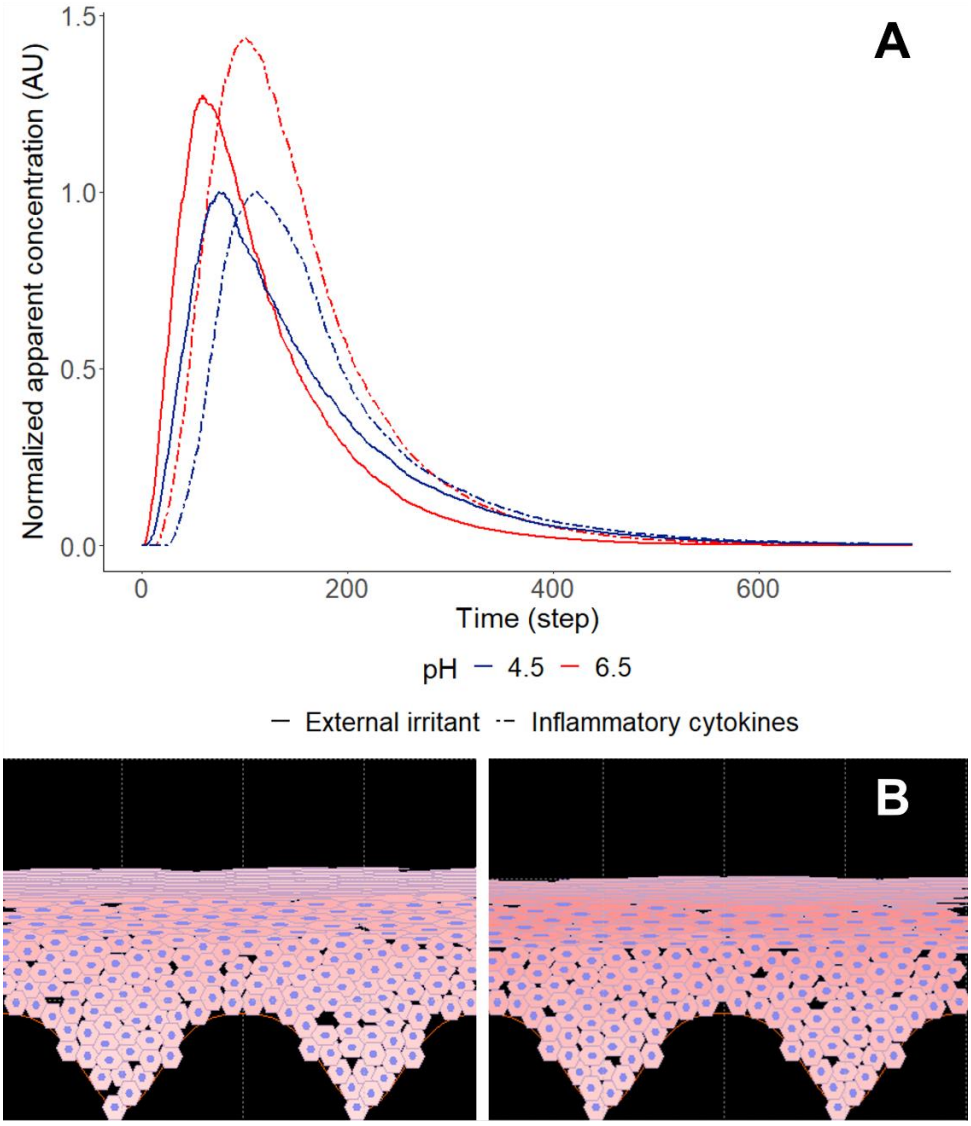

Figure II.4-6: Impaired skin barrier function at higher pH causes a more intense inflammatory reaction. *(A) The model predicts that, the same amount of irritant applied at the surface at t=0 and for 24 hours, permeates in higher quantity in the VE and therefore induces the production of more inflammatory cytokines with a skin surface pH of 6.5 compared to 4.5. The release of inflammatory cytokines also starts earlier with skin pH set to 6.5 (t= 10) compared to the more physiological pH condition of 4.5 (t=23). The evolution of the total quantity of irritant and inflammatory cytokines in VE are shown with solid and dotted line respectively. They are colored according to the pH condition and normalized to the peaks of irritant and inflammatory cytokines with pH of 4.5. (B) Graphical output of the skin inflammation peak for both pH conditions: 4.5 on the left and 6.5 on the right. The cells are colored according to their concentration in inflammatory cytokines: the redder, the higher the concentration. VE: viable epidermis.*

Table II.4.3 : Robustness of the inflammatory molecules-related model predictions to variations of the inflammation module parameter values

Parameter	Average $\Delta_{IM}(pH\ 6.5 - pH\ 4.5)$	Standard-Deviation $\Delta_{IM}(pH\ 6.5 - pH\ 4.5)$	Coefficient of variation $\Delta_{IM}(pH\ 6.5 - pH\ 4.5)$
irritation_threshold	2616	47.4	0.018
$\boldsymbol{p_i}$	2089	338.3	0.162
$\boldsymbol{d_i}$	2293	477.2	0.208

II.5. Discussion

While the model introduced here clearly demonstrates the effects of skin pH elevation that are relevant to AD (increased water-loss, higher permeability to irritants and more intense inflammation), it could be further developed to include additional aspects of AD pathology, including the involvement of microbiome dysbiosis (Paller et al. 2019), the role of allergens (Friedmann 1998), or a more complex inflammation pathway involving specific cytokines (IL-4, IL-13, IL-33 (Gandhi et al. 2016; Seltmann et al. 2015)) and Th2 cells. Moreover, the model can also be further developed to include aspects of AD lesional skin, like keratinocytes hyperproliferation, reduced secretion of lamellar granules (therefore less KLK), and SC hyperkeratosis (Igawa et al. 2017). The latter phenomenon however could be countered by an increased KLK expression stimulated by Th2 cytokines (Morizane et al. 2012). The integration of these additional modules in the model would necessarily require data, preferably measured *in vivo*, that currently do not exist.

In our qualitative model, the parameter values related to the inflammatory reaction were selected arbitrarily due to the lack of *in vivo* data involving irritants that trigger skin inflammation without disrupting skin barrier function. For example, surfactants like sodium lauryl sulphate (SLS) are disturbing skin lipid content and organization, effects that would need

to be considered in the simulation separately. As presented in our previous work (Stamatas et al. 2021), experimentally determined concentration profiles would be required for tuning the permeation parameters of an externally applied substance. If this substance is a skin irritant, this can be technically challenging. Furthermore, it is difficult to track quantitatively the production of inflammatory molecules *in vivo*. Nevertheless, parameter values related to the inflammatory reaction are shared by both pH conditions tested in this model, meaning that the qualitative comparison between them will remain the same. Due to the predicted alteration of the epidermal structure, the irritant substance will reach the VE sooner and in higher amounts, inducing a higher inflammatory response, regardless of the values given to these parameters.

Inflammation is a very complex physiological process involving different molecular cascades and activation sequences of several different cell types. In the present work we only considered the initial events of such an inflammatory cascade. In the future it is conceptually feasible to integrate in the model further downstream aspects of skin inflammation, for example to investigate the key role played by Th2 cells in AD. Additionally, several studies have demonstrated that besides their activity on corneodesmosomes, certain kallikreins like KLK5 and KLK14, are able to activate proteinase-activated receptor-2 (PAR2) (Stefansson et al. 2008; Briot et al. 2009). PAR2 is a transmembrane receptor present in keratinocytes that downregulates the lamellar bodies secretion (Hachem et al. 2006) and triggers a proinflammatory and proallergic pathway upon activation (Briot et al. 2009). Integrating this influence of KLK on barrier formation and inflammation in the model would increase our understanding of the extent of KLK impact on epidermis homeostasis.

In this work we modeled the effects of a skin pH value as a constant within the SC. This approximation resulted in reasonable results, however a more detailed model would consider that pH actually follows a gradient in the SC, from neutral pH at the interface with SG to acidic at the skin surface (Hanson et al. 2002). As discussed earlier, the enzymatic reactions involving KLK and LEKTI are highly sensitive to pH (Deraison et al. 2007). In that case both the inhibition of KLK by LEKTI and the cleaving of corneodesmosomes by active KLK would be depth dependent. Additionally, the impact of pH on skin barrier, is not limited to its action on

enzymatic activity. A recent study has shown that a more neutral pH prevents the right formation of the SC lipid structure, leading to even more water loss (Nováčková et al. 2021). Such effects would go in the same direction, namely that pH elevation leads to barrier impairment, and further support our conclusions.

Chapter III - Skin Microbiome Model: Stability versus Meta-stability

III.1. Introduction

Located at the interface between the organism and the surrounding environment, the skin constitutes the first line of defense against external threats, including irritants and pathogens. In order to control potential colonization of the skin surface by pathogens, the epidermal cells, called keratinocytes, produce AMPs (Pazgier et al. 2006). The physiologically acidic skin surface pH also helps to control the growth of bacterial populations (Proksch 2018; Korting et al. 1990). Another contributor to the defense against pathogen colonization are commensal bacteria in the community of microorganisms living on the skin, commonly referred to as the skin microbiome. Over the past decade, several studies have highlighted the key role played by such commensal bacterial species defending against invading pathogens, as well as their contribution to the regulation of the immune system (Lai et al. 2009; Cogen, Yamasaki, Muto, et al. 2010; Lai et al. 2010; Kong 2011; Belkaid and Segre 2014; Byrd, Belkaid, and Segre 2018).

Alterations in the composition of the skin microbiome resulting in a dominance by a pathogenic species, also called dysbiosis, have been associated with skin conditions such as acne or AD (Leyden et al. 1975; Kong et al. 2012). In the case of AD, the patient skin is often colonized by *S. aureus*, especially on the lesions (Kong et al. 2012). Treatment strategies targeting non-specific elimination of cutaneous microflora, such as bleach baths, have shown conflicting results regarding their capacity to reduce the disease severity (Chopra et al. 2017). On the other hand, treatments involving introduction of commensal species, like *Staphylococcus hominis* (Nakatsuji et al. 2021) on the skin surface appear promising. Accordingly, the interactions between the commensal populations, pathogens and skin cells seem at the heart of maintaining microbiome balance. There is therefore a necessity to investigate further those interactions and the drivers of dominance of one population over

others. Unfortunately, it is challenging to perform *in vitro* experiments involving more than one or two different species, even more so on skin explants or skin equivalents.

Mathematical models of population dynamics have been developed and used for more than two hundred years (Malthus 1798). Here, we introduce a model based on ODE, describing the interactions of a population of commensal species with one of opportunistic pathogens and the skin cells. We study the factors influencing the dominance of one population over the other on a microbiologically relevant timescale of a couple of days corresponding to biological experimental data. More specifically, we identify constraining relationships on the parameter values, based on published experimental data (Nakatsuji et al. 2017; Kohda et al. 2021), corresponding to special cases of our model, allowing us to reduce the parametric dimension of our model from 13 to 5 parameters. Interestingly, we observe in the reduced model a phenomenon of meta-stability (Tognoli and Kelso 2014; Radulescu et al. 2015), also called quasi-stability, in which the seemingly stable state reached after 30 hours following the initiation of the experiment, is followed after 300 hours by a reversed stable state. On the time scale of the experiments, we show that certain changes in the environment, like an elevation of skin surface pH, create favorable conditions for the emergence and colonization of the skin by the opportunistic pathogen population. Such predictions can help identify potential therapeutic strategies for the treatment of skin conditions involving microbiome dysbiosis and underscore the importance of meta-stable states in the real biological processes at their different time scales.

III.2. Initial ODE model with 13 parameters

The model built in this paper considers two types of bacterial populations. The first population, S_c, regroups commensal bacteria species having an overall beneficial effect for the skin, and the second population, S_p, represents opportunistic pathogens. The differential equations for both bacterial populations are based on the common logistic growth model (Zwietering et al. 1990), considering non-explicitly the limitations in food and space. The limited resources are included in the parameters $K_{sc}$and K_{sp}, representing the optimum concentration of the populations in a given environment, considering the available resources.

The bactericidal effect of AMPs produced by skin cells, Amp_h, on S_p is included with a Hill function. This type of highly non-linear functions have been used previously to model the effect of antibiotics on bacterial populations (Meredith et al. 2015). For the sake of simplicity, the AMPs produced by skin cells is introduced as a constant parameter, $[Amp_h]$, in the model. It represents the average concentration of these AMPs among surface cells, under given human genetic background and environmental conditions.

Several studies revealed that commensal bacterial populations, like *S. epidermidis* or *S. hominis*, are also able to produce AMPs targeted against opportunistic pathogens, such as *S. aureus* (Nakatsuji et al. 2017; Cogen, Yamasaki, Sanchez, et al. 2010). For these reasons, we introduce in the model AMPs of bacterial origin, Amp_b, acting similarly to Amp_h on the pathogenic population S_p. Amp_b is produced at rate k_c by S_c, and degraded at rate d_a. Furthermore, we include a defense mechanism of S_p against S_c with a direct killing effect.

Altogether, this gives us the following ODE system with 3 variables and 13 parameters, all taking non-negative values:

$$\begin{cases} \dfrac{d[S_c]}{dt} = \left(r_{sc}\left(1-\dfrac{[S_c]}{K_{sc}}\right) - \dfrac{d_{sc}[S_p]}{C_1+[S_p]}\right)[S_c] \\ \dfrac{d[S_p]}{dt} = \left(r_{sp}\left(1-\dfrac{[S_p]}{K_{sp}}\right) - \dfrac{d_{spb}[Amp_b]}{C_{ab}+[Amp_b]} - \dfrac{d_{sph}[Amp_h]}{C_{ah}+[Amp_h]}\right)[S_p] \\ \dfrac{d[Amp_b]}{dt} = k_c[S_c] - d_a\,[Amp_b] \end{cases} \qquad (1)$$

The model is illustrated on Figure III.2-1 and Table III.2.**1** recapitulates the variables and the parameters with their unit. Such a model cannot be solved analytically. Furthermore, the use of optimization algorithms to infer the 13 parameter values from data resulted in many valid sets of parameter values. Therefore, it is clearly necessary to restrict the number of parameters by identifying some of them, to be able to analyze the model.

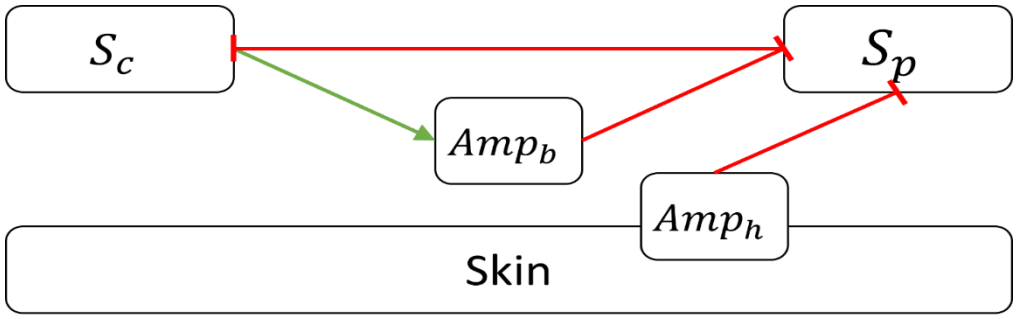

***Figure III.2-1: Model overview**, green arrow representing production and red T-lines representing killing effect.*

***Table III.2.1: List of the parameters and variables of our mathematical model with their units.** CFU = Colony forming unit, AU = Arbitrary Unit, ASU = Arbitrary Surface Unit*

Variables	**Interpretation (unit)**
$[S_c]$	Surface apparent concentration of S_c $(CFU.ASU^{-1})$
$[S_p]$	Surface apparent concentration of S_p $(CFU.ASU^{-1})$
$[Amp_b]$	Concentration of Amp_b $(AU.ASU^{-1})$
Parameter	**Interpretation (unit)**
r_{sc}	Growth rate of S_c (h^{-1})
r_{sp}	Growth rate of S_p, (h^{-1})
K_{sc}	Optimum concentration of S_c $(CFU.ASU^{-1})$
K_{sp}	Optimum concentration of S_p $(CFU.ASU^{-1})$
d_{sc}	Maximal killing rate of S_c by S_p (h^{-1})
C_1	Concentration of S_p inducing half the maximum killing rate d_{sc} $(CFU.ASU^{-1})$
d_{spb}	Maximal killing rate of S_p by Amp_b, (h^{-1})
C_{ab}	Concentration of Amp_b inducing half the maximum killing rate d_{spb} $(AU.ASU^{-1})$
d_{sph}	Maximal killing rate of S_p by Amp_h, (h^{-1})
C_{ah}	Concentration of Amp_h inducing half the maximum killing rate d_{sph} $(AU.ASU^{-1})$
$[Amp_h]$	Concentration of AMPs produced by the skin cells $(AU.ASU^{-1})$
k_c	Production rate of Amp_b by S_c $(AU.h^{-1}.CFU^{-1})$
d_a	Degradation rate of Amp_b $(AU.h^{-1})$

III.3. Parameter space reduction by steady-state reasoning

The amount of quantitative experimental data available for the model calibration is very limited due to the difficulty of carrying out experiments involving co-cultures of different bacterial species, because of their different food requirements. Most of the published work focuses on single species or on measuring the relative abundances of species living on the skin, which is highly variable between individuals and skin sites (Grice et al. 2009). In the case of AD specifically, *S. aureus* is considered pathogenic and *S. epidermidis* commensal (Geoghegan, Irvine, and Foster 2018; Koh, Ong, and Common 2021). Published data exist however for those species which we can use to constrain the parameter values of the model.

Two series of *in vitro* of experiments are considered (Nakatsuji et al. 2017; Kohda et al. 2021). While *in vitro* cultures, even on epidermal equivalent, do not entirely capture the native growth of bacteria on human skin, since they necessarily abstract from certain interactions within the microbiome and with the skin, they provide useful quantitative data that would be very difficult to measure *in vivo*.

In the first experiment (Kohda et al. 2021), mono-cultures and co-cultures of *S. epidermidis* and *S. aureus* were allowed to develop on a 3D epidermal equivalent. Table III.3.1 recapitulates the population sizes of the two species measured after 48 hours of incubation. Kohda *et al.* also performed another co-culture experiment where *S. epidermidis* was inoculated 4 hours prior to *S. aureus* in the media. This data is not used here as it requires additional manipulation to match the situation represented by the model. However, it would be interesting to use it in the future for model validation.

Table III.3.1: Experimental data from Kohda et. al (Kohda et al. 2021) used for identifying parameter values.

	S. epidermidis **(CFU/well)**	***S. aureus*** **(CFU/well)**
Mono-cultures	$4.10^8 \pm 7.10^7$	$3.10^9 \pm 4.10^8$
Co-cultures	$1.10^8 \pm 3.10^7$	$1.10^9 \pm 8.10^7$

In the second experiment (Nakatsuji et al. 2017) the impact of several concentrations of human (LL-37) and bacterial (*Sh*-lantibiotics) AMPs on *S. aureus* survival was studied. The experiments were performed *in vitro*, in culture medium, and the *S. aureus* population size was measured after 24 hours of incubation. Table III.3.2 summarizes the experimental observations from (Nakatsuji et al. 2017) used here.

Table III.3.2: Experimental data from Nakatsuji et. al (Nakatsuji et al. 2017) used for identifying parameter relations.

***Sh*-lantibiotics (μM)**	**LL-37 (μM)**	***S. aureus* (CFU/mL)**
0	4	10^9
0	8	6.10^5
0.32	0	5.10^8
0.64	0	3.10^3

III.3.1. Parameter values inferred from mono-culture experiment data

We consider first the monocultures experiments from Kohda *et al.* (Kohda et al. 2021), representing the simplest experimental conditions. *S. epidermis* is a representative of the commensal population S_c, and *S. aureus* of the pathogenic one, S_p.

Since the two species are not interacting, the set of equations simplifies to:

$$\begin{cases} \dfrac{d[S_c]}{dt} = \left(r_{sc}\left(1 - \dfrac{[S_c]}{K_{sc}}\right)\right)[S_c] \\ \dfrac{d[S_p]}{dt} = \left(r_{sp}\left(1 - \dfrac{[S_p]}{K_{sp}}\right)\right)[S_p] \end{cases} \quad (2)$$

At steady state, the population concentrations are either zero, or equal to their optimum capacities (K_{sc} or K_{sp}) when the initial population concentration is non-zero. Given the rapid growth of bacterial population, the experimental measurements done after 45 hours of incubation can be considered as corresponding to a steady state, which gives:

$$K_{sc} = 4.10^8\ CFU.ASU^{-1} \quad (3)$$

$$K_{sp} = 3.10^9\ CFU.ASU^{-1} \quad (4)$$

III.3.2. Parameter relations inferred from experimental data on AMP

The experimental conditions of Nakatsuji *et al.* (Nakatsuji et al. 2017) correspond to the special case where there is no commensal bacteria alive in the environment, only the bacterial AMPs, in addition to those produced by the skin cells. Our system of equations then reduces to:

$$\frac{d[S_p]}{dt} = \left(r_{sp}\left(1 - \frac{[S_p]}{K_{sp}}\right) - \frac{d_{spb}[Amp_b]}{C_{ab} + [Amp_b]} - \frac{d_{sph}[Amp_h]}{C_{ah} + [Amp_h]}\right)[S_p] \quad (5)$$

The concentrations in LL-37 and *Sh*-lantibiotics, translated in our model into $[Amp_h]$ and $[Amp_b]$ respectively, are part of the experimental settings. Therefore, we consider them as constants over time. At steady state, we get:

$$[S_p]^* = 0 \quad or \quad [S_p]^* = K_{sp}\left(1 - \frac{d_{spb}[Amp_b]}{r_{sp}(C_{ab} + [Amp_b])} - \frac{d_{sph}[Amp_h]}{r_{sp}(C_{ah} + [Amp_h])}\right) \quad (6)$$

Let us first focus on the special case where no *Sh*-lantibiotics were introduced in the media, translating into $[Amp_b] = 0$ in our model. We consider again that the biological observations after 24 hours of incubation correspond to steady-state and substitute the experimental values measured:

($[Amp_h] = 4\ \mu M$; $[S_p]^* = 10^9$ CFU), and ($[Amp_h] = 8\ \mu M$; $[S_p]^* = 6.10^5$ CFU),

together with the values of K_{sc} and K_{sp} (from (3) and (4)) in (6), to obtain the following equations:

$$\begin{cases} \frac{d_{sph}}{r_{sp}} = \frac{4 + C_{ah}}{6} \\ \frac{d_{sph}}{r_{sp}} = \frac{(10^4 - 2)(C_{ah} + 8)}{8.10^4} \end{cases} \quad (7)$$

which reduce to $C_{ah} = 8$ and $\frac{d_{sph}}{r_{sp}} = 2$.

Following the same method with the experimental conditions without any LL-37 (*i.e.* $[Amp_h] = 0$) and using two data points:

($[Amp_b] = 0.32$; $[S_p]^* = 5.10^8$ CFU) and ($[Amp_b] = 0.64$ µM; $[S_p]^* = 3.10^3$ CFU),

we get $C_{ab} = 0.16$ and $\frac{d_{spb}}{r_{sp}} = \frac{5}{4}$.

It is notable that the maximum killing rates of S_p by Amp_b and Amp_h are both proportional to S_p growth rate. Interestingly, such proportional relation has been observed experimentally between the killing rate of *Escherichia coli* by an antibiotic and the bacterial growth rate (Tuomanen et al. 1986).

To be consistent with the ranges of *Sh*-lantibiotics concentrations described in Nakatsuji *et al.* (Nakatsuji et al. 2017), $[Amp_b]$ should take positive values below 10. Given that $[Amp_b]^* = \frac{k_c[S_c]^*}{d_a}$ at steady-state, and that $K_{sc} = 4.10^8$ CFU is the upper bound for $[S_c]^*$, we obtain the following constraint:

$$\frac{k_c}{d_a} \leq \frac{1}{4.10^7} \quad (8)$$

III.3.3. Parameter relations inferred from co-culture data

The initial model described earlier is representative of the experimental settings of the co-culture conditions described in Kohda *et al.* (Kohda et al. 2021). At steady state, the system (1) gives:

$$[S_c]^* = 0 \quad or \quad [S_c]^* = K_{sc}\left(1 - \frac{d_{sc}[S_p]^*}{r_{sc}(C_1 + [S_p]^*)}\right) \tag{9}$$

$$[S_p]^* = 0 \quad or \quad [S_p]^* = K_{sp}\left(1 - \frac{d_{spb}[Amp_b]}{r_{sp}(C_{ab} + [Amp_b])} - \frac{d_{sph}[Amp_h]}{r_{sp}(C_{ah} + [Amp_h])}\right) \tag{10}$$

$$[Amp_b]^* = \frac{k_c[S_c]^*}{d_a} \tag{11}$$

Considering that what is observed experimentally after 48 hours of incubation is at steady-state, one can replace $[S_c]^*$ and $[S_p]^*$ with the experimental data point (*S. epidermidis* $= 10^8$ CFU; *S.aureus*$= 10^9$ CFU) in (9) and (10) to get the following parameter relation:

$$\frac{d_{sc}}{r_{sc}} = \frac{3}{4.10^9}C_1 + \frac{3}{4} \tag{12}$$

$$\frac{2}{3}r_{sp} = \frac{d_{sph}[Amp_h]}{C_{ah} + [Amp_h]} + \frac{10^8 d_{spb}k_c}{d_a C_{ab} + 10^8 k_c} \tag{13}$$

By integrating the values found for C_{ah} and C_{ab}, and the relations involving d_{sph} and d_{spb} into (13), we end up with:

$$d_a = 10^8 k_c \frac{56 + 31[Amp_h]}{2.56\,(4 - [Amp_h])} \quad with\ [Amp_h] < 4 \tag{14}$$

III.4. Reduced parameter space with 5 parameters

Using the previously mentioned experimental data, and assuming they represent steady state conditions of the initial model (1), we have reduced the parametric dimension of the model from 13 to 5. Specifically, out of the original 13 parameters, we could define the values of 4 of them, and derive 4 functional dependencies from the values of the remaining parameters, as summarized in Table III.4.1.

In our skin microbiome model (1), the parameters that remain unknown are thus:

- r_{sc}, the growth rate of S_c which can reasonably take values between 0 and 2 h^{-1} following (Czock and Keller 2007; Campion, McNamara, and Evans 2005);
- r_{sp}, the growth rate of S_p, taking similar values in the interval between 0 and 2 h^{-1};
- C_1, the concentration of S_p that induces half the maximum killing rate d_{sc} (in AU) and is thus bounded by the optimum concentration of S_p, i.e. $K_{sp} = 3.10^9 AU$;
- k_c, the production rate of $[Amp_b]$ which, as a bacterial production, generally takes values between 0 and 0.1 $AU.h^{-1}.CFU^{-1}$;
- $[Amp_h]$, the concentration in $AU.ASU^{-1}$ of AMPs produced by skin cells between 0 and 4 (equation 14).

The resulting system is the following:

$$\begin{cases} \dfrac{d[S_c]}{dt} = r_{sc}\,[S_c]\left(1 - \dfrac{[S_c]}{4.10^8} - \dfrac{3}{4}\,\dfrac{(10^{-9}C_1 + 1)[S_p]}{C_1 + [S_p]}\right) \\ \dfrac{d[S_p]}{dt} = r_{sp}[S_p]\left(1 - \dfrac{[S_p]}{3.10^9} - \dfrac{5\,[Amp_b]}{0.64 + 4\,[Amp_b]} - \dfrac{2\,[Amp_h]}{8 + [Amp_h]}\right) \\ \dfrac{d[Amp_b]}{dt} = k_c\left([S_c] - 10^8[Amp_b]\dfrac{56 + 31\,[Amp_h]}{2.56\,(4 - [Amp_h])}\right) \end{cases}$$

The following simulations and analyses are performed using the Biocham Software (Calzone, Fages, and Soliman 2006), and the corresponding notebook can be found in annex of this manuscript.

Table III.4.1: Summary of the parameter relations embedded in the reduced model.

Parameter	Value or relation to other parameters
K_{sc}	4.10^8
K_{sp}	3.10^9
C_{ah}	8
C_{ab}	0.16
d_{sph}	$2\,r_{sp}$
d_{spb}	$\frac{5}{4}\,r_{sp}$
d_{sc}	$r_{sc}\left(\frac{3}{4.10^9}\,C_1+\frac{3}{4}\right)$
d_a	$10^8 k_c\,\frac{56+31[Amp_h]}{2.56\,(4-[Amp_h])}\quad with\ \ [Amp_h]<4$

III.4.1. Simulations at the time scale of the experiments

In order to reproduce what was observed by Kohda *et. al* (Kohda et al. 2021) in the co-culture experiment, that is a dominant pathogenic population after 50 hours which can thus be considered as dysbiosis in our skin microbiome model, it is sufficient to fix a relatively low concentration of Amp produced by the skin cells, i.e. $Amph_h = 1.5$, and some fixed values for the four other parameters chosen in their intervals described above. Among a continuum of possible solutions, we chose $r_{sc} = 0.5$, $r_{sp} = 1$, $C_1 = 5.10^6$, $k_c = 0.01$.

The doses of *S. epidermidis* and *S. aureus* applied at the surface of the 3D epidermal equivalent at the beginning of the experiment ($10^5 CFU/mL$ and $10^3 CFU/mL$ respectively) are used as the initial concentrations for $[S_c]$ and $[S_p]$ respectively.

Figure III.4-1 shows the result of a numerical simulation of our model with those parameters which are in accordance with the co-culture experiments of Kohda *et. al* and reproduce a consistent qualitative behavior (Kohda et al. 2021). The evolution of bacterial

populations is shown on a linear scale here, since the model was historically built with normalized linear variables before the introduction of experimental data described in the previous section. Simulations with logarithmic scale are shown in section III.4.3.

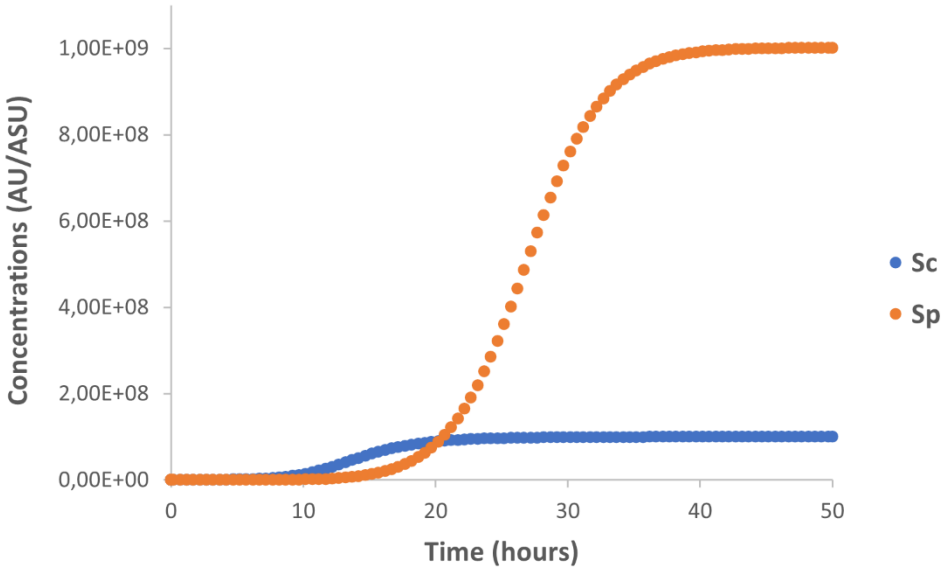

***Figure III.4-1: Numerical simulation of the reduced ODE model over 50 hours**, with initial conditions* $[S_c] = 10^5$, $[S_p] = 10^3$, $[Amp_b] = 0$ *and parameter values* $[Amp_h] = 1.5$, $r_{sc} = 0.5$, $r_{sp} = 1$, $C_1 = 5.10^6$, $k_c = 0.01$ *to fit Kohda et al. co-culture data (53) (Table III.3**.1**).*

Our model can also be used to reproduce what is considered a balanced microbiome, corresponding to the commensal population being significantly more abundant than the pathogenic one (Kong et al. 2012). This requires modifying some parameter values to represent a less virulent pathogenic population, closer to the physiological context, given that the experiments from Kohda *et. al* (Kohda et al. 2021) were performed using a virulent methicillin-resistant *S. aureus* strain.

We chose $r_{sp} = 0.5$, $C_1 = 2.10^8$ and a higher production of AMPs by the skin cells, $[Amp_h] = 3$, to compensate for feedback loops or stimuli that might be missing in the 3D epidermal equivalent used. Figure III.4-2 shows a simulation trace obtained under those conditions which clearly indicates the dominance of the non-pathogenic population under those conditions.

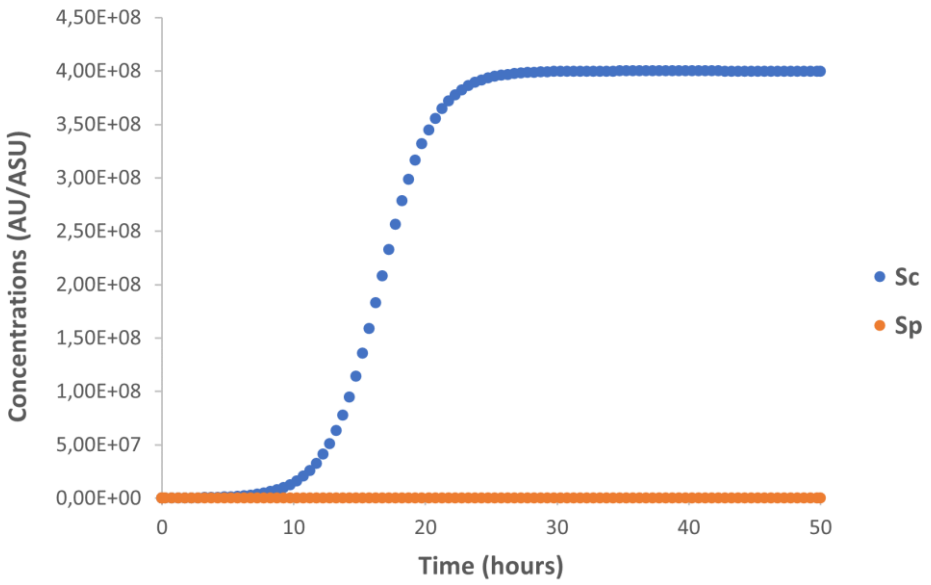

***Figure III.4-2: Numerical simulation of the reduced ODE model over 50 hours**, with initial conditions* $[S_c] = 10^5$, $[S_p] = 10^3$, $[Amp_b] = 0$ *and parameter values* $r_{sc} = r_{sp} = 0.5$, $C_1 = 2.10^8$, $k_c = 0.01$, $[Amp_h] = 3$.

III.4.2. Parameter sensitivity and robustness analyses

Since the previous simulations rely on some choices of values for the unknown parameters, it is important to evaluate the robustness of the predictions of our model by performing an analysis of sensitivity to the parameter values. This is possible in Biocham by specifying the property of interest in quantitative temporal logic (Rizk et al. 2011). The interesting property here is the stabilization at the time scale of the experiments around 48 hours of the bacterial population sizes to the values given by simulation (Figure III.4-2). Here we use the temporal logic formula:

$$F\left(Time == 40 \wedge NSc = x1 \wedge NSp = y1 \wedge F\big(G(NSc = x2 \wedge NSp = y2)\big)\right)$$

and objective values equal to 1 for the free variables $x1, x2, y1, y2$, to express that the normalized variables NSc and NSp, i.e. current values of $[S_c]$ and $[S_p]$ divided by their expected value at steady state, respectively 10^8 and 10^9 in the pathogenic case of Kohda *et al.* experiments, is reached (F, finally) at time around 40 and finally at the end of the time horizon (FG) of 50 hours. On a given simulation trace, the free variables of the formula have a validity domain (here fixed values) which is used to define a continuous degree of satisfaction of the property as a distance to the objective values, and a robustness degree by sampling

with a normal distribution the parameter values around their nominal values (Rizk et al. 2011). The robustness degree is defined as the mean satisfaction degree, with respect to variations of the parameter values.

The sensitivity analysis (Table III.4.2) reveals that the dominance of the commensal population is highly sensitive to variations of the initial concentration of the pathogen. To a lesser extent, the dominant population is also sensitive to the growth rates (r_{sc} and r_{sp}) and the concentration of human AMPs ($[Amp_h]$). On the other hand, C_1 and k_c do not seem to affect the relative proportions of the bacterial populations.

Table III.4.2: Sensitivity of the model to variations of the parameters and initial concentrations *for the property of reaching the same values at time 40 and time horizon 50 as in Figure III.4-2.*

Parameter	Coefficient of variation	Robustness degree
r_{sc}	0.1	0.74
r_{sp}	0.1	0.67
C_1	10	0.95
k_c	0.1	0.95
$[Amp_h]$	0.1	0.62
$[S_p]_0$	10	0.16
$[S_c]_0$	10	0.57
(r_{sc}, r_{sp})	0.1	0.64
$([S_c]_0, [S_p]_0)$	10	0.34

III.4.3. Meta-stability revealed by simulation on a long timescale

Interestingly, by extending the simulation time horizon to a longer time scale of 500 hours, one can observe a meta-stability phenomenon, shown in Figure III.4-3. The seemingly stable state observed in Figure III.4-2 at the relevant time scale of 50 hours of the experiments, is thus not a mathematical steady state, but a meta-stable state, also called quasi-stable state, that slowly evolves, with $\frac{d[S_c]}{dt} \neq 0$ and $\frac{d[S_p]}{dt} \neq 0$, towards a true stable state of the model reached around 300 hours in which the population density are reversed.

The S_c population almost reaches its optimum capacity K_{sc} after approximately 30 hours and stays relatively stable for around 100 hours more, that is over 4 days, which can reasonably be considered stable on the microbiological time scale. Meanwhile, the S_p population is kept at a low concentration compared to S_c, even though it is continuously increasing and eventually leading to its overtake of S_c. This continuous increase of S_p can be seen more clearly with a logarithmic scale (Figure III.4-4). By varying the parameters values, it appears that this meta-stability phenomenon emerges above a threshold value of 2.5 for $[Amp_h]$, that is for almost half of its possible values (see sectionIII.3). More generally, the metastability phenomenon observed here is probably due to the difference in magnitude between parameters ($C_1 = 2.10^8$) and variables ($[S_p] \sim 10^5$ on the short timescale), causing a phenomenon that was neglectable at first to become dominant after a certain period of time.

That phenomenon of meta-stability, also called quasi-stability, is a classical notion of dynamical systems theory, particularly well-studied in the case of oscillatory systems for which analytical solutions exist, and as models of brain activity (Tognoli and Kelso 2014). It is worth noting that it has also been considered in the computational systems biology community with respect to model reduction methods based on the identification of different regimes corresponding to different preponderant terms of the ODEs, for which simplified dynamics can be defined, and chained within a hybrid automaton (Radulescu et al. 2015).

More generally, this raises the question of the existence and importance of meta-stability in real biological processes, as well as the validity of the steady state assumptions made in mathematical modeling methods to fit the models to the observed experimental data.

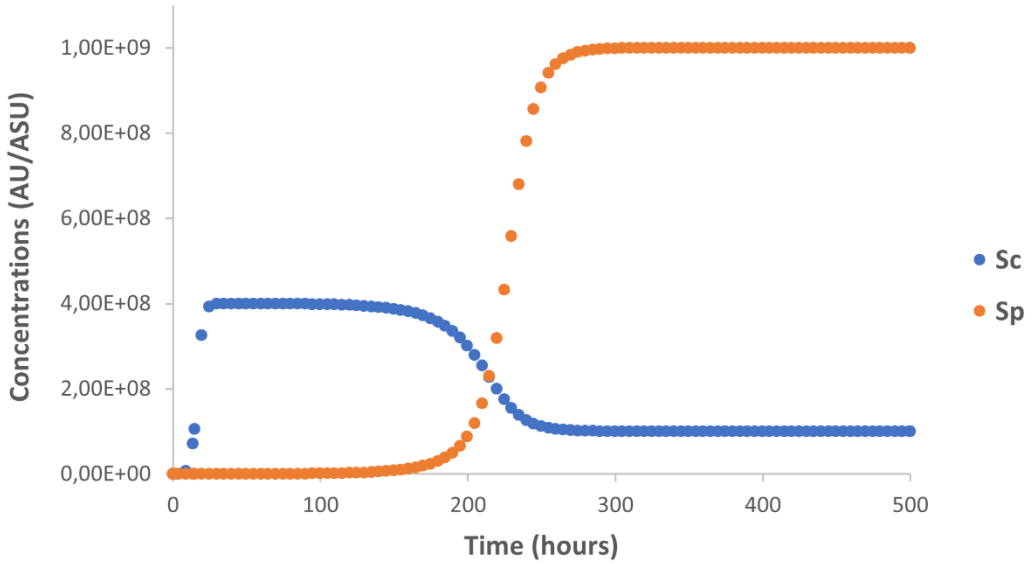

Figure III.4-3: Numerical simulation of the reduced ODE model on a longer time scale of 500 hours, *with the same initial concentrations and parameter values as in Figure III.4-2, showing an inversion of the dominant bacterial population after 220 hours.*

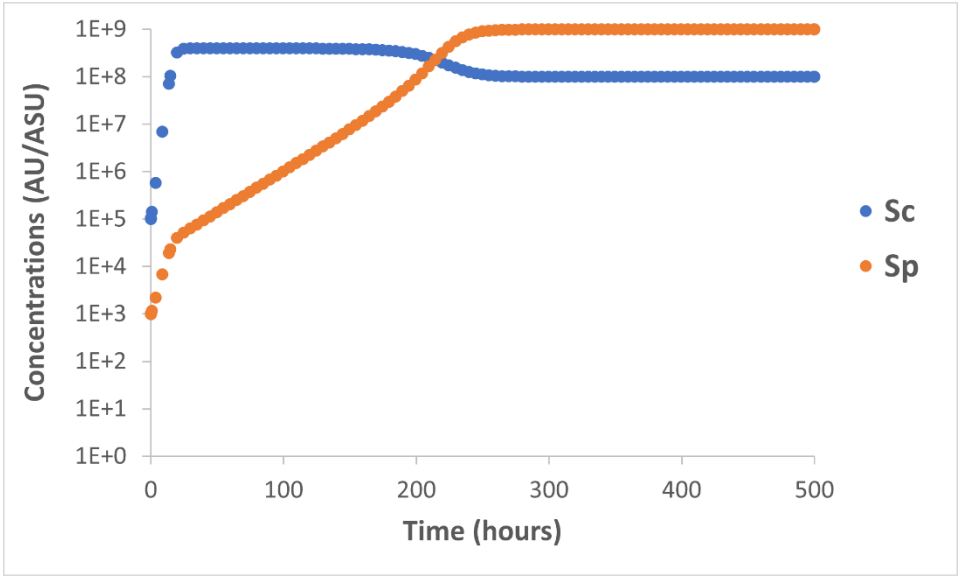

Figure III.4-4: Numerical simulation of the reduced ODE model on a longer time scale of 500 hours with a logarithmic scale, *with the same initial concentrations and parameter values as in Figure III.4-2, showing an inversion of the dominant bacterial population after 220 hours.*

III.5. Results on conditions favoring the pathogenic population

Whether the dysbiosis observed in AD is the cause or the result of the disease is unclear (T. Kobayashi et al. 2015; Koh, Ong, and Common 2021). Infants developing AD do not necessarily have more *S. aureus* present on their skin prior to the onset of the disease compared to the healthy group (Kennedy et al. 2017). This suggests that atopic skin has some characteristics enabling the dominance of *S. aureus* over the other species of the microbiome. To test this hypothesis, we investigate two changes of the skin properties observed in AD patients (skin surface pH elevation (Eberlein-König et al. 2000) and reduced production of AMPs (Ong et al. 2002)) and their impact on the dominant species at steady-state. More specifically, we study the behavior of the system following the introduction of a pathogen and whether the pathogen will colonize the media depending on the initial concentrations of the bacterial populations and the particular skin properties mentioned before.

III.5.1. Skin surface pH elevation

According to Proksch (Proksch 2018), the physiological range for skin surface pH is 4.1-5.8. However, in certain skin conditions, like AD, an elevation of this pH has been observed. Dasgupta *et al.* studied *in vitro* the influence of pH on the growth rates of *S. aureus* and *S. epidermidis* (Dasgupta et al. 2020). Their experimental results show that, when the pH is increased from 5 to 6.5, the growth rate of *S.epidermidis* is multiplied by 1.8, whereas the one of *S.aureus* is multiplied by more than 4 (Table III.5.1).

Their data can be used to select values for the growth rates r_{sc} and r_{sp} in our model, corresponding to healthy skin with a skin surface pH of 5 and compromised skin with a pH of 6.5. Because the experiments from Dasgupta *et al.* were performed *in vitro* and the bacterial population sizes measured with optical density (OD) instead of CFU, the growth rates cannot be directly translated into r_{sc} and r_{sp}. We use $r_{sc} = 0.5$ as the reference value for the commensal growth rate at pH 5, following on from previous simulation (Figure III.4-2). Maintaining the ratio between the two population growth rates at pH 5 and the multiplying

factors following the pH elevation from Dasgupta *et al.* experimental data, we can define two sets of values for r_{sc} and r_{sp}:

skin surface pH of 5 ⇒ $r_{sc} = 0.5, r_{sp} = 0.3$

skin surface pH of 6.5 ⇒ $r_{sc} = 0.9, r_{sp} = 1.3$

Table III.5.1: Experimental data from Dasgupta et. al (Dasgupta et al. 2020) showing the influence of pH on growth rates of S. epidermidis and S. aureus.

pH	Growth rate (ΔOD/hour)	
	S. aureus	***S. epidermidis***
5	0.03	0.05
5.5	0.04	0.07
6	0.09	0.08
6.5	0.13	0.09
7	0.14	0.10

Considering the healthy skin scenario with a skin surface pH of 5, the influence of the bacterial populations' initial concentrations on the dominant species after 50 hours is evaluate using the temporal logic formula:

$$F\left(Time == 40 \wedge \left([S_c] > u1 * [S_p]\right) \wedge F\left(G\left([S_c] > u2 * [S_p]\right)\right)\right)$$

where $u1$ and $u2$ are free variables representing the abundance factors between both populations, evaluated at $Time = 40$ and at the last time point of the trace respectively (F stands for finally and G for globally at all future time points), i.e., at the time horizon of the experiments of 50 hours.

When given with an objective value, *e.g.* $u1 = 10$, the distance between that value and the validity domain of the formula, i.e. the set of values for $u1$ that satisfy the formula, provides a violation degree which is used to evaluate the satisfaction degree of the property.

Here, we evaluate how much the temporal formula:

$$F\left(Time == 40 \wedge \left([S_c] > u1 * [S_p]\right) \wedge F\left(G\left([S_c] > u2 * [S_p]\right)\right)\right), u1 \to 10,\ u2 \to 10,$$

is satisfied given variations of the initial concentrations of two populations. The model predicts that, under the healthy skin condition, the commensal population will always dominate after 50 hours, except when introduced at a relatively low concentration ($< 2.10^4$) while the initial concentration of the pathogenic population is high ($> 5.10^5$) (Figure III.5-1).

The model predicts a higher vulnerability of the skin regarding invading pathogens with an elevated skin surface pH. When evaluating the same temporal formula with growth rates values corresponding to a skin surface pH of 6.5, we observe that even when the initial concentration of commensal is high ($> 10^7$), the pathogenic population is able to colonize the skin when introduced at a concentration as low as 3.10^4 (Figure III.5-2). Such predictions highlight the protective effect of the skin surface acidic pH against the invasion of pathogenic bacteria.

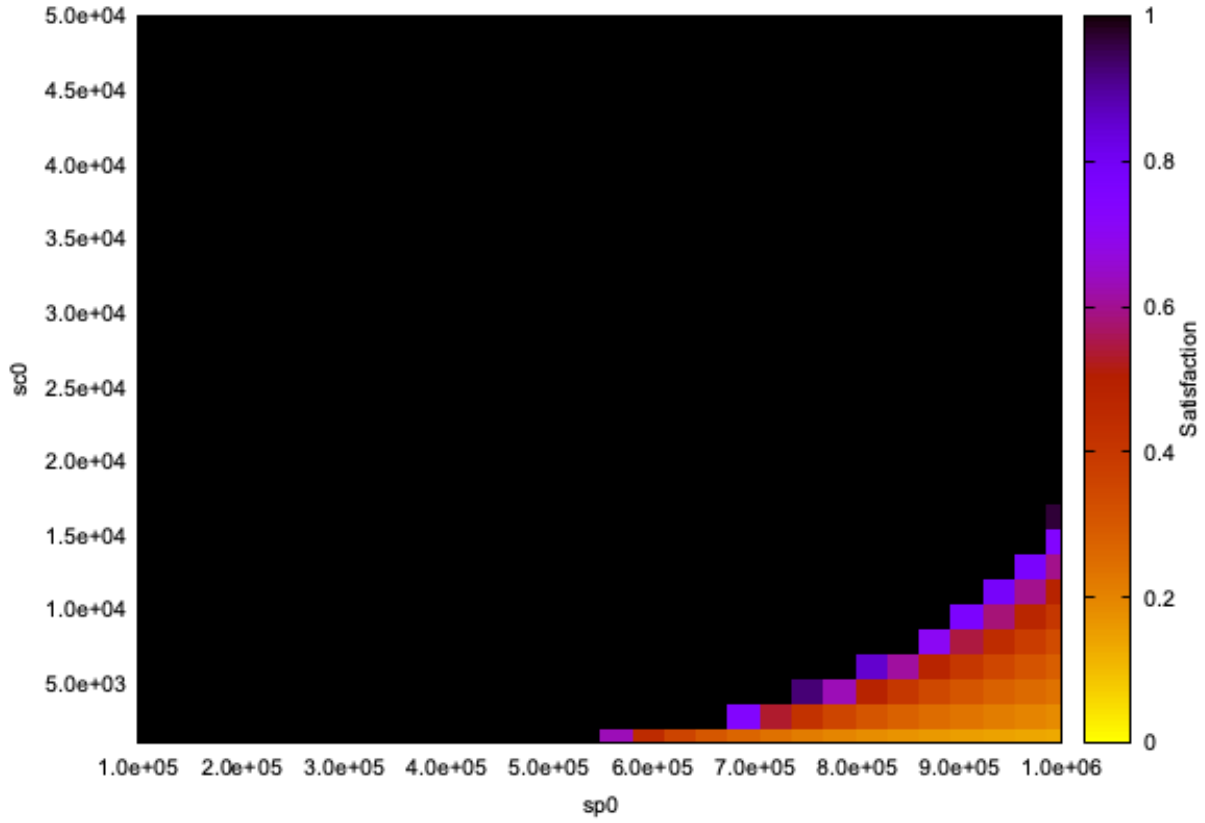

Figure III.5-1: Landscape of satisfaction degree of the temporal formula corresponding to healthy skin with a skin surface pH of 5 ($r_{sc} = 0.5$ and $r_{sp} = 0.3$). *The x and y axis represent variations of the initial quantities of $[S_p]$ and $[S_c]$ respectively. The color coding corresponds to the satisfaction degree of the temporal logic formula. Values used for the other parameters: $C_1 = 2.10^8$, $k_c = 0.01$, $[Amp_h] = 3$.*

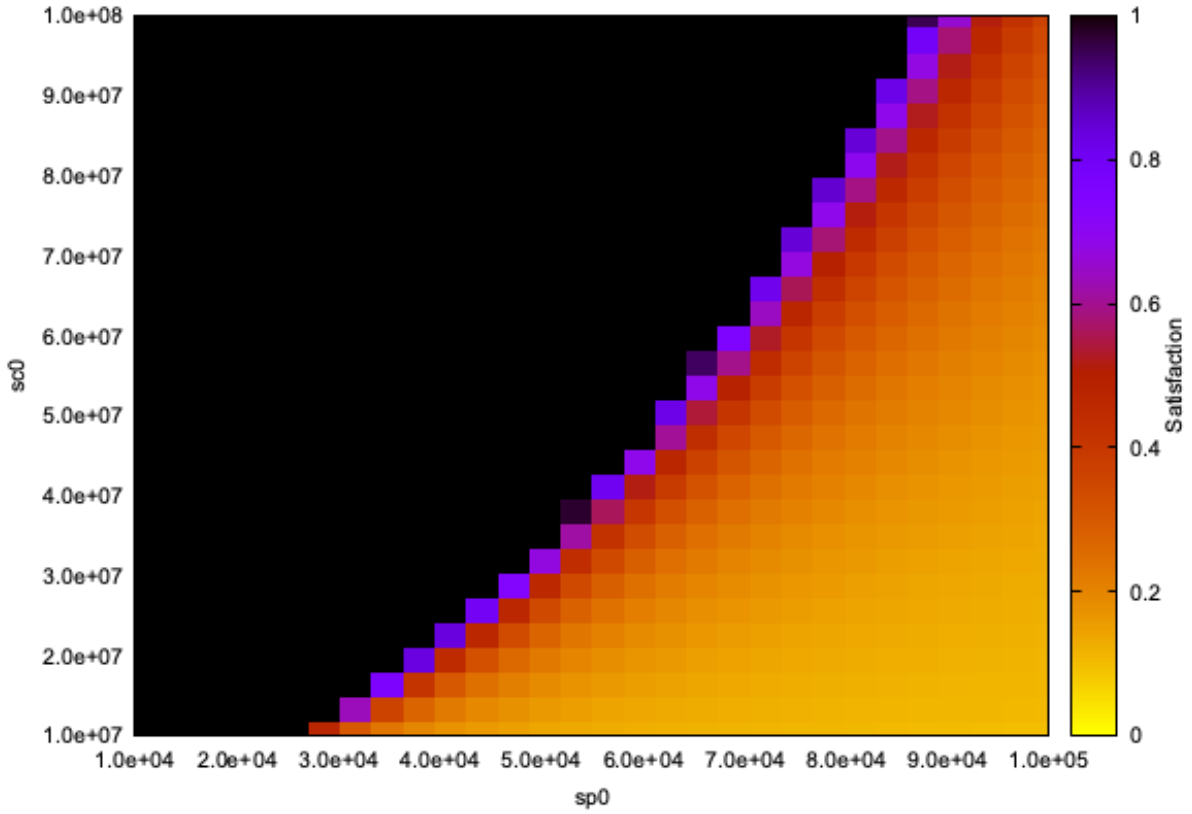

Figure III.5-2: Landscape of satisfaction degree of the temporal formula corresponding to compromised skin with a skin surface pH of 6.5 ($r_{sc} = 0.9$ and $r_{sp} = 1.3$). *The x and y axis represent variations of the initial quantities of $[S_p]$ and $[S_c]$ respectively. The color coding corresponds to the satisfaction degree of the temporal logic formula. Values used for the other parameters: $C_1 = 2.10^8$, $k_c = 0.01$, $[Amp_h] = 3$.*

III.5.2. Reduced production of skin AMPs

As mentioned before, human keratinocytes constitutively produce AMPs as a defense against pathogens. In atopic dermatitis, the expression of AMPs is dysregulated, leading to lower concentration levels of AMPs in the epidermis (Nakatsuji et al. 2017). Similarly, to the analysis done for skin surface pH, our model can be used to study how skin microbiome reacts to modulation of the AMPs production by the skin cells.

Two situations are considered: an impaired production of AMPs by the skin cells ($[Amp_h] = 0.5$) and a higher concentration with $[Amp_h] = 3$. Using the same methodology as in the case of skin surface pH, the temporal logic formula $F\left(Time == 40 \wedge\right.$

$\left([S_c] > u1 * [S_p]) \wedge F\left(G([S_c] > u2 * [S_p])\right)\right)$, $u1 \to 10,\ u2 \to 10,$ is evaluated for variations of the initial concentrations of both populations for $[Amp_h] = 0.5$ and $[Amp_h] = 3$ (Figure III.5-3).

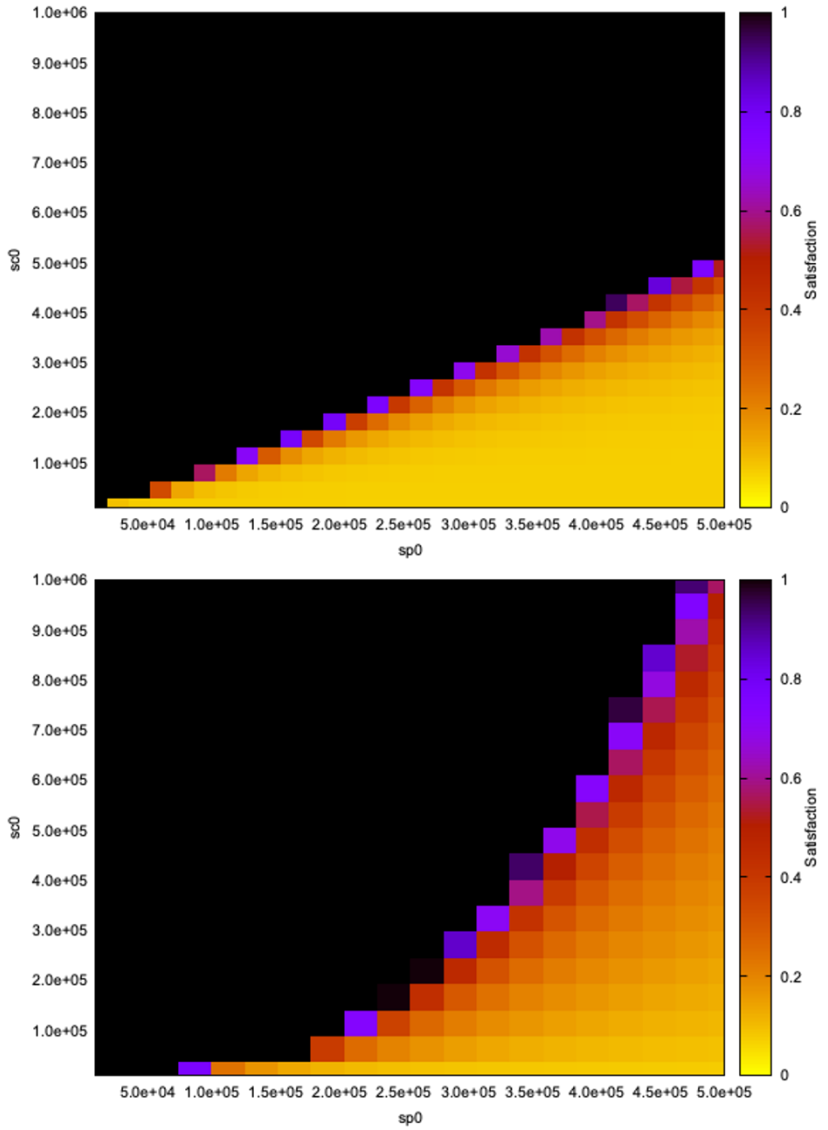

Figure III.5-3: Landscape of satisfaction degree of the healthy condition formula with a low concentration of human AMPs on the upper graph ($[Amp_h] = 0.5$) and a high concentration at the bottom ($[Amp_h] = 3$). *The x and y axis represent variations of the initial quantities of $[S_p]$ and $[S_c]$ respectively. The color coding corresponds to the satisfaction degree of the temporal logic formula. Values used for the other parameters: $r_{sc} = r_{sp} = 0.5$, $C_1 = 2.10^8$, $k_c = 0.01$.*

The model predicts a slightly protective effect of Amp_h regarding the colonization of the skin by a pathogenic population, for low initial concentrations. However, when both populations are introduced in high concentrations, the increase of $[Amp_h]$ appears to have the opposite effect of facilitating the colonization by the pathogenic population. This mitigated effect might be due to the presence of $[Amp_h]$ in the constraint related to the degradation rate of $[Amp_b]$ (equation 14) and deserves further investigation.

III.6. Discussion

Based on the few available experimental data, a method based on steady-state assumption was introduced to identify parameter values and define parameters as functions of others. This process already enabled a significant reduction of the parametric dimension of the model. To further calibrate the model, and improve its analysis, this approach could be combined with other methods for parameter inference. Optimization algorithms or parameter value search with temporal logic could be apply on the sub models representative of the experimental conditions. The use of several methods could help to exploit the entirety of the experimental data, such as the delayed introduction of *S. aureus* in the media presented by Kohda *et al.*(Kohda et al. 2021), and the dose-response curves of *S. aureus* survival exposed simultaneously to LL-37 and l-antibiotics (Nakatsuji et al. 2017). Moreover, the observation of metastability and timescale consideration might be indicators to find alternative methods to overcome the steady-state assumption, even though this assumption is biologically relevant when studying bacterial populations.

Because of the difficulty to obtain quantitative *in vivo* data related to the microbiome and even more to the AMPs, the parameter inference was achieved using *in vitro* experiments data. These data were assumed to be representative of the bacterial populations' behavior on the human skin. The influence of this assumption could be assessed by a robustness analysis of the model behavior following variations of the 8 parameters inferred using *in vitro* data. Even though it is reasonable to think that the qualitative behavior of the system will be preserved, further investigations focusing on the main differences between *in vitro* and *in vivo* could be recommended.

The unexpected, and not necessarily desired, metastability phenomenon observed under certain parametric conditions, brings food for thoughts on two different aspects. First, reconciliate the steady-state assumptions made during the parameter inference step with the resulting system's behavior on the timescale of this experiment. This could be done by defining additional constraints on the growth rates, to impose the stability of both bacterial population under 50 hours of simulation. This could be challenging to solve mathematically but could be achieved empirically, using temporal logic with a long time-horizon. On the other hand, from a modelling point of view, it is worth investigating what is causing the appearance of this metastability phenomenon.

Chapter IV - Connecting and integrating the modules in the Agent-Based Model

IV.1. Introduction

The structure of the epidermis is the result of a dynamic homeostasis, from proliferation at the basal layer to desquamation at the surface. This dynamic nature is likely to affect the bacteria community living on the skin surface. The cutaneous microbiome is indeed in close interaction with the skin cells, known to influence its population composition. For instance, different cutaneous microbiome compositions have been associated with distinct skin sites (oily, moist, dry, etc.) (Byrd, Belkaid, and Segre 2018).

Commensal bacteria are not only taking advantage of the resources provided by the skin. Some commensal species such as *Staphylococcus hominis*, contribute to the defense against invading pathogens by producing AMPs, acting in synergy with the AMPs produced by keratinocytes (Nakatsuji et al. 2017). The progress made in the omics fields enables the study of the microbiome in more details, even though the cutaneous microbiome remains less understood than that of the gut. In an effort to better understand the factors influencing the microbiome balance, it seems important to study the impact of the continuous removal and renewal of the surface cells on which the bacteria are growing.

The interactions between skin commensal and pathogens have already been studied with computational models. Nakaoka *et al.* introduced a model combining ODE and delayed differential equations to look at the competition dynamic between 2 populations of bacteria exposed to cytokines (Nakaoka et al. 2016). Miyano *et al.* designed a QSP model including the interactions between *S. aureus* and coagulase negative *Staphylococcus* to evaluate AD treatment strategies targeting specifically *S. aureus* (Miyano, Irvine, and Tanaka 2022). Although these models provided interesting insights and predictions regarding the

microbiome balance, they did not consider the potential impact of surface cell renewal on bacterial growth.

Agent-based models appear as a relevant tool to investigate this aspect due to their capacity to recapitulate the dynamic homeostasis of the epidermis. In this chapter, we integrate the ODE model introduced in Chapter III into the agent-based model of the epidermis described in Chapter II. This hybrid model is used to study how the corneocytes desquamation and renewal impact microbiome kinetics.

IV.2. From ODE to agent-based

The agent-based model and ODE formalisms are compatible and can be combined. However, working at the agent- level, as opposed to the averaged population level, brings up several specificities that need to be considered carefully during the integration process. This section focuses on these aspects and how they were solved in this model.

IV.2.1. Location

The focus of this model is the bacteria population living on the surface of the skin. The microbiome present in hair follicles is not considered, as the agent-based model used here represents only the inter-follicular region of the epidermis. Moreover, the bacteria penetrating the skin barrier during an infection are also neglected as a first approach. Therefore, the microbiome model introduced in Chapter III is implemented only for the surface cells of the agent-based model.

IV.2.2. Discretization of time and space

Given the size difference between corneocytes and bacteria, it is reasonable to consider that the bacteria only interact with other bacteria located on the same surface cell. The movement from one cell to another will be discussed below (section IV.2.4). Consequently, the microbiome model described in Chapter III is implemented at the agent level, for the surface cells.

The agent-based model developed in EPISIM is synchronous, meaning that the time is discretized in simulation steps at which the agents evolve, based on their behavior rules. Therefore, the microbiome ODE system, defined in section III.2, needs to be adapted to this specific consideration of time.

Unlike the KLK-LEKTI system describing reactions happening in a matter of seconds, the timescale of the microbiome model is coherent with the agent-based one. The phenomenon involved are studied over hours or days. It is possible to transform the ODE system from section III.2 into a recurrence relation:

$$\begin{cases} Sc_n &= Sc_{n-1} + \frac{1}{2}\, Sc_{n-1}\left(r_{sc}\left(1 - \frac{Sc_{n-1}}{K_{sc}}\right) - \frac{d_{sc}\, Sp_{n-1}}{C_1 + Sp_{n-1}}\right) \\ Sp_n &= Sp_{n-1} + \frac{1}{2}\, Sp_{n-1}\left(r_{sp}\left(1 - \frac{Sp_{n-1}}{K_{sp}}\right) - \frac{d_{spb}\, AMPb_{n-1}}{C_{ab} + AMPb_{n-1}} - \frac{d_{sph}\, AMPh}{C_{ah} + AMPh}\right) \\ AMPb_n &= AMPb_{n-1} + \frac{1}{2}\,(k_c Sc_{n-1} - d_a AMPb_n) \end{cases}$$

(15)

where X_{n-1} and X_n represent the concentrations of the variable X on one agent at the previous and current step respectively. To match the time unit of the original ODE model (hour) to the agent-based time unit (one simulation step = 30min), a $\frac{1}{2}$ factor is added to the recurrence relation. The degradation of $AMPb$ at step n depends on its concentration at the same step, to avoid approximation errors and negative values. The $AMPb$ recurrence equation can be simplified to:

$$AMPb_n = \frac{2\, AMPb_{n-1} + k_c Sc_{n-1}}{2 \;+\; da}$$

(16)

The following recurrence system can then be implemented on each surface cell of the model:

$$\begin{cases} Sc_n &= Sc_{n-1} + \frac{1}{2} Sc_{n-1}\left(r_{sc}\left(1 - \frac{Sc_{n-1}}{K_{sc}}\right) - \frac{d_{sc}\, Sp_{n-1}}{C_1 + Sp_{n-1}}\right) \\ Sp_n &= Sp_{n-1} + \frac{1}{2} Sp_{n-1}\left(r_{sp}\left(1 - \frac{Sp_{n-1}}{K_{sp}}\right) - \frac{d_{spb}\, AMPb_{n-1}}{C_{ab} + AMPb_{n-1}} - \frac{d_{sph}\, AMPh}{C_{ah} + AMPh}\right) \\ AMPb_n &= \frac{2\, AMPb_{n-1} + k_c Sc_{n-1}}{2 + da} \end{cases}$$

(17)

The system's behavior observed with the original ODE model is preserved with the recurrence relation (Figure IV.2-1).

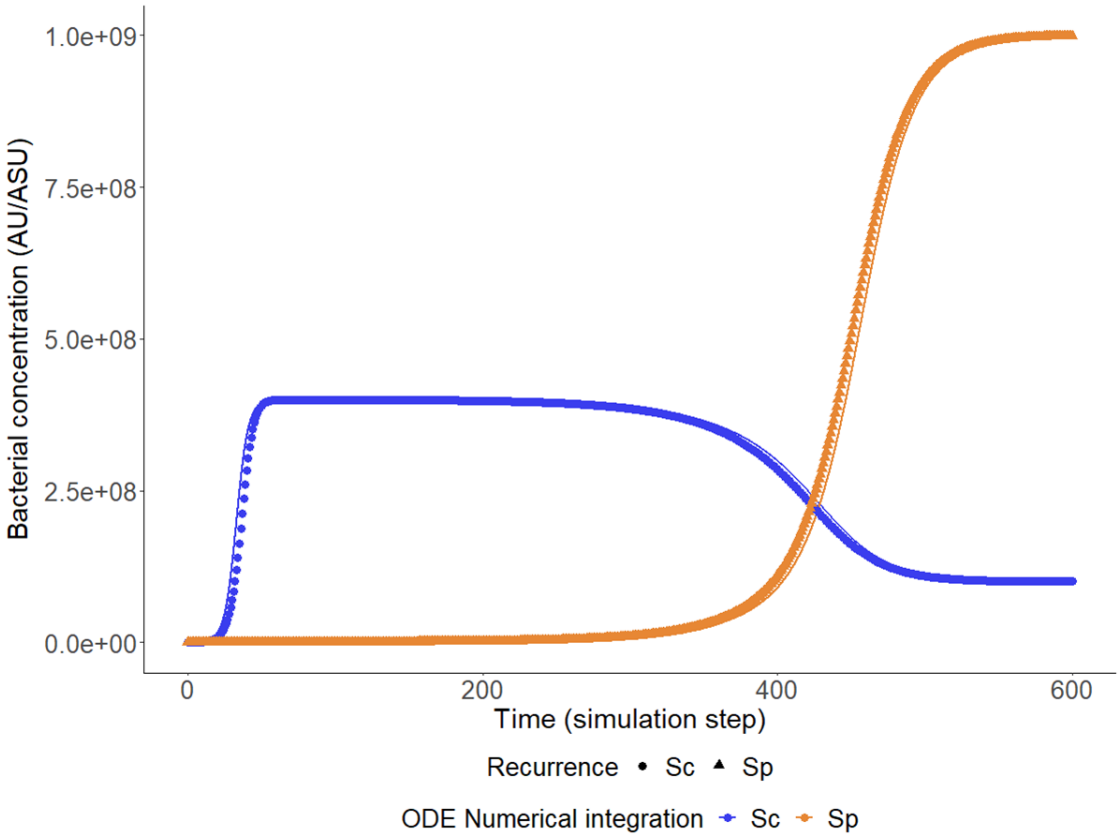

Figure IV.2-1: Comparison of the microbiome kinetics with the recurrence relation and the ODE numerical integration. *The concentrations relations of Sc and Sp are shown in blue and orange respectively, with lines for the result of the ODE numerical integration with the lsoda function in R, and with dots or triangle for the recurrence relation. The time unit is ½ hour, corresponding to one simulation step in the agent-based model. Parameter values used:* $r_{sc} = r_{sp} = 0.5$; $k_c = 0.01$; $C_1 = 2.10^8$; $[AMPh] = 3$; $[S_c](t=0) = 10^5$; $[S_p](t=0) = 10^3$; $[AMP_b](t=0) = 0$

IV.2.3. Model initialization

At the beginning of an EPISIM simulation, only the stem cells of the *stratum basale* are present. The epidermis is gradually built from them and the dynamic homeostasis structure is reached after approximatively 5000 simulations steps. For this thesis, we focus on the perturbations of this homeostatic epidermis in the context of AD. Therefore, the bacteria model is only activated at epidermal homeostasis, with a user-controlled Boolean function.

The bacteria populations S_c and S_p are initialized to user-defined values $[Sc]_{init}$ and $[Sp]_{init}$ respectively, usually the initial concentrations used in the ODE model introduced in the previous chapter. It means that every cell reaching the surface is immediately colonized by Sc_{init} and Sp_{init} concentrations of the commensal population S_c and the opportunistic pathogen S_p respectively. Similarly to the ODE model simulations, the bacterial AMPs are initialized to 0. These initial values can be changed during a simulation if needed. With this approach, the user has control over the model initialization and can compare the simulation results with the analysis of the original ODE system. However, this approach assumes an arbitrary colonization of new surface cells, independently of their surroundings.

IV.2.4. Bacteria mobility and $\boldsymbol{AMP_b}$ diffusion

As discussed in section IV.2.2, the bacteria are considered to interact only with the population located on the same surface cell in the model. However, biologically, the skin surface constitutes an open environment on which bacteria can move freely. In the model, it is translated by a proportion *popMouv* of each bacteria population moving to the neighboring surface cells, independently of the bacteria concentrations on the receiving cells. It is implemented using EPISIM *Send()* function, described by Sütterlin *et al.* (Sütterlin et al. 2009). This function equally distributes the amount of the variable (here the bacterial population) among the neighboring agents, checking that the variable amount does not go below or above the defined minimum or maximum value of the variable, for the sending and receiving agent respectively. In the event that the amount to be exchanged exceeds the variable limits, the amount effectively exchanged corresponds to the maximum variable amount respecting the constraints from both the sending and receiving agents.

The exchange of AMP_b between neighboring cells is implemented as a molecular diffusion, similarly to what is described in section II.2.2 for inflammatory molecules. At each step, AMP_b diffuses to neighboring surface cells based on the concentration gradient and a diffusion coefficient *amp_diff*. This process is also implemented with the *Send()* function from (Sütterlin et al. 2009).

IV.2.5. Microbiome module overview

Figure IV.2-2 shows a screenshot of the microbiome module implementation in EPISIM Modeller (Sütterlin et al. 2013; 2009). It recapitulates the modelling choices described above, regarding the location of the reactions, time discretization, exchange with neighbors, and model initialization. This module is integrated in the global cellular workflow including the previously existing modules such as cell differentiation, desquamation, substance permeation, water flow from (Sütterlin et al. 2017; Stamatas et al. 2021), as well as the other modules developed during this thesis: inflammation and KLK-LEKTI interactions.

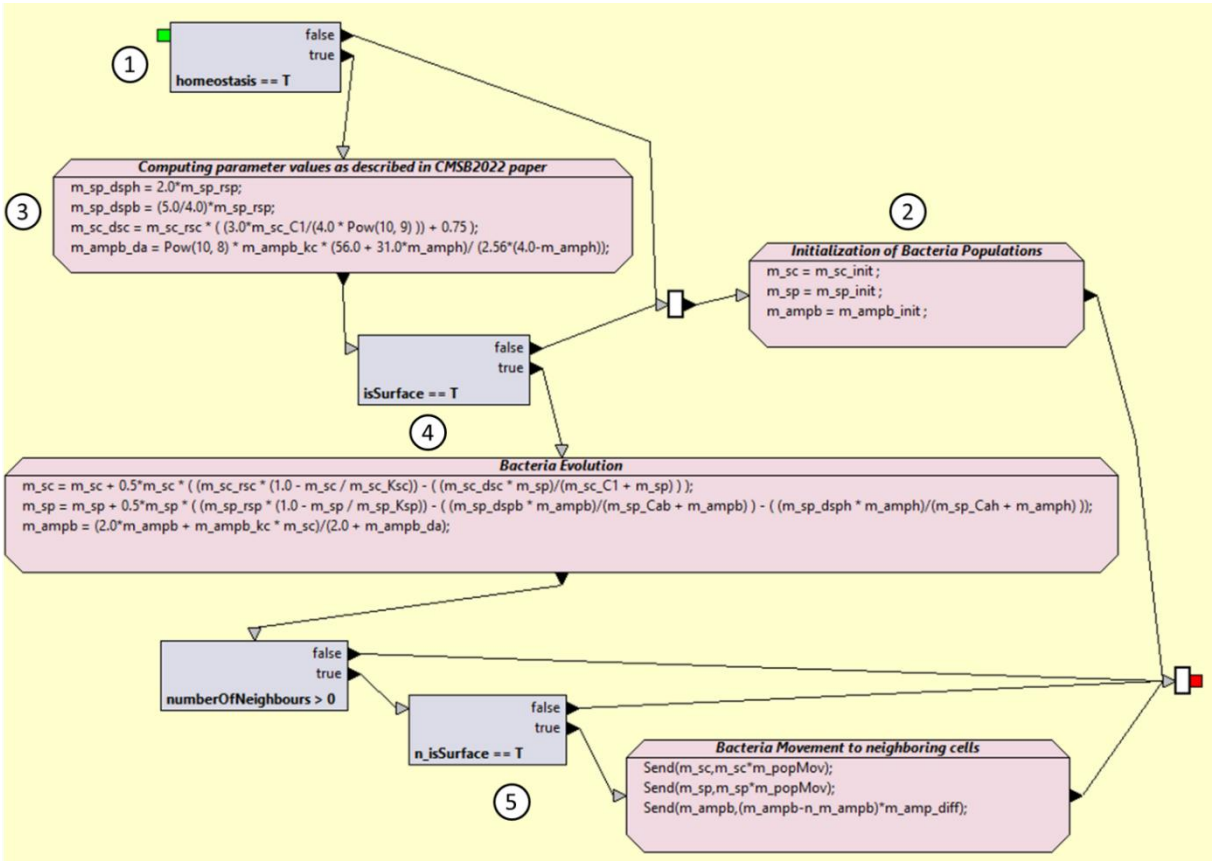

Figure IV.2-2: Screenshot of the microbiome module implementation in EPISIM Modeller *(Sütterlin et al. 2013; 2009) 1) When the user considers the epidermis to be stable, that is to say when the thickness of the different layers are stable (usually after 5000 simulation steps), they turn the homeostasis Boolean function to True (T), triggering the activation of bacterial interactions 2) When the epidermis has not reached homeostasis yet, or when the agent is not at the surface* $[S_c]$, $[S_p]$ *and* $[AMP_b]$ *are initialized to fixed user-defined values. 3) The values for certain parameters are computed according to the relations defined in section III.4 4) If the agent is at the surface, the bacterial populations interact and the new concentrations are computed following the recurrence relations defined in section IV.2.2. 5) If the agent has surface neighbors, a proportion popMouv of each bacterial population moves to these neighboring surface cells. The agent also exchanges* $[AMP_b]$ *according to the concentration gradient and a diffusion coefficient with its surface neighbors.*

IV.3. Simulations of the microbiome kinetics in the agent-based model

The ODE population model introduced in Chapter III is adapted to be integrated in the agent-based model of the epidermis described in Chapter II. This gives the opportunity to study the impact of the epidermis dynamic nature on the microbiome kinetics and balance. All simulations are done on a fully built and stable epidermis after 5000 simulations steps. The *homeostasis* Boolean switch is set to True at step 5000.

IV.3.1. Comparison with the ODE model

First, the agent-based model is simulated with the microbiome-related parameter values corresponding to Figure III.4-2 with the original ODE model. To better isolate the effect of surface cells desquamation on the microbiome kinetics, *popMouv* and *ampb_diff* are temporarily set to 0.

Two main differences can be observed when comparing the microbiome kinetics in the agent-based model (Figure IV.3-1 A and Figure IV.3-2 A) to the original ODE model (Figure IV.3-1 B and Figure IV.3-2 B). The most obvious is the disappearance of the quasi-stability phenomenon observed with the ODE model. The reversed stable state reached around 300 hours (equivalent to 600 simulations steps) seems to be completely absent in the agent-based model, even when simulated over 2000 steps. The other difference that can be noted concerns the concentration level reached by S_c and AMP_b. On the quasi-stable state of the ODE model, $[S_c]$ and $[AMP_b]$ stabilize around 4.10^8 and 0.07 AU respectively. However, in the agent-based model, the average $[S_c]$ and $[AMP_b]$ over all surface cells oscillate around significantly lower values.

A possible explanation for the latter is that what is observed is an average between cells that have just reached the surface, and cells that have been at the surface for several time steps. This results in a discrepancy of the bacterial population kinetics among the surface cells. The other possible contributing factor, which can also explain the disappearance of the quasi-stability phenomenon, is that the desquamation process limits bacterial growth in time.

Indeed, when a surface cell is desquamated, its bacterial population is removed from the simulation together with the cell.

The desquamation process in this model is taken from the multi-agent model from (Sütterlin et al. 2017), except for the addition of KLK* impact on cell-to-cell adhesion decay (see II.2.1). The decision for a cell to be desquamated is controlled by a stochastic process based on the progressive loss of adhesion its neighbors. Given that in the model the adhesion loss process is deterministic and constant, the stochasticity of how long a cell remains at the surface results from the time it takes for the cell to reach the surface. This period depends on the stochastic cellular movement. Therefore, a corneocyte moving slowly to the surface, will have lost a significant proportion of its adhesion to its neighbors when reaching the surface, and will be desquamated quickly.

To confirm this hypothesis, the microbiome kinetics of single surface cells was observed with the model, using the same parameter values as for Figure IV.3-1 and Figure IV.3-2. During the simulation, the microbiome kinetics of a randomly selected single surface cell are observed (Figure IV.3-3). When this cell is desquamated, the model randomly selects another surface cell for the observation and so on. For the moment, there is no straight forward way of selecting a cell that has just reached the surface, therefore the kinetics are often caught partway through. Nevertheless, it is still helpful to dissect the average behavior of Figure IV.3-1 and Figure IV.3-2 on the single-cell scale.

Figure IV.3-3 clearly highlights the impact of desquamation on microbiome kinetics. The commensal population barely has time to reach its quasi-stable state before desquamation. Likewise, the cells do not stay at the surface long enough for the opportunistic pathogens to outgrow the commensals. This confirms the explanation for the disappearance of the quasi-stability and the long-term steady-state observed with the original ODE model.

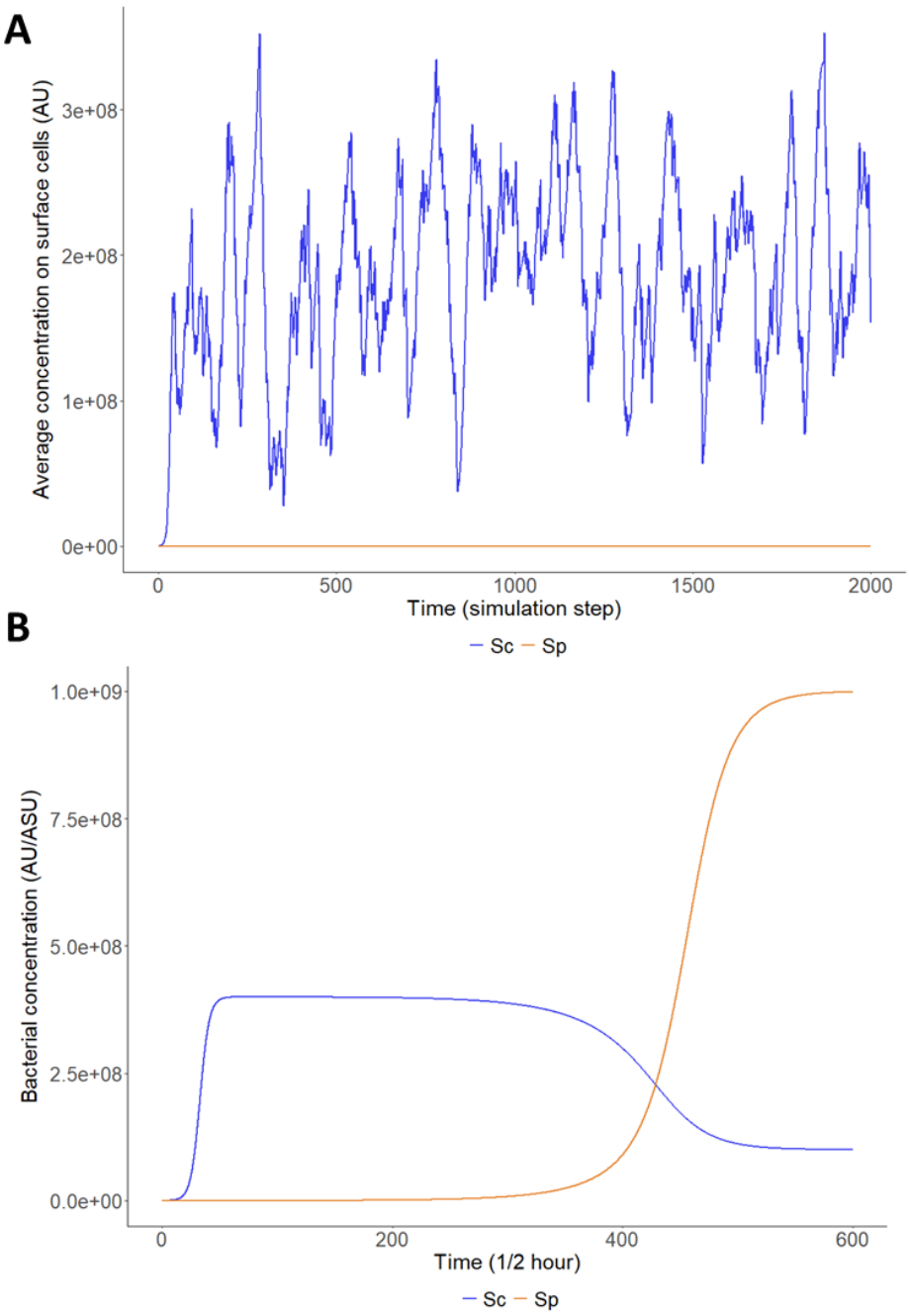

Figure IV.3-1: Comparison of the average bacterial populations kinetics at the skin surface in the agent-based model (A) with the ODE model's behavior (B). *The concentration of the commensal population S_c, and the opportunistic pathogen one S_p are shown in blue and orange respectively. The time unit is ½ hour, corresponding to 1 simulation step. The corresponding kinetics of $[AMP_b]$ are shown in Figure IV.3-2. Parameter values used for both the agent-based and the ODE model : $r_{sc} = r_{sp} = 0.5$; $k_c = 0.01$; $C_1 = 2.10^8$; $[AMPh] = 3$; $[Sc]_{init} = 10^5$; $[Sp]_{init} = 10^3$; $[AMPb]_{init} = 0$. Parameter values specific to the agent-based model: popMouv = 0 ; amp_diff = 0*

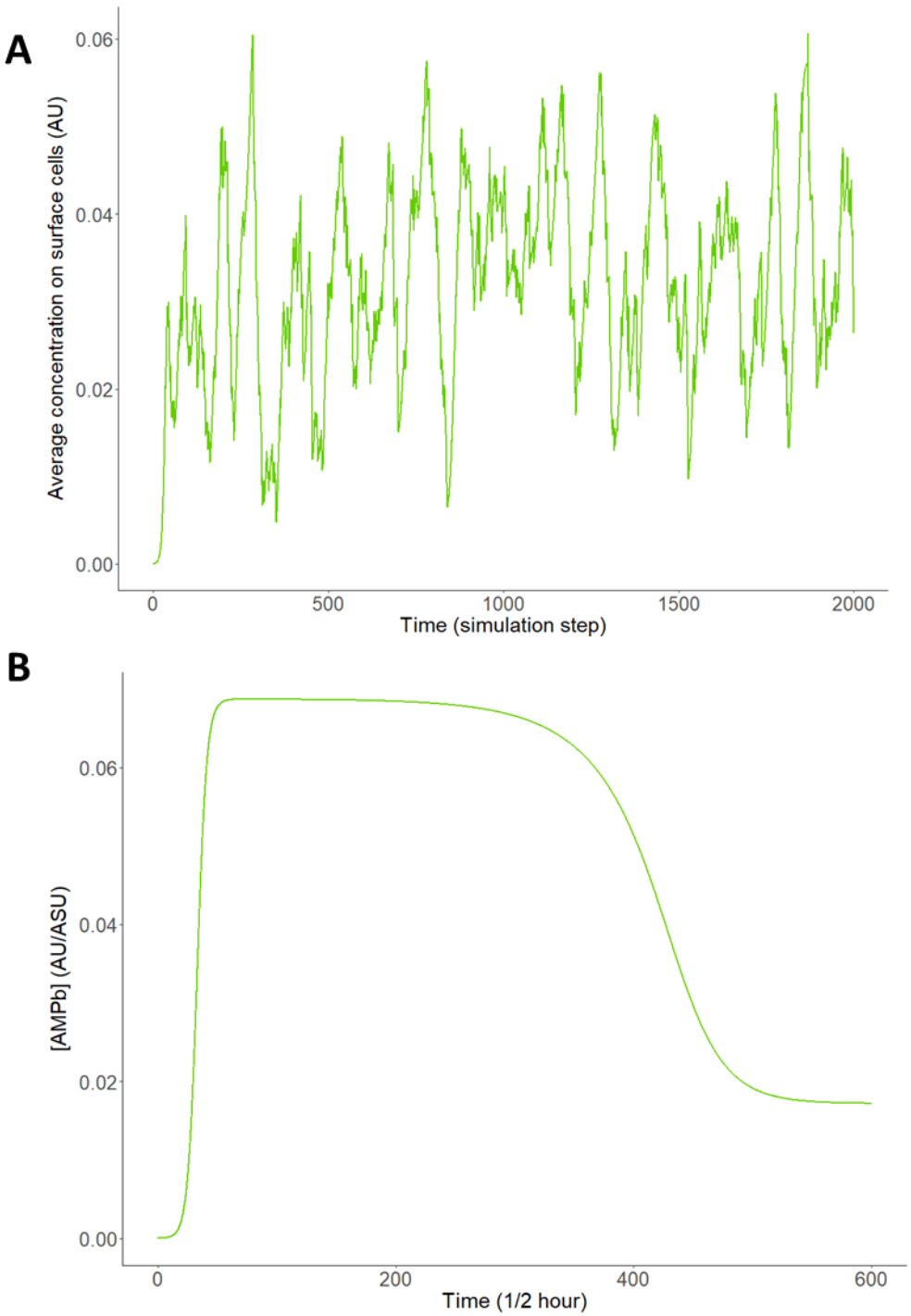

Figure IV.3-2: Comparison of the average AMPb kinetics at the skin surface in the agent-based model (A) with the ODE model's behavior (B). *The time unit is ½ hour, corresponding to 1 simulation step. The corresponding bacterial population kinetics are shown in Figure IV.3-1. Parameter values used for both the agent-based and the ODE model :* $r_{sc} = r_{sp} = 0.5$ *;* $k_c = 0.01;\ C_1 = 2.10^8\ ;\ [AMPh] = 3;\ [Sc]_{init} = 10^5;\ [Sp]_{init} = 10^3;\ [AMPb]_{init} = 0.$ *Parameter values specific to the agent-based model: popMouv = 0 ; amp_diff = 0*

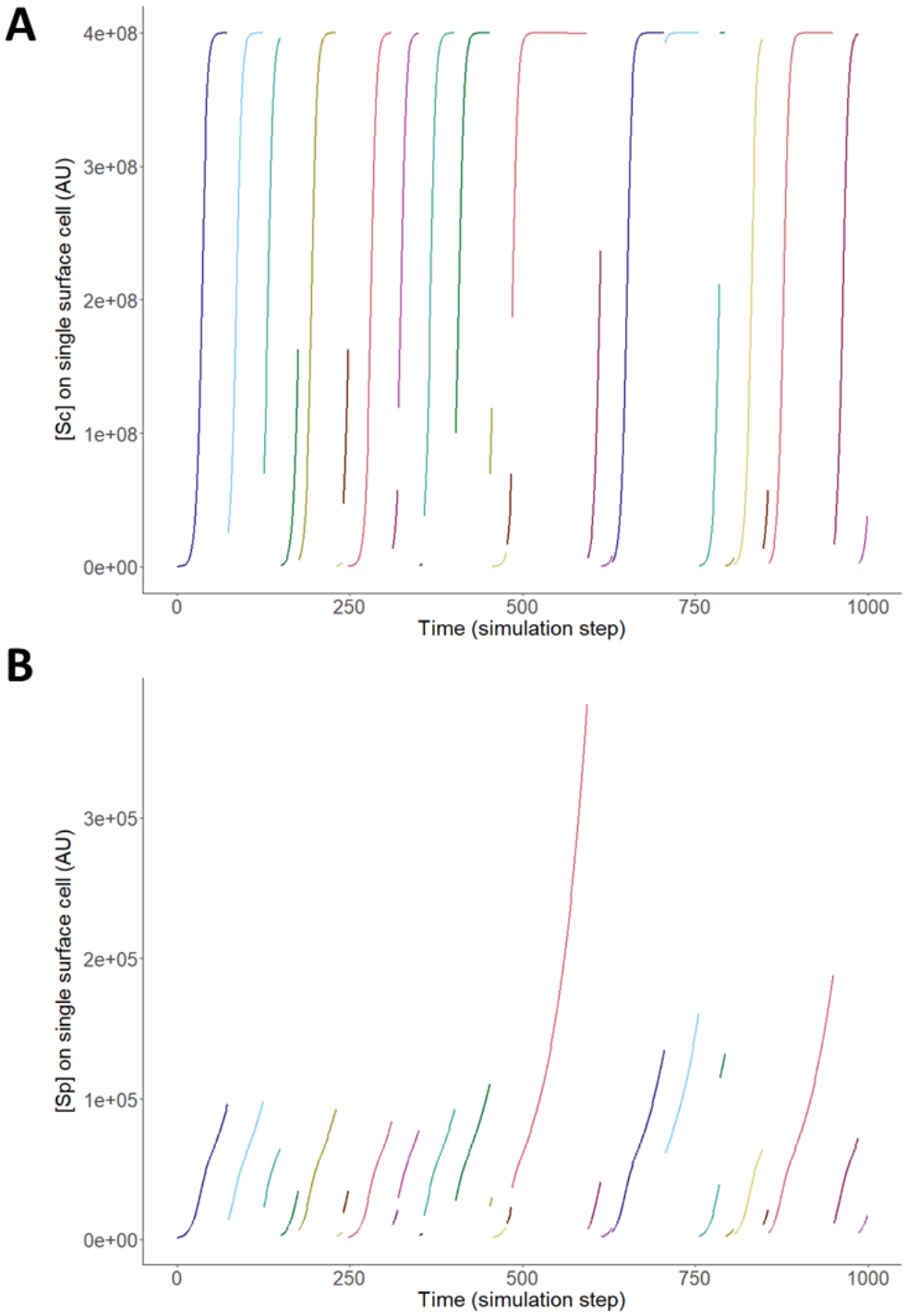

Figure IV.3-3 : Microbiome kinetics on individual surface cells. *The evolution of the commensal population* $[S_c]$ *and the opportunistic pathogen* $[S_p]$ *on single surface cells of the agent-based model are displayed on A) and B) respectively. Each color corresponds to the trajectory observed on one randomly selected surface cell. The time unit is a simulation step, representing 30 minutes. Parameter values used :* $r_{sc} = r_{sp} = 0.5$ *;* $k_c = 0.01$*;* $C_1 = 2.10^8$ *;* $[AMPh] = 3$*;* $[Sc]_{init} = 10^5$*;* $[Sp]_{init} = 10^3$*;* $[AMPb]_{init} = 0$*; popMouv = 0 ; amp_diff = 0.*

IV.3.2. Impact of bacterial mobility on microbiome balance

Now that the impact of desquamation on microbiome kinetics has been established, we shift the focus on the influence of bacterial mobility on microbiome balance. Simulations of the agent-based model with the same parameter values as Figure IV.3-1 and Figure IV.3-2, with different values of *popMouv* are shown on Figure IV.3-4 and Figure IV.3-5. With 1% of each bacterial population moving to neighboring surface cells each step (Figure IV.3-4), the metastable switch still does not appear. However, it can be noticed that the variance of oscillation is reduced compared to Figure IV.3-1 A. This suggests that, thanks to the higher rates of bacterial movement, newly arisen surface cells reach the short time-scale quasi-stable state faster. The average commensal population over all surface cells is therefore more stable and less driven down due to low values, coming from the newly arisen surface cells.

Interestingly, increasing *popMouv* to 0.1 leads to the reemergence of the longer time-scale steady-state observed with the original ODE model (Figure IV.3-5). It takes approximately 1600 simulations steps (corresponding to 800 hours) for the pathogenic population to outgrow the commensal, globally. It appears that this level of bacterial mobility enables a proportion of the pathogenic population to survive longer than the cells average residence time at the surface. Then, once the pathogenic population becomes dominant, the newly arisen surface cells receive a significant amount of $[S_p]$ through bacterial mobility, which ensures a maintained pathogen dominance.

In contrast, high *popMouv* values seem to be detrimental to the opportunistic pathogen population (Figure IV.3-6). The bacterial mobility was gradually increased during one simulation. S_p becomes the most abundant population after around 1700 simulations steps. However, as the *popMouv* values increase, the average $[S_p]$ over the skin surface undergoes a stepwise decrease, in accordance with the *popMouv* value. This suggests that high bacterial mobility slows down the overall population growth. It can also be noticed that the commensal population does not seem to be affected as much as the pathogenic one by a higher *popMouv* value.

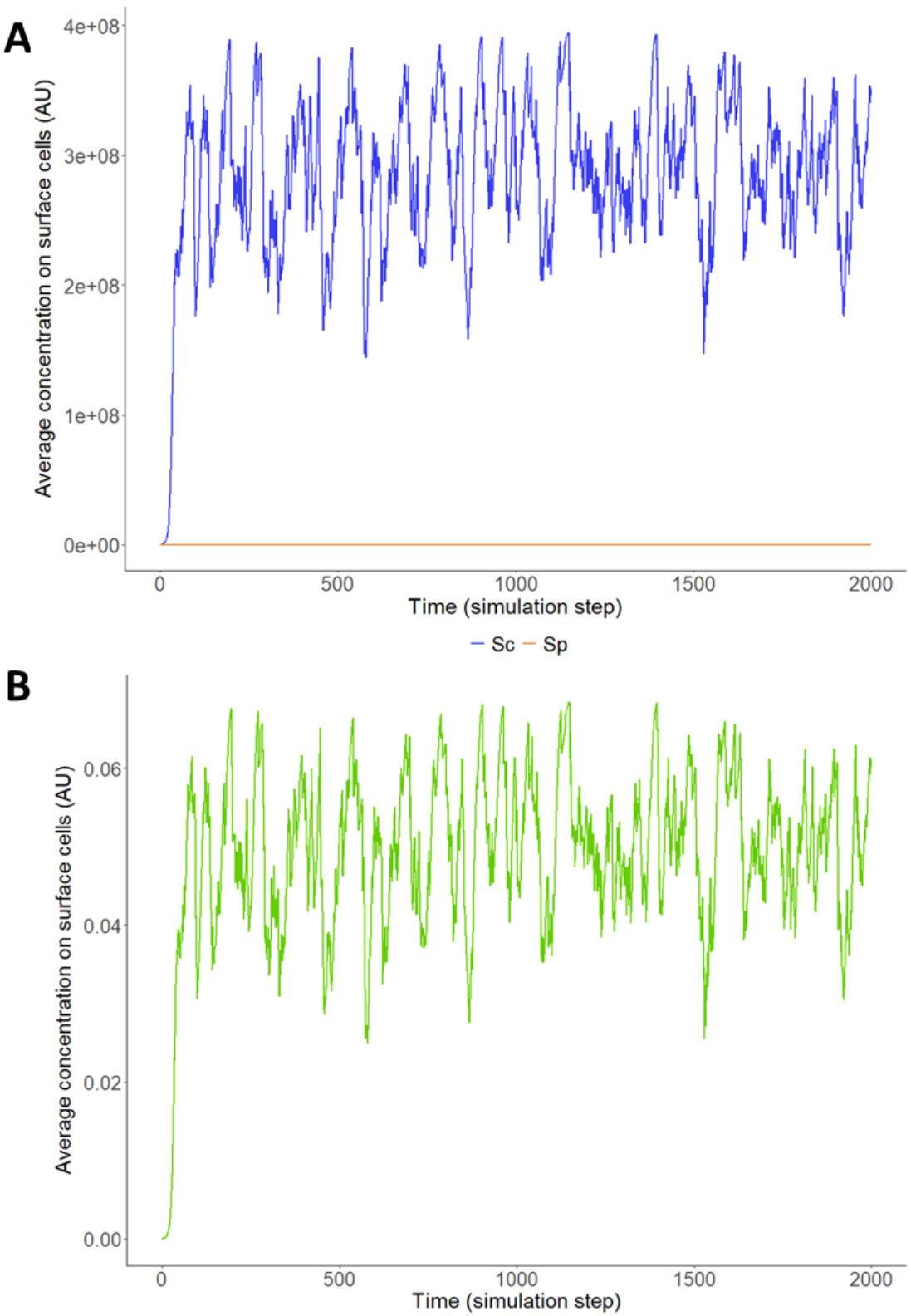

Figure IV.3-4: Simulations of the average surface bacterial population kinetics (A) and $[AMP_b]$ ***evolution (B) of the agent-based model popMouv = 0.01.*** *The time unit is one simulation step, corresponding to 30 minutes. Other parameter values used:* $r_{sc} = r_{sp} = 0.5$ *;* $k_c = 0.01$*;* $C_1 = 2.10^8$ *;* $[AMPh] = 3$*;* $[Sc]_{init} = 10^5$*;* $[Sp]_{init} = 10^3$*;* $[AMPb]_{init} = 0$*; amp_diff = 0.*

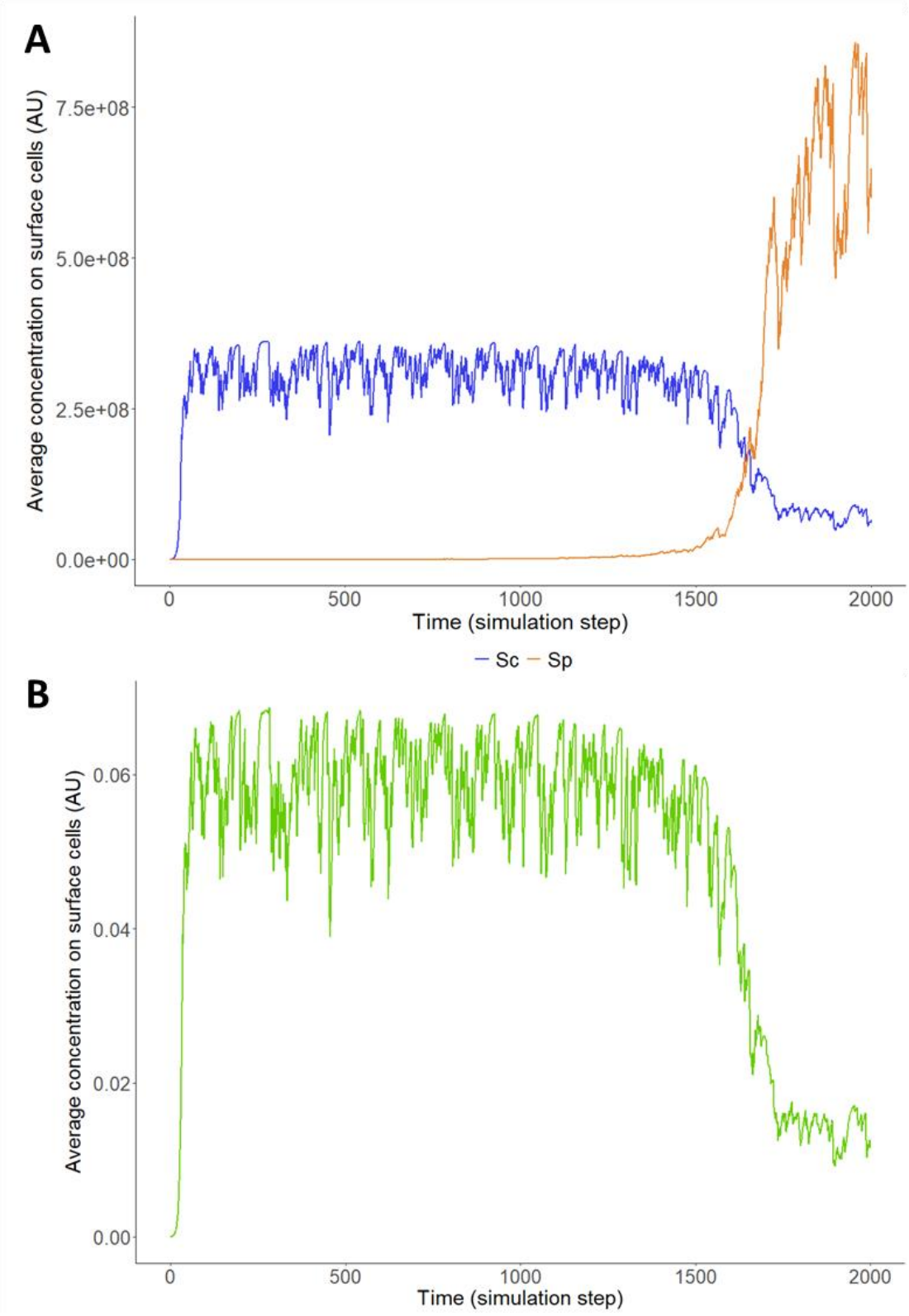

Figure IV.3-5: Simulations of the average surface bacterial population kinetics (A) and $[AMP_b]$ ***evolution (B) of the agent-based model with popMouv = 0.1.*** *The time unit is one simulation step, corresponding to 30 minutes. Other parameter values used:* $r_{sc} = r_{sp} = 0.5$ *;* $k_c = 0.01$*;* $C_1 = 2.10^8$ *;* $[AMPh] = 3$*;* $[Sc]_{init} = 10^5$*;* $[Sp]_{init} = 10^3$*;* $[AMPb]_{init} = 0$*; amp_diff = 0.*

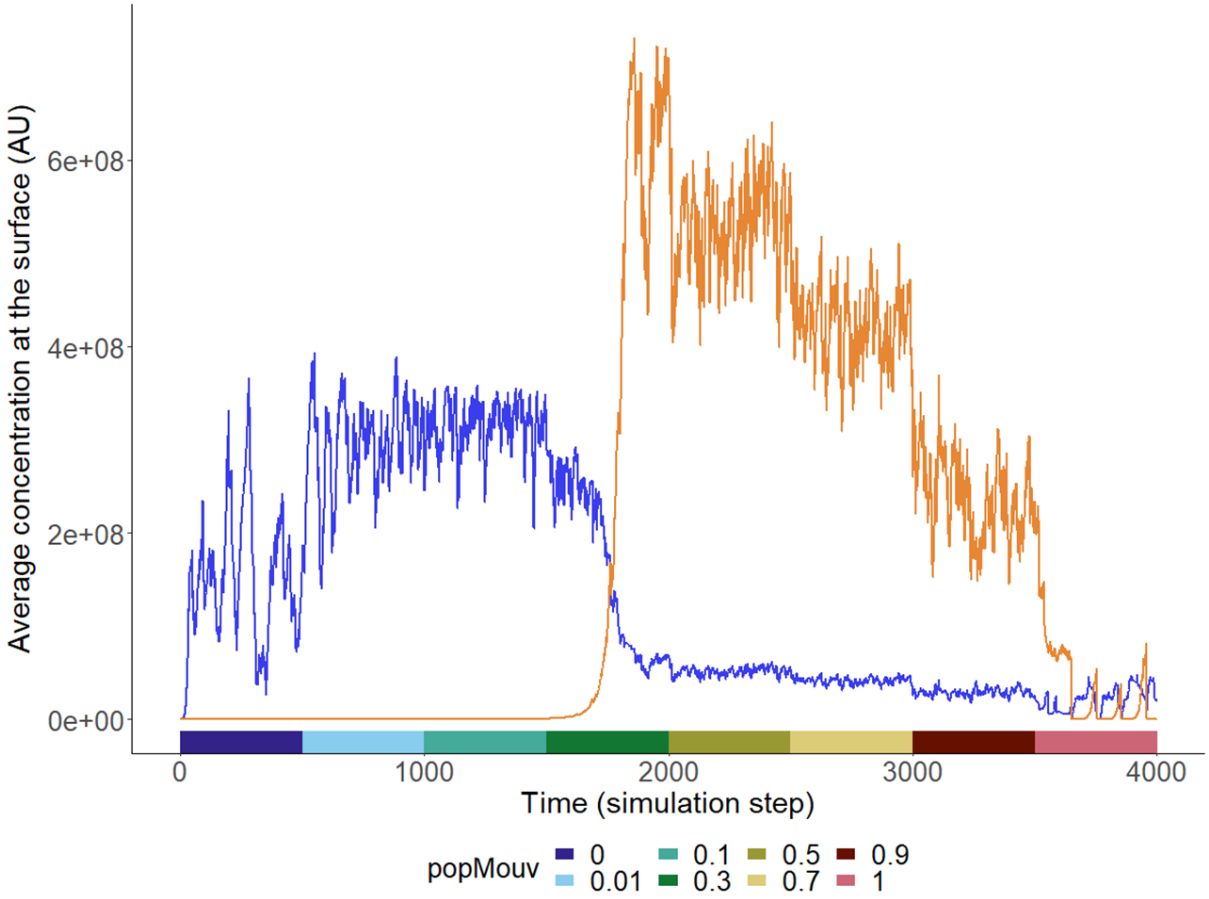

Figure IV.3-6: Variation of the bacterial mobility during one simulation. *The average concentrations of S_c and S_p are shown in blue and orange respectively. The value of popMouv used at a particular time point in the simulation is indicated with colors on the y-axis. The time unit is one simulation step, corresponding to 30 minutes. Other parameter values used:* $r_{sc} = r_{sp} = 0.5 \quad ; \quad k_c = 0.01; \quad C_1 = 2.10^8 \quad ; \quad [AMPh] = 3; \quad [Sc]_{init} = 10^5; \quad [Sp]_{init} = 10^3; \quad [AMPb]_{init} = 0;$ *amp_diff = 0.*

IV.3.3. Impact of $\boldsymbol{AMP_b}$ diffusion

So far, in order to analyze the effect of bacterial mobility separately, the diffusion coefficient of AMP_b was set to 0. The focus will now shift to how *amp_diff* values impact the microbiome balance. The value of *popMouv* is thus temporarily set to 0.

Similarly to what was done for *popMouv*, the value of *amp_diff* was progressively increased during one simulation (Figure IV.3-7). Looking at the resulting microbiome kinetics, it appears that the value of *amp_diff* has no influence on the microbiome balance, under these conditions.

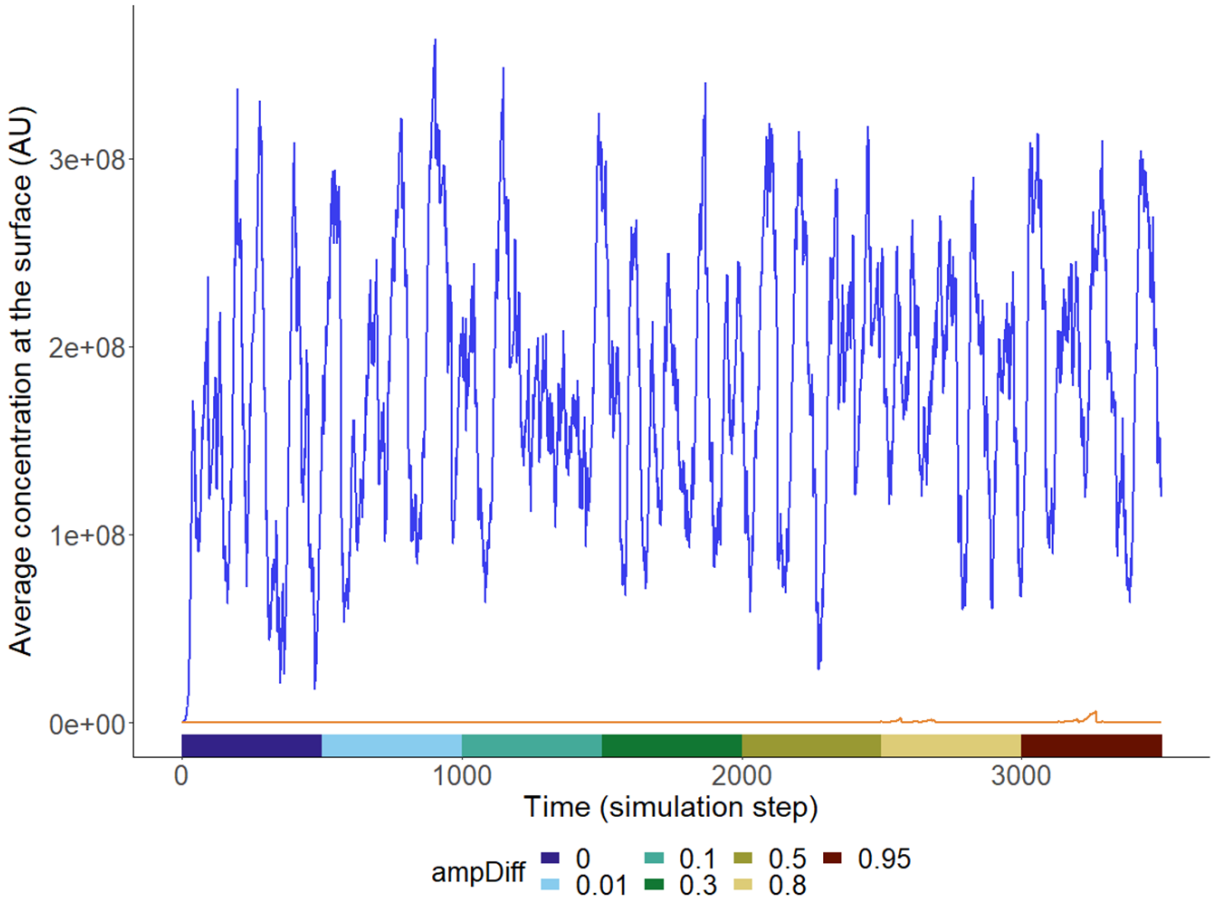

Figure IV.3-7: Variation of the AMPb diffusion during one simulation. *The average concentrations of S_c and S_p are shown in blue and orange respectively. The value of amp_diff used at a particular time point in the simulation is indicated with colors on the y-axis. The time unit is one simulation step, corresponding to 30 minutes. Other parameter values used:* $r_{sc} = r_{sp} = 0.5 \quad ; \quad k_c = 0.01; \quad C_1 = 2.10^8 \quad ; \quad [AMPh] = 3; \quad [Sc]_{init} = 10^5; \quad [Sp]_{init} = 10^3; \quad [AMPb]_{init} = 0;$ *popMouv = 0.*

IV.3.4. Behavior of the system with bacterial mobility and $\boldsymbol{AMP_b}$ diffusion

Following the analysis done in the previous sections, the values of popMouv and amp_diff are both fixed to 0.1. The simulation results for the average surface values are shown on Figure IV.3-8, and the single-cell kinetics on Figure IV.3-9. The dynamics of the microbial population on a single corneocyte can help us understand the emergence of the pathologic population on the long term. For the first 1000 steps approximately, the commensal population is dominant and quickly grows from its initial concentration (10^5) to a relatively stable state below 4.10^8 AU. After a thousand steps, cell 1 (and probably others that are not shown) represented in pink in Figure IV.3-9 A-B stays at the surface long enough for the pathogenic population to emerge. A transition phase can be seen between 1000 and 1500 steps after the simulation start. During this phase, there are cells on which the commensal population is still dominant (cell 2) and cells where the pathogenic population is emerging (cell 3). Thanks to the bacterial mobility, the pathogenic population colonizes neighboring as well as newly arriving surface cells, maintaining its dominance on the long-time horizon.

The model was also tested with parameter values that did not result in quasi-stability with the original ODE model (Figure IV.3-10 and Figure IV.3-11). The model behavior observed with the ODE model is overall reproduced in the agent-based model. Notably, the average surface $[S_p]$ reaches higher level in the agent-based model. This is due to bacterial mobility, which increases the microbial concentration on single-cells beyond the steady-state value observed with the ODE model (Figure IV.3-12).

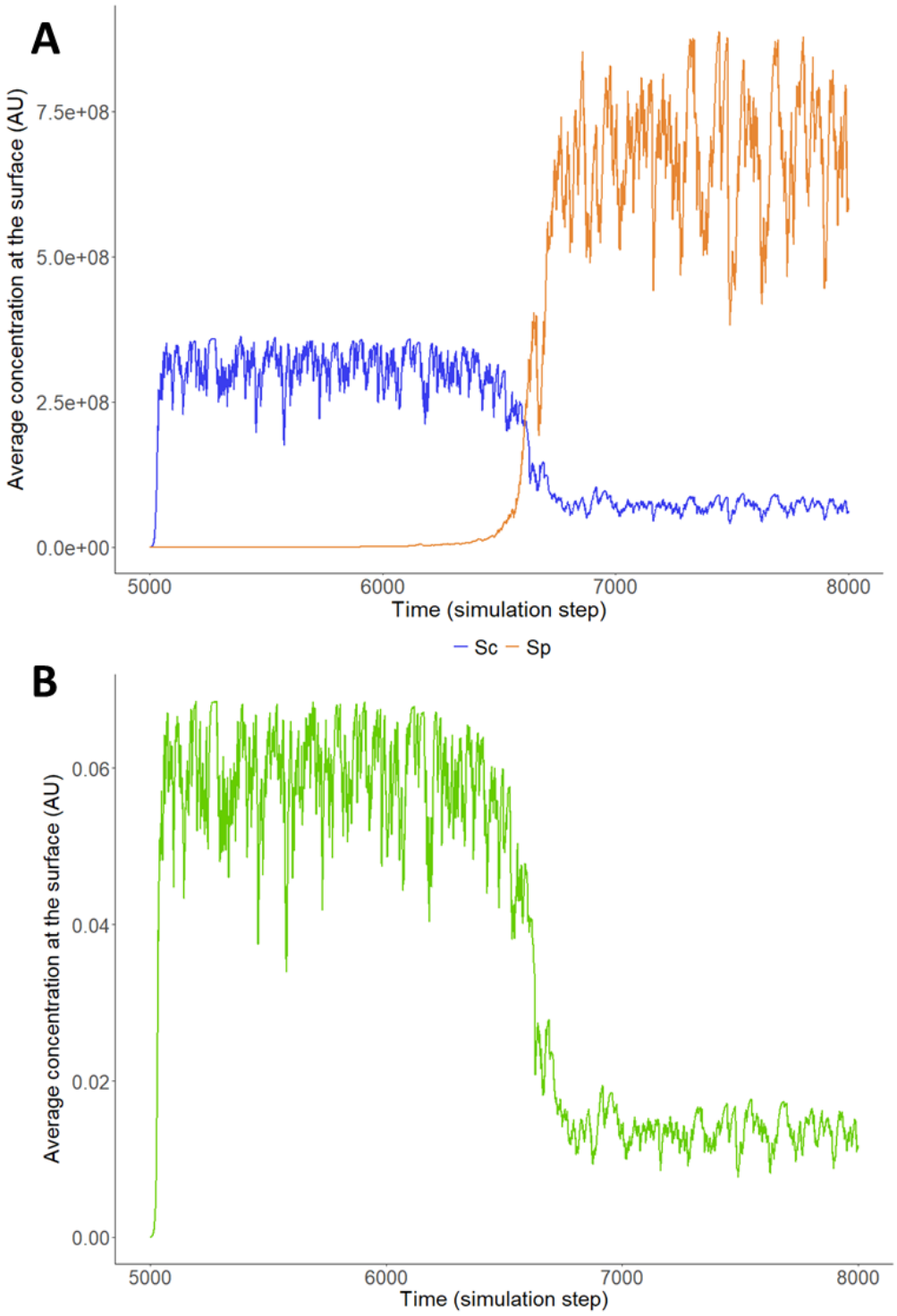

Figure IV.3-8: Simulation of the system including bacterial mobility and $[AMP_b]$ diffusion. *Evolution of the average concentrations of bacterial populations (A) and $[AMP_b]$ (B) at the surface with popMouv =0.1 and amp_diff=0.1. The time unit is a simulation step, representing 30 minutes. The associated single-cell trajectories are shown in Figure IV.3-9. Parameter values used : $r_{sc} = r_{sp} = 0.5$; $k_c = 0.01$; $C_1 = 2.10^8$; $[AMPh] = 3$; $[Sc]_{init} = 10^5$; $[Sp]_{init} = 10^3$; $[AMPb]_{init} = 0$*

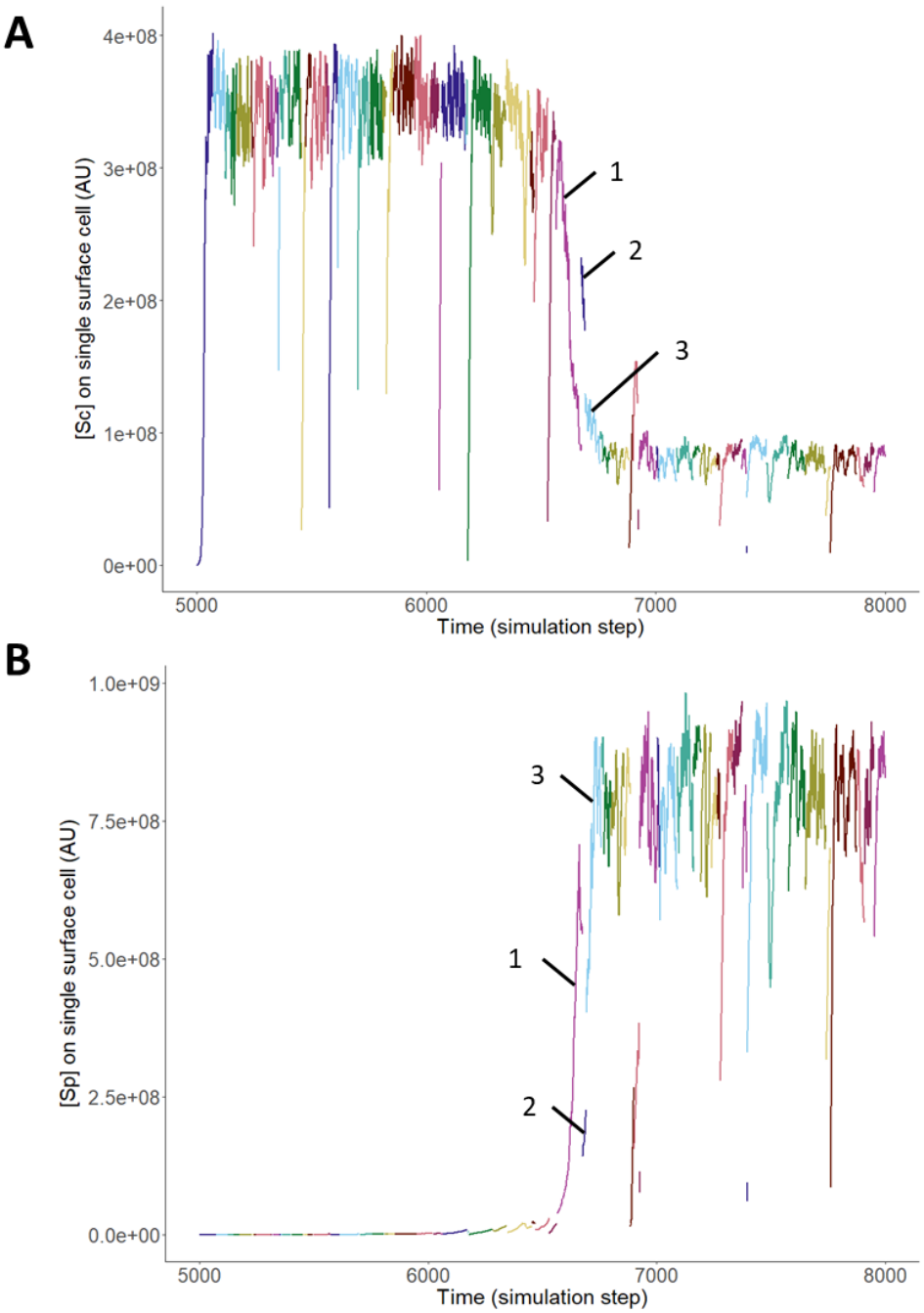

Figure IV.3-9: Microbiome kinetics on individual surface cells considering bacterial mobility and $[\boldsymbol{AMP_b}]$ ***diffusion****. The single cell trajectories of the commensal population* $[S_c]$ *and the oportunistic pathogen* $[S_p]$ *on single surface cells, with popMouv =0.1 and amp_diff=0.1, are shown in (A) and (B) respectively. Each color corresponds to the trajectory observed on one randomly selected surface cell. The time unit is a simulation step, representing 30 minutes. The numbers indicate the trajectories of bacterial populations on the 3 surface cells of interest mentioned in section IV.3.4. Parameter values used :* $r_{sc} = r_{sp} = 0.5$ *;* $k_c = 0.01$*;* $C_1 = 2.10^8$ *;* $[AMPh] = 3$*;* $[Sc]_{init} = 10^5$*;* $[Sp]_{init} = 10^3$*;* $[AMPb]_{init} = 0$

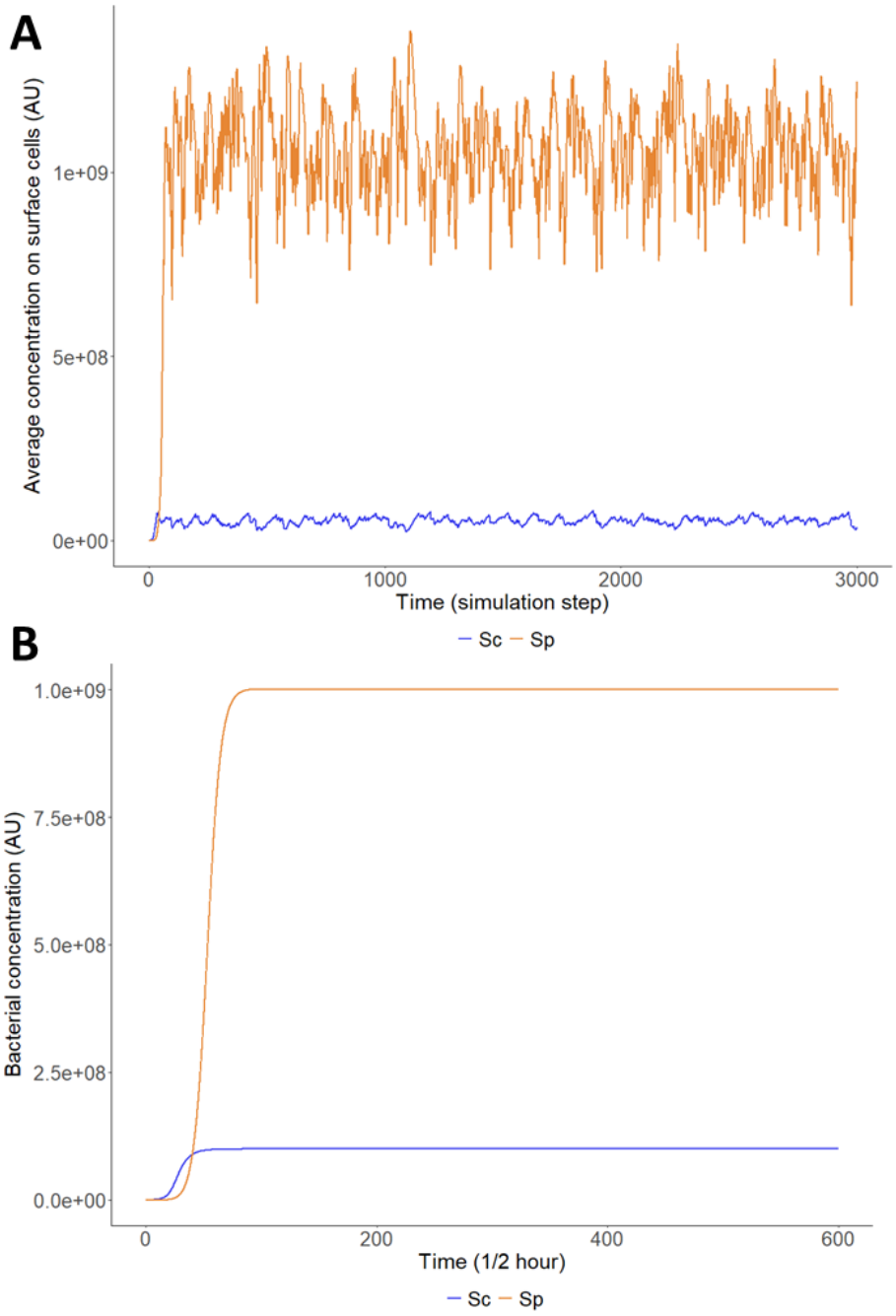

Figure IV.3-10: Simulation of the microbiome kinetics in the agent-based model including bacterial mobility and $[AMP_b]$ diffusion (A) compared to the ODE model (B). *The concentration of the commensal population S_c, and the opportunistic pathogen one S_p are shown in blue and orange respectively. The time unit is ½ hour, corresponding to 1 simulation step. The corresponding kinetics of $[AMP_b]$ are shown in Figure IV.3-11.Parameter values used for both the agent-based and the ODE model : $r_{sc} = 0.5$; $r_{sp} = 1$; $k_c = 0.01$; $C_1 = 5.10^6$; $[AMPh] = 1.5$; $[Sc]_{init} = 10^5$; $[Sp]_{init} = 10^3$; $[AMPb]_{init} = 0$. Parameter values specific to the agent-based model : popMouv = 0.1 ; amp_diff = 0.1*

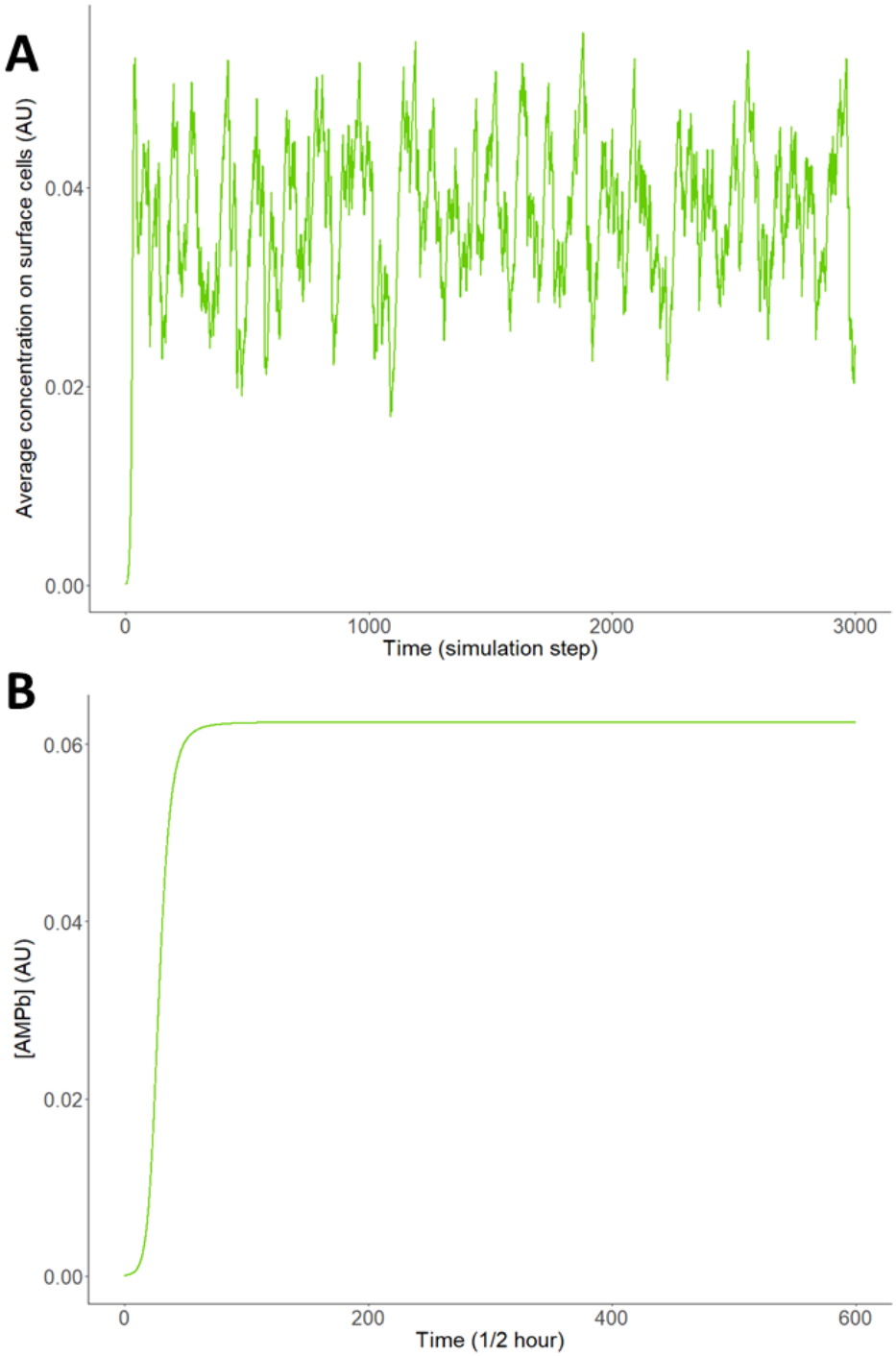

Figure IV.3-11: Simulation of the AMPb kinetics in the agent-based model including bacterial mobility and $[AMP_b]$ diffusion (A) compared to the ODE model (B). *The time unit is ½ hour, corresponding to 1 simulation step. The corresponding bacterial populations kinetics are shown in Figure IV.3-10.Parameter values used for both the agent-based and the ODE model :* $r_{sc} = 0.5$ *;* $r_{sp} = 1$*;* $k_c = 0.01$*;* $C_1 = 5.10^6$ *;* $[AMPh] = 1.5$*;* $[Sc]_{init} = 10^5$*;* $[Sp]_{init} = 10^3$*;* $[AMPb]_{init} = 0$*. Parameter values specific to the agent-based model: popMouv = 0.1; amp_diff = 0.1*

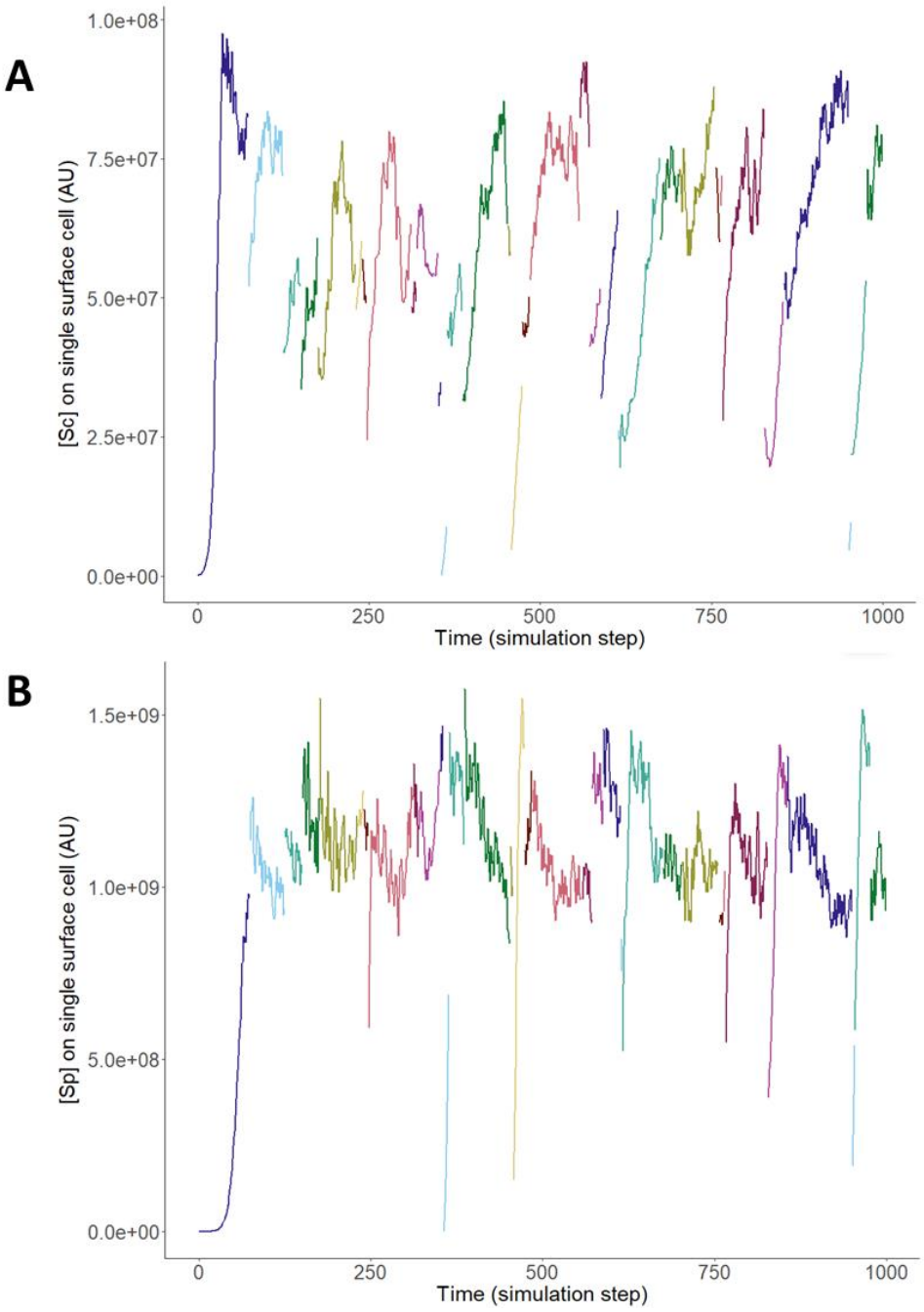

Figure IV.3-12: ***Microbiome kinetics on individual surface cells considering bacterial mobility and*** $[\boldsymbol{AMP_b}]$ ***diffusion, corresponding to the average kinetics from Figure IV.3-10****. The single cell trajectories of the commensal population* $[S_c]$ *and the oportunistic pathogen* $[S_p]$ *on single surface cells, with popMouv =0.1 and amp_diff=0.1, are shown in (A) and (B) respectively. Each color corresponds to the trajectory observed on one randomly selected surface cell. The time unit is a simulation step, representing 30 minutes.* $r_{sc} = 0.5$ *;* $r_{sp} = 1$*;* $k_c = 0.01$*;* $C_1 = 5.10^6$ *;* $[AMPh] = 1.5$*;* $[Sc]_{init} = 10^5$*;* $[Sp]_{init} = 10^3$*;* $[AMPb]_{init} = 0$*.*

IV.4. Host-microbiome interactions

Integrating a model of 2 competitive bacterial populations into an agent-based model already provides interesting insights on how the dynamic nature of the epidermis might influence the microbiome balance. To go towards a more integrative model of atopic dermatitis, it would be relevant to connect this simple model of microbiome evolution with the epidermal barrier function and inflammatory reaction. This section discusses potential ways to implement the interactions between the different phenomenon and some early developments explored.

IV.4.1. AMPs

As a first approach, the human AMPs, were implemented as a user-defined constant, AMPs, contributing to the killing of the pathogen population S_p. Even though it is reasonable to consider $[Amp_h]$ constant at the surface given stable genetic background and environmental conditions, a more realistic approach would take into account the kinetics of AMPs production by the keratinocytes. Only the cells of the viable epidermis are capable of synthetic activity. However, enzymatic activity is still possible within the SC (Pouillot et al. 2008). Therefore, a possible recurrence reaction for $[Amp_h]$ kinetics could be:

$$[Amp_h]_n = [Amp_h]_{n-1} + p_{ah}[Amp_h]_{n-1} - d_{ah}[Amp_h]_n$$

Where $[Amp_h]_n$, $[Amp_h]_{n-1}$, represent the intracellular concentration of Amp_h at the current and previous simulation step respectively. The production rate would be set to 0 for cells of the SC. Similarly, to the discretization strategy chosen for Amp_b in section IV.2.2, the degradation rate d_{ah} is applied to the concentration of Amp_h at the current step.

The recurrence relation can be reduced to the following geometric progression:

$$[Amp_h]_n = \frac{1 + pah}{1 + dah}[Amp_h]_{n-1}$$

Assuming $p_{ah} > d_{ah}$, the concentration of Amp_h will increase gradually in the viable epidermis. Once the keratinocyte differentiates into a corneocyte and loses the synthetic capacity, $[Amp_h]$ will converge to 0. Therefore, the value of d_{ah} needs to be selected so that there is still some $[Amp_h]$ present when the agent reaches the surface and interacts with the bacteria.

The AMPs produced by the keratinocytes would also be brought to the surface through a gradient-based diffusion process. At each time step, the agents would exchange $[Amp_h]$ with their neighbors, proportionally to the concentration gradient and a diffusion coefficient *amph_diff*. Variations of p_{ah} and d_{ah} will be used to model the reduced level of AMPs observed in AD skin.

IV.4.2. Bacterial metabolites

Several studies suggest that some species of the microbiome influence the skin metabolism. Commensals such as *S. epidermidis,* stimulate the production of ceramides (Zheng et al. 2022), or produce anti-inflammatory molecules (Yu et al. 2019). On the other side, pathogens such as *S. aureus* stimulate the inflammatory reaction (Laborel-Préneron et al. 2015). All the mechanisms previously mentioned either happen or are initialized in the viable epidermis, below the SC. As stated before, the bacteria rarely permeate through SC barrier outside of an infection. This implies the existence of a mechanism allowing bacteria to act on cells of the viable epidermis from the surface.

In the agent-based model, a production of population-specific metabolites could be implemented, proportionally to the population sizes. The bacterial metabolites will then diffuse through the skin in a gradient-dependent manner, to reach the viable epidermis. Once in the viable epidermis, the bacterial metabolites could influence the production or degradation of human AMPs or trigger the production of inflammatory molecules.

IV.4.3. Amino acids

A recent multi-omics analysis on skin, combining microbiome and metabolome data, revealed the existence of three major clusters, associating bacterial genus with metabolic pathways (P.-F. Roux, Oddos, and Stamatas 2022). One of these three clusters regroups several genera, including *Staphylococcus*, with sugars, amino acids (AA), peptides and vitamin B6. This correlation could be implemented in the agent-based, with some simplification assumption, considering that the bacterial populations described in the microbiome module belong to the Staphylococcus genus.

The effect of AA could be implemented as a ratio R_{AA} influencing the growth rates of both populations, although the exact nature of this positive correlation remains unclear:

$$\begin{cases} Sc_n &= Sc_{n-1} + \frac{1}{2}\, Sc_{n-1}\left(r_{sc}\left(R_{AA} - \frac{Sc_{n-1}}{K_{sc}}\right) - \frac{d_{sc}\, Sp_{n-1}}{C_1 + Sp_{n-1}}\right) \\ Sp_n &= Sp_{n-1} + \frac{1}{2}\, Sp_{n-1}\left(r_{sp}\left(R_{AA} - \frac{Sp_{n-1}}{K_{sp}}\right) - \frac{d_{spb}\, AMPb_{n-1}}{C_{ab} + AMPb_{n-1}} - \frac{d_{sph}\, AMPh}{C_{ah} + AMPh}\right) \\ AMPb_n &= \frac{2\, AMPb_{n-1} + k_c Sc_{n-1}}{2 \;+\; da} \end{cases}$$

(18)

R_{AA} equal to 1 would correspond to ideal growth conditions for the bacterial populations.

It has been established that filaggrin breakdown products are responsible for 70% of the AA present in the SC (Scott, Harding, and Barrett 1982). As a first approach, it seems reasonable to consider filaggrin as the unique direct source of AA production in the model. Filaggrin is already present in the agent-based model and contributes to the differentiation of granulosum cells into corneocytes. However, filaggrin breakdown was not implemented in the model described by Stamatas *et al.* (Stamatas et al. 2021).

The following recurrence relations describe the degradation of filaggrin into AA in each SC cell, at each step:

$$[filag]_n = [filag]_{n-1} - d_{filag}$$

$$[AA]_n = [AA]_{n-1} + C_{AA} d_{filag}$$

where $[X]_n$ and $[X]_{n-1}$ represent the concentrations of the variable X at the current and previous step respectively. d_{filag} corresponds to the breakdown rate of filaggrin and C_{AA} is a scaling factor between filaggrin and AA.

Clinical data of AA concentration according to skin depth measured with Raman spectroscopy were used to calibrate the model and define parameter values (Nikolovski et al. 2008). The fit of simulated AA profile to clinical data is shown of Figure IV.4-1.

The computation of R_{AA} based on the intracellular [AA] is still to be defined. Given the complexity brought by the agent-based model, it would be relevant to study how the addition of R_{AA} impacts the microbiome model separately, before implementing it in EPISIM. This correlation between AA and bacterial growth would be interesting to study, especially in the context of AD, where filaggrin and AA levels are significantly lower compared to healthy skin.

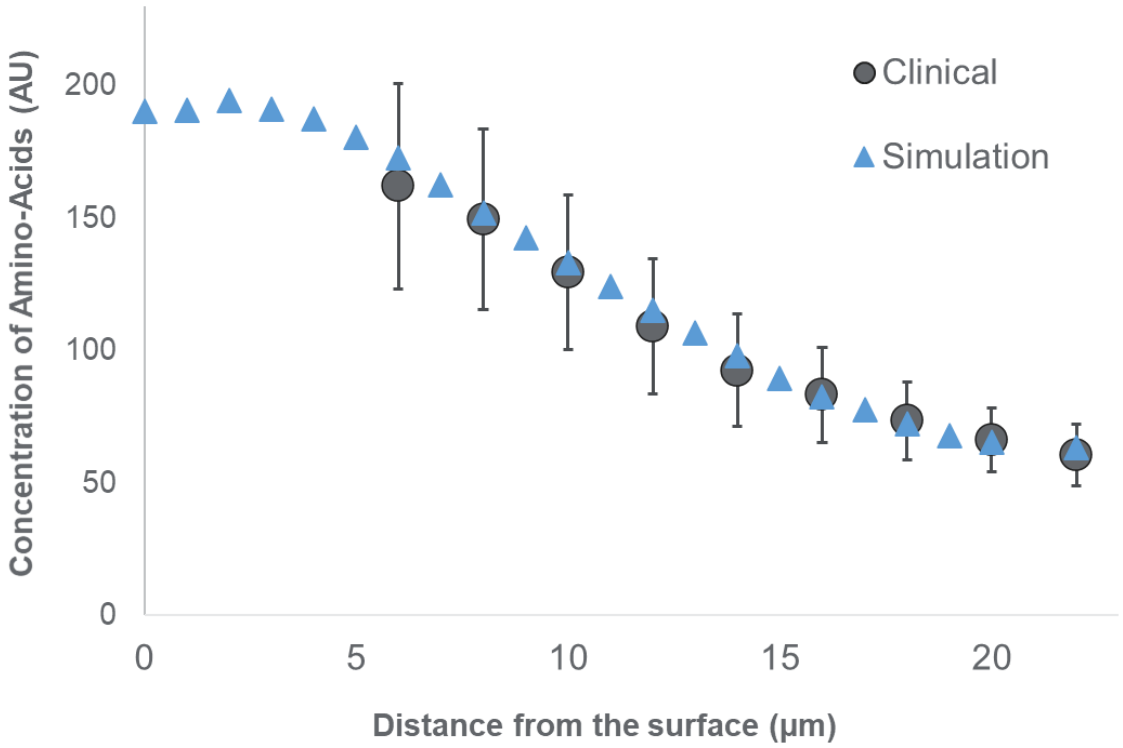

Figure IV.4-1: Simulated amino-acids (AA) profile in the stratum corneum (SC) compared to clinical data. *The baseline quantity of AA in the cells is set to 60,* $C_{AA} = 5$ *and* $d_{filag} = 0.035$*. The clinical data were measured in vivo with Raman spectroscopy on 14 adults (103).*

IV.5. Discussion

The multi-agent model of the epidermis integrating the microbiome kinetics module predicts that the constant renewal of surface cells significantly affects bacterial growth, acting as a time-limiting factor. A high bacterial mobility also seems to impact negatively the pathogenic population and to a lesser extent, the commensal one. This would be an interesting aspect to investigate further, although it would be challenging to test *in vitro*. Further investigation on the computational model is warranted, to ensure the robustness of this observation to the modelling choices made.

The quasi-stability phenomenon observed on the long timescale in the original ODE system can be reproduced by the agent-based model, provided that bacterial mobility values are sufficiently high. Under those conditions, the inverse steady state appears after the equivalent of 30 to 40 days (compared to approximately 12 days with the ODE model) of simulation. The biological relevance of such a long-time horizon may be challenged, as it is unlikely that the skin would be exposed to the exact same environment for 30 days.

The implementation of host-microbiome interactions is still at an early stage. Several mechanisms could be included to allow for a more accurate modulization of microbiome dysbiosis on the skin surface. For instance, positive impact of the commensal population on the lipid and AMPs production could be implemented. Similarly, the contribution of the pathogenic population to the AD vicious circle of exacerbating inflammation and damaging the skin barrier, is also an important aspect to consider.

Chapter V - Conclusions and Perspectives

V.1. Conclusions about our hybrid multiscale computational model of AD

To answer our first research question on the influence of pH elevation on epidermis structure and function, we introduced a hybrid multiscale model. It combines a pre-existing ODE model describing the interactions between KLK and its inhibitor LEKTI at molecular scale, with an agent-based model of the epidermis. The molecular interactions, happening on a short timescale, impact the cellular scale through their action on corneocyte adhesion, subsequently affecting global tissue properties on a longer timescale.

This hybrid multiscale model enabled us to better understand and visualize the role played by skin surface pH on the skin barrier function. By simulating two scenarios differing only in terms of KLK activity level, our model illustrates the key role played by pH on the barrier. An increase of KLK activity alone, due to a less acidic pH, is sufficient to affect significantly both the skin capacity to retain water and its permeability to irritant. Moreover, this alteration of the skin barrier function can result in a more intense inflammatory reaction. The effects highlighted here can begin to explain the propensity to irritation and dryness observed in AD or irritant contact dermatitis related to an elevation of skin pH.

The second component of our computational model of AD concerns the microbiome. The objective of this research was the identification of conditions which might favor or inhibit the emergence of pathogenic populations in the skin microbiome. Such analyses can lead to insights about potential treatment strategies aiming at restoring a balanced microbiome.

We have developed a simple ODE model of skin microbiome with 3 variables and 13 parameters which were reduced to 5 parameters by using published data from the literature and steady state reasoning on the observations made in the biological experiments. Our bacterial population model is generic in the sense that we did not consider the peculiarities of

some specific bacterial populations, but on some general formulas of adversary population dynamics and influence factors.

Perhaps surprisingly, we also showed that this simple model exhibits a meta-stability phenomenon, over a large range of biologically relevant parameter values, revealed by allowing the simulation to continue for times one order of magnitude longer than the reported experimental times. This observation questions the existence and importance of meta-stability phenomena in real biological processes. It needs to be noted that an important assumption made in building the mathematical model was that the experimental data used to fit the model parameters correspond to “stable” states of the mathematical model.

Finally, by combining the hybrid multiscale model with our bacterial population dynamic ODE system, we introduced the first multi-agent model of the epidermis including microbiome kinetics. This model is used to study how the constant renewal of surface cells impacts the microbiome balance. It predicts that the desquamation process poses an important constraint on bacterial growth, that can delay or even prevent the emergence of the opportunistic pathogen population dominance, under certain conditions. The model also predicts a detrimental effect of high bacterial mobility, requiring further investigation.

The presence of the metastability phenomenon observed during the ODE model study, depends on a certain level of bacterial mobility on surface cells in the multi-agent model. Furthermore, the emergence of the true mathematical steady state is significantly delayed in the dynamic model of the epidermis, questioning even further its biological relevance. However, it is worth noticing that, a few cells staying long enough at the surface to reach the mathematical steady state are sufficient to induced a sustained switch of the overall surface microbiome.

This work highlights the added value that hybrid models can bring in the study of complex systems. The combination of agent-based modelling with ODE system enables the simulation of population kinetics combined with dynamic structure. Moreover, it shows the value of studying the ODE model’s behavior independently prior to its integration in the agent-based model. It facilitates greatly the analysis of the global behaviors observed when simulating the agent-based model.

Altogether, the computational model presented here provides a good baseline to the implementation of a dynamic integrative model of the epidermis representative of AD skin. Our hybrid model already enabled relevant predictions and raised interesting questions at the biological as well as the computational aspect.

V.2. Perspectives for future work

More aspects of the complex AD pathophysiology could be investigated as additional modules on the hybrid multiscale model introduced here.

First, the study of how molecular mechanisms might affect the epidermis structure and function could be advanced. As mentioned previously, some cytokines which are overly expressed in AD, are downregulating filaggrin, contributing to the barrier dysfunction. This phenomenon could be implemented in the model by introducing in the model parameters and functions relating to cytokine production and effect on filaggrin in the granulosum layer. This may affect the cell differentiation processes in the model, since a certain amount of filaggrin is necessary to trigger the cornification of granular cells. Eventually, consequences on the formation and the quality of the skin barrier function could be expected, as well as potential structural disorganization of the SC.

Moreover, integrating the altered lipids and ceramides expression observed in AD skin could be considered in our multi-agent model. The water exchanged between neighboring cells is directly dependent on the lipid concentration, which can enable the study of the impact of altered lipid expression on the skin capacity to retain water.

The role of pH could be investigated further by implementing it as a gradient in the SC, instead of considering it as constant. The parameters for the KLK-LEKTI module could then be computed according to this gradient. The gradient from neutral to acidic would result in the successive activation and inhibition of KLK.

The microbiome model could be improved by the addition of a synergy mechanism between the commensal bacterial and the human AMPs against the pathogenic population, or the stimulation of keratinocyte production of AMPs by the commensal population. This

would reinforce the role played by AMPs on microbiome balance, an important mechanism in the context of AD. The AMP degradation by the pathogenic population could also be considered.

Host-microbiome interactions is an active area of research where much remains to be understood. Part of it could be investigated with computational models, such as the one presented here. For instance, it would be interesting to study the opposite effects that commensal and pathogens seem to have on skin barrier and inflammation. Commensals such *S. epidermidis* produce anti-inflammatory molecules, whereas pathogens such as *S. aureus* exacerbate the inflammation process by producing superantigens. Implementing these kinds of mechanisms in our model will give a new dimension to the study of microbiome balance with specific consequences on skin physiology.

We demonstrated with the hybrid model that surface cell desquamation has a significant impact on microbiome kinetics. Therefore, it would be relevant to study further this phenomenon in infant skin, especially as AD affects primarily children. Indeed, infant skin differs from that of the adult, both structurally and physiologically, with a continuously maturing barrier function and higher proliferation rates of basal cells, among other things. This higher proliferation is associated with higher desquamation rates of surface cells, which would then impact bacterial growth. This hypothesis could be tested by implementing our ODE model of microbiome into the agent-based model of infant epidermis described by Stamatas et al. (Stamatas et al. 2021).

On the modeling methodology aspects, the metastability phenomenon observed with the ODE model is worth further investigation. Given that the metastable state turns out to be dominating in the hybrid agent-based model, it would be useful to be able to compute it mathematically and study it, like we usually do with steady states. “What is causing metastability?”, “Can we mathematically define conditions when it will be observed or not?”, are examples of questions that could be the subject of future research.

The agent-based formalism could be exploited even further to introduce cell-to-cell variability in the model parameters. Instead of defining parameter values common for all agents, the parameter values will be defined at the agent level, following a probability distribution. This will introduce more stochasticity in the model, which will be coherent with the variability observed in biology in general.

Finally, when the interactions between skin barrier inflammation and microbiome are more thoroughly implemented in the model, it will be possible to assess the relative impact of each of these factors on AD. This type of model could be used to identify potential strategies to compensate one aspect or improve the symptoms in the long term. For instance, it would be useful to know if the enhancement of the commensal population with prebiotics or probiotics will be sufficient to break the vicious cycle characteristic of AD and recover microbiome balance.

References

Abuabara, K., A. M. Yu, J.-P. Okhovat, I. E. Allen, and S. M. Langan. 2018. "The Prevalence of Atopic Dermatitis beyond Childhood: A Systematic Review and Meta-Analysis of Longitudinal Studies." *Allergy* 73 (3): 696–704. https://doi.org/10.1111/all.13320.

Adra, Salem, Tao Sun, Sheila MacNeil, Mike Holcombe, and Rod Smallwood. 2010. "Development of a Three Dimensional Multiscale Computational Model of the Human Epidermis." *PLOS ONE* 5 (1): e8511. https://doi.org/10.1371/journal.pone.0008511.

Apfelbacher, C. J., T. L. Diepgen, and J. Schmitt. 2011. "Determinants of Eczema: Population-Based Cross-Sectional Study in Germany." *Allergy* 66 (2): 206–13. https://doi.org/10.1111/j.1398-9995.2010.02464.x.

Belkaid, Yasmine, and Julia A. Segre. 2014. "Dialogue between Skin Microbiota and Immunity." *Science* 346 (6212): 954–59. https://doi.org/10.1126/science.1260144.

Brattsand, Maria, Kristina Stefansson, Christine Lundh, Ylva Haasum, and Torbjörn Egelrud. 2005. "A Proteolytic Cascade of Kallikreins in the Stratum Corneum." *Journal of Investigative Dermatology* 124 (1): 198–203. https://doi.org/10.1111/j.0022-202X.2004.23547.x.

Briot, Anaïs, Céline Deraison, Matthieu Lacroix, Chrystelle Bonnart, Aurélie Robin, Céline Besson, Pierre Dubus, and Alain Hovnanian. 2009. "Kallikrein 5 Induces Atopic Dermatitis–like Lesions through PAR2-Mediated Thymic Stromal Lymphopoietin Expression in Netherton Syndrome." *The Journal of Experimental Medicine* 206 (5): 1135–47. https://doi.org/10.1084/jem.20082242.

Bylund, S, L Kobyletzki, M Svalstedt, and A Svensson. 2020. "Prevalence and Incidence of Atopic Dermatitis: A Systematic Review." *Acta Dermato Venereologica* 100 (12): adv00160. https://doi.org/10.2340/00015555-3510.

Byrd, Allyson L., Yasmine Belkaid, and Julia A. Segre. 2018. "The Human Skin Microbiome." *Nature Reviews Microbiology* 16 (3): 143–55. https://doi.org/10.1038/nrmicro.2017.157.

Calzone, L., F. Fages, and S. Soliman. 2006. "BIOCHAM: An Environment for Modeling Biological Systems and Formalizing Experimental Knowledge." *Bioinformatics* 22 (14): 1805–7. https://doi.org/10.1093/bioinformatics/btl172.

Campion, Jeffrey J., Patrick J. McNamara, and Martin E. Evans. 2005. "Pharmacodynamic Modeling of Ciprofloxacin Resistance in Staphylococcus Aureus." *Antimicrobial Agents and Chemotherapy* 49 (1): 209–19. https://doi.org/10.1128/AAC.49.1.209-219.2005.

Chopra, Rishi, Paras P. Vakharia, Ryan Sacotte, and Jonathan I. Silverberg. 2017. "Efficacy of Bleach Baths in Reducing Severity of Atopic Dermatitis: A Systematic Review and Meta-Analysis." *Annals of Allergy, Asthma & Immunology* 119 (5): 435–40. https://doi.org/10.1016/j.anai.2017.08.289.

Christodoulides, Panayiotis, Yoshito Hirata, Elisa Domínguez-Hüttinger, Simon G. Danby, Michael J. Cork, Hywel C. Williams, Kazuyuki Aihara, and Reiko J. Tanaka. 2017. "Computational Design of Treatment Strategies for Proactive Therapy on Atopic Dermatitis Using Optimal Control Theory." *Philosophical Transactions. Series A, Mathematical, Physical, and Engineering Sciences* 375 (2096): 20160285. https://doi.org/10.1098/rsta.2016.0285.

Cogen, Anna L., Kenshi Yamasaki, Jun Muto, Katheryn M. Sanchez, Laura Crotty Alexander, Jackelyn Tanios, Yuping Lai, Judy E. Kim, Victor Nizet, and Richard L. Gallo. 2010. "Staphylococcus Epidermidis Antimicrobial δ-Toxin (Phenol-Soluble Modulin-γ) Cooperates with Host Antimicrobial Peptides to Kill Group A Streptococcus." *PLOS ONE* 5 (1): e8557. https://doi.org/10.1371/journal.pone.0008557.

Cogen, Anna L., Kenshi Yamasaki, Katheryn M. Sanchez, Robert A. Dorschner, Yuping Lai, Daniel T. MacLeod, Justin W. Torpey, et al. 2010. "Selective Antimicrobial Action Is Provided by Phenol-Soluble Modulins Derived from Staphylococcus Epidermidis, a Normal Resident of the

Skin." *Journal of Investigative Dermatology* 130 (1): 192–200. https://doi.org/10.1038/jid.2009.243.
Czock, David, and Frieder Keller. 2007. "Mechanism-Based Pharmacokinetic-Pharmacodynamic Modeling of Antimicrobial Drug Effects." *Journal of Pharmacokinetics and Pharmacodynamics* 34 (6): 727–51. https://doi.org/10.1007/s10928-007-9069-x.
Dasgupta, Anindya, Vidula Iyer, Janhavi Raut, and Amy Qualls. 2020. "16502 Effect of PH on Growth of Skin Commensals and Pathogens." *Journal of the American Academy of Dermatology* 83 (6): AB180. https://doi.org/10.1016/j.jaad.2020.06.808.
Deraison, Celine, Chrystelle Bonnart, Frederic Lopez, Celine Besson, Ross Robinson, Arumugam Jayakumar, Fredrik Wagberg, et al. 2007. "LEKTI Fragments Specifically Inhibit KLK5, KLK7, and KLK14 and Control Desquamation through a PH-Dependent Interaction." *Molecular Biology of the Cell* 18 (9): 3607–19. https://doi.org/10.1091/mbc.e07-02-0124.
Domínguez-Hüttinger, Elisa, Panayiotis Christodoulides, Kosuke Miyauchi, Alan D. Irvine, Mariko Okada-Hatakeyama, Masato Kubo, and Reiko J. Tanaka. 2017. "Mathematical Modeling of Atopic Dermatitis Reveals 'Double-Switch' Mechanisms Underlying 4 Common Disease Phenotypes." *Journal of Allergy and Clinical Immunology* 139 (6): 1861-1872.e7. https://doi.org/10.1016/j.jaci.2016.10.026.
Domínguez-Hüttinger, Elisa, Masahiro Ono, Mauricio Barahona, and Reiko J. Tanaka. 2013. "Risk Factor-Dependent Dynamics of Atopic Dermatitis: Modelling Multi-Scale Regulation of Epithelium Homeostasis." *Interface Focus* 3 (2): 20120090. https://doi.org/10.1098/rsfs.2012.0090.
Drucker, Aaron M., Annie R. Wang, Wen-Qing Li, Erika Sevetson, Julie K. Block, and Abrar A. Qureshi. 2017. "The Burden of Atopic Dermatitis: Summary of a Report for the National Eczema Association." *Journal of Investigative Dermatology* 137 (1): 26–30. https://doi.org/10.1016/j.jid.2016.07.012.
Eberlein-König, B., T. Schäfer, J. Huss-Marp, U. Darsow, M. Möhrenschlager, O. Herbert, D. Abeck, U. Krämer, H. Behrendt, and J. Ring. 2000. "Skin Surface PH, Stratum Corneum Hydration, Trans-Epidermal Water Loss and Skin Roughness Related to Atopic Eczema and Skin Dryness in a Population of Primary School Children." *Acta Dermato-Venereologica* 80 (3): 188–91. https://doi.org/10.1080/000155500750042943.
Eissa, Azza, and Eleftherios P. Diamandis. 2008. "Human Tissue Kallikreins as Promiscuous Modulators of Homeostatic Skin Barrier Functions." *Biological Chemistry* 389 (6). https://doi.org/10.1515/BC.2008.079.
Évora, Ana S., Michael J. Adams, Simon A. Johnson, and Zhibing Zhang. 2021. "Corneocytes: Relationship between Structural and Biomechanical Properties." *Skin Pharmacology and Physiology* 34 (3): 146–61. https://doi.org/10.1159/000513054.
Fages, François, Steven Gay, and Sylvain Soliman. 2015. "Inferring Reaction Systems from Ordinary Differential Equations." *Theoretical Computer Science* 599 (September): 64–78. https://doi.org/10.1016/j.tcs.2014.07.032.
Finney, A., J.C. Doyle, H. Kitano, B.L. Kovitz, M. Hucka, B.E. Shapiro, A. Funahashi, et al. 2004. "Evolving a Lingua Franca and Associated Software Infrastructure for Computational Systems Biology: The Systems Biology Markup Language (SBML) Project." *Systems Biology* 1 (1). https://doi.org/10.1049/sb:20045008.
Fluhr, Joachim W., and Peter M. Elias. 2002. "Stratum Corneum PH: Formation and Function of the 'Acid Mantle.'" *Exogenous Dermatology* 1 (4): 163–75. https://doi.org/10.1159/000066140.
Friedmann, P S. 1998. "Allergy and the Skin. II—Contact and Atopic Eczema." *BMJ : British Medical Journal* 316 (7139): 1226.
Gandhi, Namita A., Brandy L. Bennett, Neil M. H. Graham, Gianluca Pirozzi, Neil Stahl, and George D. Yancopoulos. 2016. "Targeting Key Proximal Drivers of Type 2 Inflammation in Disease." *Nature Reviews Drug Discovery* 15 (1): 35–50. https://doi.org/10.1038/nrd4624.

Geoghegan, Joan A., Alan D. Irvine, and Timothy J. Foster. 2018. “Staphylococcus Aureus and Atopic Dermatitis: A Complex and Evolving Relationship.” *Trends in Microbiology* 26 (6): 484–97. https://doi.org/10.1016/j.tim.2017.11.008.

Grice, Elizabeth A., Heidi H. Kong, Sean Conlan, Clayton B. Deming, Joie Davis, Alice C. Young, Gerard G. Bouffard, et al. 2009. “Topographical and Temporal Diversity of the Human Skin Microbiome.” *Science (New York, N.Y.)* 324 (5931): 1190–92. https://doi.org/10.1126/science.1171700.

Hachem, Jean-Pierre, Evi Houben, Debra Crumrine, Mao-Quiang Man, Nanna Schurer, Truus Roelandt, Eung H. Choi, et al. 2006. “Serine Protease Signaling of Epidermal Permeability Barrier Homeostasis.” *Journal of Investigative Dermatology* 126 (9): 2074–86. https://doi.org/10.1038/sj.jid.5700351.

Halling-Overgaard, A.-S., S. Kezic, I. Jakasa, K.a. Engebretsen, H. Maibach, and J.p. Thyssen. 2017. “Skin Absorption through Atopic Dermatitis Skin: A Systematic Review.” *British Journal of Dermatology* 177 (1): 84–106. https://doi.org/10.1111/bjd.15065.

Hanson, Kerry M., Martin J. Behne, Nicholas P. Barry, Theodora M. Mauro, Enrico Gratton, and Robert M. Clegg. 2002. “Two-Photon Fluorescence Lifetime Imaging of the Skin Stratum Corneum PH Gradient.” *Biophysical Journal* 83 (3): 1682–90. https://doi.org/10.1016/S0006-3495(02)73936-2.

Howell, Michael D., Byung Eui Kim, Peisong Gao, Audrey V. Grant, Mark Boguniewicz, Anna DeBenedetto, Lynda Schneider, Lisa A. Beck, Kathleen C. Barnes, and Donald Y.M. Leung. 2007. “Cytokine Modulation of Atopic Dermatitis Filaggrin Skin Expression.” *Journal of Allergy and Clinical Immunology* 120 (1): 150–55. https://doi.org/10.1016/j.jaci.2007.04.031.

Hurault, Guillem, Jean François Stalder, Sophie Mery, Alain Delarue, Markéta Saint Aroman, Gwendal Josse, and Reiko J. Tanaka. 2022. “EczemaPred: A Computational Framework for Personalised Prediction of Eczema Severity Dynamics.” *Clinical and Translational Allergy* 12 (3): e12140. https://doi.org/10.1002/clt2.12140.

Igawa, Satomi, Mari Kishibe, Masako Minami-Hori, Masaru Honma, Hisashi Tsujimura, Junko Ishikawa, Tsutomu Fujimura, Masamoto Murakami, and Akemi Ishida-Yamamoto. 2017. “Incomplete KLK7 Secretion and Upregulated LEKTI Expression Underlie Hyperkeratotic Stratum Corneum in Atopic Dermatitis.” *Journal of Investigative Dermatology* 137 (2): 449–56. https://doi.org/10.1016/j.jid.2016.10.015.

Irvine, Alan D. 2007. “Fleshing Out Filaggrin Phenotypes.” *Journal of Investigative Dermatology* 127 (3): 504–7. https://doi.org/10.1038/sj.jid.5700695.

Jang, Hyosun, Akira Matsuda, Kyungsook Jung, Kaoru Karasawa, Kenshiro Matsuda, Kumiko Oida, Saori Ishizaka, et al. 2016. “Skin PH Is the Master Switch of Kallikrein 5-Mediated Skin Barrier Destruction in a Murine Atopic Dermatitis Model.” *Journal of Investigative Dermatology* 136 (1): 127–35. https://doi.org/10.1038/JID.2015.363.

Jungersted, J. M., H. Scheer, M. Mempel, H. Baurecht, L. Cifuentes, J. K. Høgh, L. I. Hellgren, G. B. E. Jemec, T. Agner, and S. Weidinger. 2010. “Stratum Corneum Lipids, Skin Barrier Function and Filaggrin Mutations in Patients with Atopic Eczema.” *Allergy* 65 (7): 911–18. https://doi.org/10.1111/j.1398-9995.2010.02326.x.

Kennedy, Elizabeth A, Jennifer Connolly, Jonathan O’B Hourihane, Padraic G Fallon, W H Irwin McLean, Deirdre Murray, Jay-Hyun Jo, Julia A Segre, Heidi H Kong, and Alan D Irvine. 2017. “Skin Microbiome before Development of Atopic Dermatitis: Early Colonization with Commensal Staphylococci at 2 Months Is Associated with a Lower Risk of Atopic Dermatitis at 1 Year.” *J ALLERGY CLIN IMMUNOL* 139 (1): 7.

Kezic, Sanja, Patrick M. J. H. Kemperman, Ellen S. Koster, Cindy M. de Jongh, Hok Bing Thio, Linda E. Campbell, Alan D. Irvine, Irwin W. H. McLean, Gerwin J. Puppels, and Peter J. Caspers. 2008. “Loss-of-Function Mutations in the Filaggrin Gene Lead to Reduced Level of Natural Moisturizing Factor in the Stratum Corneum.” *Journal of Investigative Dermatology* 128 (8): 2117–19. https://doi.org/10.1038/jid.2008.29.

Kobayashi, Tetsuro, Martin Glatz, Keisuke Horiuchi, Hiroshi Kawasaki, Haruhiko Akiyama, Daniel H. Kaplan, Heidi H. Kong, Masayuki Amagai, and Keisuke Nagao. 2015. “Dysbiosis and Staphylococcus Aureus Colonization Drives Inflammation in Atopic Dermatitis.” *Immunity* 42 (4): 756–66. https://doi.org/10.1016/j.immuni.2015.03.014.

Kobayashi, Yasuaki, Yusuke Sawabu, Hiroyuki Kitahata, Mitsuhiro Denda, and Masaharu Nagayama. 2016. “Mathematical Model for Calcium-Assisted Epidermal Homeostasis.” *Journal of Theoretical Biology* 397 (May): 52–60. https://doi.org/10.1016/j.jtbi.2016.02.032.

Kobayashi, Yasuaki, Yusuke Yasugahira, Hiroyuki Kitahata, Mika Watanabe, Ken Natsuga, and Masaharu Nagayama. 2018. “Interplay between Epidermal Stem Cell Dynamics and Dermal Deformation.” *Npj Computational Materials* 4 (1): 1–9. https://doi.org/10.1038/s41524-018-0101-z.

Koh, Li Fang, Ruo Yan Ong, and John E. Common. 2021. “Skin Microbiome of Atopic Dermatitis.” *Allergology International*, November, S1323893021001404. https://doi.org/10.1016/j.alit.2021.11.001.

Kohda, Katsunori, Xuan Li, Naoki Soga, Risa Nagura, Tie Duerna, Saeko Nakajima, Ichiro Nakagawa, Masakazu Ito, and Akinori Ikeuchi. 2021. “An In Vitro Mixed Infection Model With Commensal and Pathogenic Staphylococci for the Exploration of Interspecific Interactions and Their Impacts on Skin Physiology.” *Frontiers in Cellular and Infection Microbiology* 11 (September): 712360. https://doi.org/10.3389/fcimb.2021.712360.

Kong, Heidi H. 2011. “Skin Microbiome: Genomics-Based Insights into the Diversity and Role of Skin Microbes.” *Trends in Molecular Medicine* 17 (6): 320–28. https://doi.org/10.1016/j.molmed.2011.01.013.

Kong, Heidi H., Julia Oh, Clay Deming, Sean Conlan, Elizabeth A. Grice, Melony A. Beatson, Effie Nomicos, et al. 2012. “Temporal Shifts in the Skin Microbiome Associated with Disease Flares and Treatment in Children with Atopic Dermatitis.” *Genome Research* 22 (5): 850–59. https://doi.org/10.1101/gr.131029.111.

Korting, H. C., K. Hübner, K. Greiner, G. Hamm, and O. Braun-Falco. 1990. “Differences in the Skin Surface PH and Bacterial Microflora Due to the Long-Term Application of Synthetic Detergent Preparations of PH 5.5 and PH 7.0. Results of a Crossover Trial in Healthy Volunteers.” *Acta Dermato-Venereologica* 70 (5): 429–31.

Laborel-Préneron, Emeline, Pascale Bianchi, Franck Boralevi, Philippe Lehours, Frédérique Fraysse, Fanny Morice-Picard, Motoyuki Sugai, et al. 2015. “Effects of the Staphylococcus Aureus and Staphylococcus Epidermidis Secretomes Isolated from the Skin Microbiota of Atopic Children on CD4+ T Cell Activation.” *PLOS ONE* 10 (10): e0141067. https://doi.org/10.1371/journal.pone.0141067.

Lai, Yuping, Anna L. Cogen, Katherine A. Radek, Hyun Jeong Park, Daniel T. MacLeod, Anke Leichtle, Allen F. Ryan, Anna Di Nardo, and Richard L. Gallo. 2010. “Activation of TLR2 by a Small Molecule Produced by Staphylococcus Epidermidis Increases Antimicrobial Defense against Bacterial Skin Infections.” *The Journal of Investigative Dermatology* 130 (9): 2211–21. https://doi.org/10.1038/jid.2010.123.

Lai, Yuping, Anna Di Nardo, Teruaki Nakatsuji, Anke Leichtle, Yan Yang, Anna L. Cogen, Zi-Rong Wu, et al. 2009. “Commensal Bacteria Regulate Toll-like Receptor 3-Dependent Inflammation after Skin Injury.” *Nature Medicine* 15 (12): 1377–82. https://doi.org/10.1038/nm.2062.

Leyden, James J., Richard R. Marples, and Albert M. Kligman. 1974. “Staphylococcus Aureus in the Lesions of Atopic Dermatitis.” *British Journal of Dermatology* 90 (5): 525–525. https://doi.org/10.1111/j.1365-2133.1974.tb06447.x.

Leyden, James J., Kenneth J. McGinley, Otto H. Mills, and Albert M. Kligman. 1975. “Propionibacterium Levels In Patients With And Without Acne Vulgaris.” *Journal of Investigative Dermatology* 65 (4): 382–84. https://doi.org/10.1111/1523-1747.ep12607634.

Logtestijn, Mark D. A. van, Peter J. Caspers, Sanja Kezic, Douglas R. Hoffman, David W. Koenig, Masahiro Ono, Georgios N. Stamatas, and Reiko J. Tanaka. 2016. “Water Resistance Profile as

a Marker of Skin Barrier Damage in Atopic Dermatitis Patients." *Journal of Dermatological Science* 81 (2): 126–28. https://doi.org/10.1016/j.jdermsci.2015.10.017.

Logtestijn, Mark D. A. van, Elisa Domínguez-Hüttinger, Georgios N. Stamatas, and Reiko J. Tanaka. 2015. "Resistance to Water Diffusion in the Stratum Corneum Is Depth-Dependent." *PLOS ONE* 10 (2): e0117292. https://doi.org/10.1371/journal.pone.0117292.

Malik, Erum, Sarah R. Dennison, Frederick Harris, and David A. Phoenix. 2016. "PH Dependent Antimicrobial Peptides and Proteins, Their Mechanisms of Action and Potential as Therapeutic Agents." *Pharmaceuticals* 9 (4): 67. https://doi.org/10.3390/ph9040067.

Malthus, T. R. (Thomas Robert). 1798. *An Essay on the Principle of Population, as It Affects the Future Improvement of Society. With Remarks on the Speculations of Mr. Godwin, M. Condorcet and Other Writers*. London, J. Johnson. http://archive.org/details/essayonprincipl00malt.

Matsui, Takeshi, and Masayuki Amagai. 2015. "Dissecting the Formation, Structure and Barrier Function of the Stratum Corneum." *International Immunology* 27 (6): 269–80. https://doi.org/10.1093/intimm/dxv013.

McGirt, Laura Y., and Lisa A. Beck. 2006. "Innate Immune Defects in Atopic Dermatitis." *Journal of Allergy and Clinical Immunology* 118 (1): 202–8. https://doi.org/10.1016/j.jaci.2006.04.033.

Meredith, Hannah R., Allison J. Lopatkin, Deverick J. Anderson, and Lingchong You. 2015. "Bacterial Temporal Dynamics Enable Optimal Design of Antibiotic Treatment." *PLOS Computational Biology* 11 (4): e1004201. https://doi.org/10.1371/journal.pcbi.1004201.

Meyer-Hoffert, Ulf, Zhihong Wu, and Jens-Michael Schröder. 2009. "Identification of Lympho-Epithelial Kazal-Type Inhibitor 2 in Human Skin as a Kallikrein-Related Peptidase 5-Specific Protease Inhibitor." *PLoS ONE* 4 (2). https://doi.org/10.1371/journal.pone.0004372.

Miyano, Takuya, Alan D. Irvine, and Reiko J. Tanaka. 2021. "A Mathematical Model to Identify Optimal Combinations of Drug Targets for Dupilumab Poor Responders in Atopic Dermatitis." *Allergy* n/a (n/a). https://doi.org/10.1111/all.14870.

———. 2022. "Model-Based Meta-Analysis to Optimize Staphylococcus Aureus–Targeted Therapies for Atopic Dermatitis." *JID Innovations* 2 (3). https://doi.org/10.1016/j.xjidi.2022.100110.

Morar, Nilesh, William O. C. M. Cookson, John I. Harper, and Miriam F. Moffatt. 2007. "Filaggrin Mutations in Children with Severe Atopic Dermatitis." *Journal of Investigative Dermatology* 127 (7): 1667–72. https://doi.org/10.1038/sj.jid.5700739.

Moreci, Rebecca S., and Terry Lechler. 2020. "Epidermal Structure and Differentiation." *Current Biology* 30 (4): R144–49. https://doi.org/10.1016/j.cub.2020.01.004.

Morizane, Shin, Kenshi Yamasaki, Ai Kajita, Kazuko Ikeda, Maosheng Zhan, Yumi Aoyama, Richard L. Gallo, and Keiji Iwatsuki. 2012. "Th2 Cytokines Increase Kallikrein 7 Expression and Function in Atopic Dermatitis." *The Journal of Allergy and Clinical Immunology* 130 (1): 259-261.e1. https://doi.org/10.1016/j.jaci.2012.03.006.

Mu, Zhanglei, and Jianzhong Zhang. 2020. "The Role of Genetics, the Environment, and Epigenetics in Atopic Dermatitis." In *Epigenetics in Allergy and Autoimmunity*, edited by Christopher Chang and Qianjin Lu, 107–40. Advances in Experimental Medicine and Biology. Singapore: Springer. https://doi.org/10.1007/978-981-15-3449-2_4.

Nakaoka, Shinji, Sota Kuwahara, Chang Hyeong Lee, Hyejin Jeon, Junho Lee, Yasuhiro Takeuchi, and Yangjin Kim. 2016. "Chronic Inflammation in the Epidermis: A Mathematical Model." *Applied Sciences* 6 (9): 252. https://doi.org/10.3390/app6090252.

Nakatsuji, Teruaki, Tiffany H. Chen, Saisindhu Narala, Kimberly A. Chun, Aimee M. Two, Tong Yun, Faiza Shafiq, et al. 2017. "Antimicrobials from Human Skin Commensal Bacteria Protect against Staphylococcus Aureus and Are Deficient in Atopic Dermatitis." *Science Translational Medicine* 9 (378): eaah4680. https://doi.org/10.1126/scitranslmed.aah4680.

Nakatsuji, Teruaki, Tissa R. Hata, Yun Tong, Joyce Y. Cheng, Faiza Shafiq, Anna M. Butcher, Secilia S. Salem, et al. 2021. "Development of a Human Skin Commensal Microbe for Bacteriotherapy of Atopic Dermatitis and Use in a Phase 1 Randomized Clinical Trial." *Nature Medicine* 27 (4): 700–709. https://doi.org/10.1038/s41591-021-01256-2.

Nikolovski, Janeta, Georgios N. Stamatas, Nikiforos Kollias, and Benjamin C. Wiegand. 2008. “Barrier Function and Water-Holding and Transport Properties of Infant Stratum Corneum Are Different from Adult and Continue to Develop through the First Year of Life.” *Journal of Investigative Dermatology* 128 (7): 1728–36. https://doi.org/10.1038/sj.jid.5701239.

Nishio, Y., E. Noguchi, M. Shibasaki, M. Kamioka, E. Ichikawa, K. Ichikawa, Y. Umebayashi, F. Otsuka, and T. Arinami. 2003. “Association between Polymorphisms in the SPINK5 Gene and Atopic Dermatitis in the Japanese.” *Genes & Immunity* 4 (7): 515–17. https://doi.org/10.1038/sj.gene.6363889.

Nomura, Ichiro, Elena Goleva, Michael D. Howell, Quatyba A. Hamid, Peck Y. Ong, Clifton F. Hall, Marc A. Darst, et al. 2003. “Cytokine Milieu of Atopic Dermatitis, as Compared to Psoriasis, Skin Prevents Induction of Innate Immune Response Genes.” *The Journal of Immunology* 171 (6): 3262–69. https://doi.org/10.4049/jimmunol.171.6.3262.

Nováčková, Anna, Irene Sagrafena, Petra Pullmannová, Georgios Paraskevopoulos, Anupma Dwivedi, Anisha Mazumder, Karolína Růžičková, Petr Slepička, Jarmila Zbytovská, and Kateřina Vávrová. 2021. “Acidic PH Is Required for the Multilamellar Assembly of Skin Barrier Lipids In Vitro.” *Journal of Investigative Dermatology* 141 (8): 1915-1921.e4. https://doi.org/10.1016/j.jid.2021.02.014.

Ohno, Kota, Yasuaki Kobayashi, Masaaki Uesaka, Takeshi Gotoda, Mitsuhiro Denda, Hideyuki Kosumi, Mika Watanabe, Ken Natsuga, and Masaharu Nagayama. 2021. “A Computational Model of the Epidermis with the Deformable Dermis and Its Application to Skin Diseases.” *Scientific Reports* 11 (June): 13234. https://doi.org/10.1038/s41598-021-92540-1.

Ong, Peck Y., Takaaki Ohtake, Corinne Brandt, Ian Strickland, Mark Boguniewicz, Tomas Ganz, Richard L. Gallo, and Donald Y. M. Leung. 2002. “Endogenous Antimicrobial Peptides and Skin Infections in Atopic Dermatitis.” *The New England Journal of Medicine* 347 (15): 1151–60. https://doi.org/10.1056/NEJMoa021481.

Paller, Amy S., Heidi H. Kong, Patrick Seed, Shruti Naik, Tiffany C. Scharschmidt, Richard L. Gallo, Thomas Luger, and Alan D. Irvine. 2019. “The Microbiome in Patients with Atopic Dermatitis.” *Journal of Allergy and Clinical Immunology* 143 (1): 26–35. https://doi.org/10.1016/j.jaci.2018.11.015.

Palmer, Colin N. A., Alan D. Irvine, Ana Terron-Kwiatkowski, Yiwei Zhao, Haihui Liao, Simon P. Lee, David R. Goudie, et al. 2006. “Common Loss-of-Function Variants of the Epidermal Barrier Protein Filaggrin Are a Major Predisposing Factor for Atopic Dermatitis.” *Nature Genetics* 38 (4): 441–46. https://doi.org/10.1038/ng1767.

Pazgier, M., D. M. Hoover, D. Yang, W. Lu, and J. Lubkowski. 2006. “Human β-Defensins.” *Cellular and Molecular Life Sciences CMLS* 63 (11): 1294–1313. https://doi.org/10.1007/s00018-005-5540-2.

Polak, Marta E., Chuin Ying Ung, Joanna Masapust, Tom C. Freeman, and Michael R. Ardern-Jones. 2017. “Petri Net Computational Modelling of Langerhans Cell Interferon Regulatory Factor Network Predicts Their Role in T Cell Activation.” *Scientific Reports* 7 (1): 668. https://doi.org/10.1038/s41598-017-00651-5.

Pouillot, Anne, Nava Dayan, Ada S Polla, Luigi L Polla, and Barbara S Polla. 2008. “The Stratum Corneum: A Double Paradox.” *Journal of Cosmetic Dermatology* 7 (2): 143–48. https://doi.org/10.1111/j.1473-2165.2008.00379.x.

Proksch, Ehrhardt. 2018. “PH in Nature, Humans and Skin.” *The Journal of Dermatology* 45 (9): 1044–52. https://doi.org/10.1111/1346-8138.14489.

Proksch, Ehrhardt, Johanna M. Brandner, and Jens-Michael Jensen. 2008. “The Skin: An Indispensable Barrier.” *Experimental Dermatology* 17 (12): 1063–72. https://doi.org/10.1111/j.1600-0625.2008.00786.x.

Radulescu, Ovidiu, Satya Swarup Samal, Aurélien Naldi, Dima Grigoriev, and Andreas Weber. 2015. “Symbolic Dynamics of Biochemical Pathways as Finite States Machines.” In *Computational Methods in Systems Biology*, edited by Olivier Roux and Jérémie Bourdon, 104–20. Lecture

Notes in Computer Science. Cham: Springer International Publishing. https://doi.org/10.1007/978-3-319-23401-4_10.

Rizk, Aurélien, Grégory Batt, François Fages, and Sylvain Soliman. 2011. “Continuous Valuations of Temporal Logic Specifications with Applications to Parameter Optimization and Robustness Measures.” *Theoretical Computer Science*, Foundations of Formal Reconstruction of Biochemical Networks, 412 (26): 2827–39. https://doi.org/10.1016/j.tcs.2010.05.008.

Roux, Pierre-François, Thierry Oddos, and Georgios Stamatas. 2022. “Deciphering the Role of Skin Surface Microbiome in Skin Health: An Integrative Multiomics Approach Reveals Three Distinct Metabolite–Microbe Clusters.” *Journal of Investigative Dermatology* 142 (2): 469-479.e5. https://doi.org/10.1016/j.jid.2021.07.159.

Scott, Ian R., Clive R. Harding, and John G. Barrett. 1982. “Histidine-Rich Protein of the Keratohyalin Granules: Source of the Free Amino Acids, Urocanic Acid and Pyrrolidone Carboxylic Acid in the Stratum Corneum.” *Biochimica et Biophysica Acta (BBA) - General Subjects* 719 (1): 110–17. https://doi.org/10.1016/0304-4165(82)90314-2.

Seltmann, Jenny, Lennart M. Roesner, Friedrich-Wilhelm von Hesler, Miriam Wittmann, and Thomas Werfel. 2015. “IL-33 Impacts on the Skin Barrier by Downregulating the Expression of Filaggrin.” *Journal of Allergy and Clinical Immunology* 135 (6): 1659-1661.e4. https://doi.org/10.1016/j.jaci.2015.01.048.

Stamatas, Georgios N., Jalil Bensaci, Elea Greugny, Simarna Kaur, Hequn Wang, Maria Victoria Dizon, Michael J. Cork, Adam J. Friedman, and Thierry Oddos. 2021. “A Predictive Self-Organizing Multicellular Computational Model of Infant Skin Permeability to Topically Applied Substances.” *Journal of Investigative Dermatology* 141 (8): 2049-2055.e1. https://doi.org/10.1016/j.jid.2021.02.012.

Stefansson, Kristina, Maria Brattsand, Dirk Roosterman, Cordula Kempkes, Georgeta Bocheva, Martin Steinhoff, and Torbjörn Egelrud. 2008. “Activation of Proteinase-Activated Receptor-2 by Human Kallikrein-Related Peptidases.” *Journal of Investigative Dermatology* 128 (1): 18–25. https://doi.org/10.1038/sj.jid.5700965.

Subramanian, Indhupriya, Vivek K. Singh, and Abhay Jere. 2018. “Elucidating Mechanistic Insights into Drug Action for Atopic Dermatitis: A Systems Biology Approach.” *BMC Dermatology* 18 (1): 3. https://doi.org/10.1186/s12895-018-0070-4.

Sun, Tao, Salem Adra, Rod Smallwood, Mike Holcombe, and Sheila MacNeil. 2009. “Exploring Hypotheses of the Actions of TGF-B1 in Epidermal Wound Healing Using a 3D Computational Multiscale Model of the Human Epidermis.” *PLOS ONE* 4 (12): e8515. https://doi.org/10.1371/journal.pone.0008515.

Sütterlin, Thomas, Simone Huber, Hartmut Dickhaus, and Niels Grabe. 2009. “Modeling Multi-Cellular Behavior in Epidermal Tissue Homeostasis via Finite State Machines in Multi-Agent Systems.” *Bioinformatics* 25 (16): 2057–63. https://doi.org/10.1093/bioinformatics/btp361.

Sütterlin, Thomas, Christoph Kolb, Hartmut Dickhaus, Dirk Jäger, and Niels Grabe. 2013. “Bridging the Scales: Semantic Integration of Quantitative SBML in Graphical Multi-Cellular Models and Simulations with EPISIM and COPASI.” *Bioinformatics*. https://doi.org/10.1093/bioinformatics/bts659.

Sütterlin, Thomas, Erika Tsingos, Jalil Bensaci, Georgios N. Stamatas, and Niels Grabe. 2017. “A 3D Self-Organizing Multicellular Epidermis Model of Barrier Formation and Hydration with Realistic Cell Morphology Based on EPISIM.” *Scientific Reports*. https://doi.org/10.1038/srep43472.

Tanaka, Reiko J., Masahiro Ono, and Heather A. Harrington. 2011. “Skin Barrier Homeostasis in Atopic Dermatitis: Feedback Regulation of Kallikrein Activity.” *PLoS ONE* 6 (5). https://doi.org/10.1371/journal.pone.0019895.

Tognoli, Emmanuelle, and J. A. Scott Kelso. 2014. “The Metastable Brain.” *Neuron* 81 (1): 35–48. https://doi.org/10.1016/j.neuron.2013.12.022.

Totté, J.e.e., W.t. van der Feltz, M. Hennekam, A. van Belkum, E.j. van Zuuren, and S.g.m.a. Pasmans. 2016. “Prevalence and Odds of Staphylococcus Aureus Carriage in Atopic Dermatitis: A

Systematic Review and Meta-Analysis." *British Journal of Dermatology* 175 (4): 687–95. https://doi.org/10.1111/bjd.14566.

Tuomanen, E., R. Cozens, W. Tosch, O. Zak, and A. Tomasz. 1986. "The Rate of Killing of Escherichia Coli by Beta-Lactam Antibiotics Is Strictly Proportional to the Rate of Bacterial Growth." *Journal of General Microbiology* 132 (5): 1297–1304. https://doi.org/10.1099/00221287-132-5-1297.

Wang, Yangyang, Christian F. Guerrero-Juarez, Yuchi Qiu, Huijing Du, Weitao Chen, Seth Figueroa, Maksim V. Plikus, and Qing Nie. 2019. "A Multiscale Hybrid Mathematical Model of Epidermal-Dermal Interactions during Skin Wound Healing." *Experimental Dermatology* 28 (4): 493–502. https://doi.org/10.1111/exd.13909.

Weidinger, Stephan, Lisa A. Beck, Thomas Bieber, Kenji Kabashima, and Alan D. Irvine. 2018. "Atopic Dermatitis." *Nature Reviews Disease Primers* 4 (1): 1. https://doi.org/10.1038/s41572-018-0001-z.

Yu, Jinlei, Yang Luo, Zhenlai Zhu, Yufeng Zhou, Licheng Sun, Jixin Gao, Jinlv Sun, Gang Wang, Xu Yao, and Wei Li. 2019. "A Tryptophan Metabolite of the Skin Microbiota Attenuates Inflammation in Patients with Atopic Dermatitis through the Aryl Hydrocarbon Receptor." *Journal of Allergy and Clinical Immunology* 143 (6): 2108-2119.e12. https://doi.org/10.1016/j.jaci.2018.11.036.

Zheng, Yue, Rachelle L. Hunt, Amer E. Villaruz, Emilie L. Fisher, Ryan Liu, Qian Liu, Gordon Y. C. Cheung, Min Li, and Michael Otto. 2022. "Commensal Staphylococcus Epidermidis Contributes to Skin Barrier Homeostasis by Generating Protective Ceramides." *Cell Host & Microbe* 30 (3): 301-313.e9. https://doi.org/10.1016/j.chom.2022.01.004.

Zipperer, Alexander, Martin C. Konnerth, Claudia Laux, Anne Berscheid, Daniela Janek, Christopher Weidenmaier, Marc Burian, et al. 2016. "Human Commensals Producing a Novel Antibiotic Impair Pathogen Colonization." *Nature* 535 (7613): 511–16. https://doi.org/10.1038/nature18634.

Zwietering, M. H., I. Jongenburger, F. M. Rombouts, and K. van 't Riet. 1990. "Modeling of the Bacterial Growth Curve." *Applied and Environmental Microbiology* 56 (6): 1875–81.

Annexes

Biocham Notebook – Simulations and analyses of the ODE model of skin microbiome

ODE Model of Skin Microbiome

companion Biocham notebook associated to the article

Stability versus Meta-stability in a Model of Skin Microbiome

Eléa Thibault Greugny(1,2), Georgios N. Stamatas(1), and François Fages(2)

1 Johnson & Johnson Santé Beauté France, Issy-les-Moulineaux, France

2 Inria Saclay, Lifeware Team, Palaiseau, France

In [1]:
```
clear_model.
set_units(time, hours).
set_units(substance, CFU).
set_units(volume, ASU).
```

Out[1]:

In [2]:
```
da*Ab for Ab=>_.
kc*Sc for Sc=>Ab+Sc.
rsp*Sp for Sp=>2*Sp.
rsc*Sc for Sc=>2*Sc.
rsp*Sp^2/Ksp for Sp=>_.
rsc*Sc^2/Ksc for Sc=>_.
dspb*Ab*Sp/(Cab+Ab) for Ab+Sp=>Ab.
dsph*Ah*Sp/(Cah+Ah) for Sp=>_.
dsc*Sp*Sc/(C1+Sp) for Sp+Sc=>Sp.
```

Out[2]:

In [3]:
```
parameter(Ksc=4e8,Ksp=3e9,Cab=0.16,Cah=8).
function dsc = rsc*((3*C1/4e9) + 3/4).
function dspb = 5*rsp/4 .
function dsph = 2*rsp.
function da = 1e8*kc*(56 + 31*Ah)/(2.56*(4-Ah)).
```

Out[3]:

In [4]:
```
present(Sp,sp0).
present(Sc,sc0).
present(Ab,0).
```

Out[4]:

In [5]:
```
list_model.
```

Out[5]:
```
Ab*da for Ab=>_.
Sc*kc for Sc=>Ab+Sc.
Sp*rsp for Sp=>2*Sp.
Sc*rsc for Sc=>2*Sc.
Sp^2/Ksp*rsp for Sp=>_.
Sc^2/Ksc*rsc for Sc=>_.
Ab*Sp*dspb/(Ab+Cab) for Ab+Sp=>Ab.
Ah*Sp*dsph/(Ah+Cah) for Sp=>_.
Sc*Sp*dsc/(C1+Sp) for Sc+Sp=>Sp.
initial_state(Sp=sp0).
initial_state(Sc=sc0).
initial_state(Ab=0).
parameter(
  Ksc = 400000000.0,
  Ksp = 3000000000.0,
  Cab = 0.16,
  Cah = 8
).
function(
  dsc = rsc*(3*C1/4000000000.0+3/4),
  dspb = 5*rsp/4,
  dsph = 2*rsp,
  da = 100000000.0*kc*(56+31*Ah)/(2.56*(4-Ah))
).
```

In [6]:
```
parameter(sp0 = 1e3, sc0 = 1e5).
draw_influences.
```

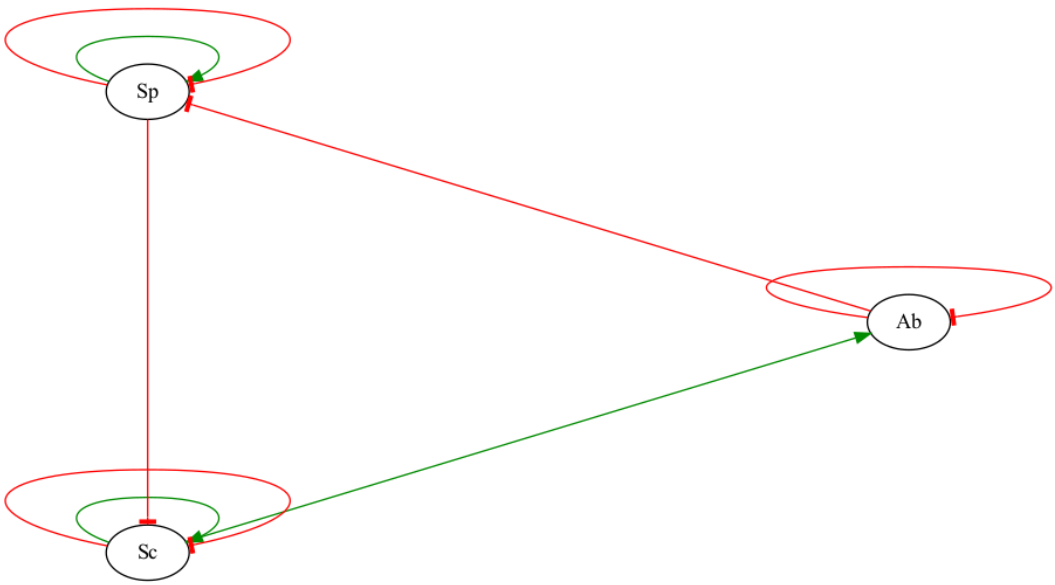

Out[6]:

Reproducing Kohda et al. (2021) coculture experimental data

Parameter values reproducing the experimental results showing

- stabilization at 40-50 hours of Sc=1e8 and Sp=1e9
- with initial conditions Sp(0)=1e3 and Sc(0)=1e5

In [7]:
```
option(time:50).
function normSc = Sc*1e-8.
function normSp = Sp*1e-9.

parameter(sp0 = 1e3, sc0 = 1e5).
```

Out[7]:

In [8]:
```
parameter(rsc=0.5,rsp=1,C1=5e6,kc=0.01,Ah=1.5).
```

Out[8]:

In [9]:
```
option(show:{Sp, Sc}).
numerical_simulation.
plot.
```

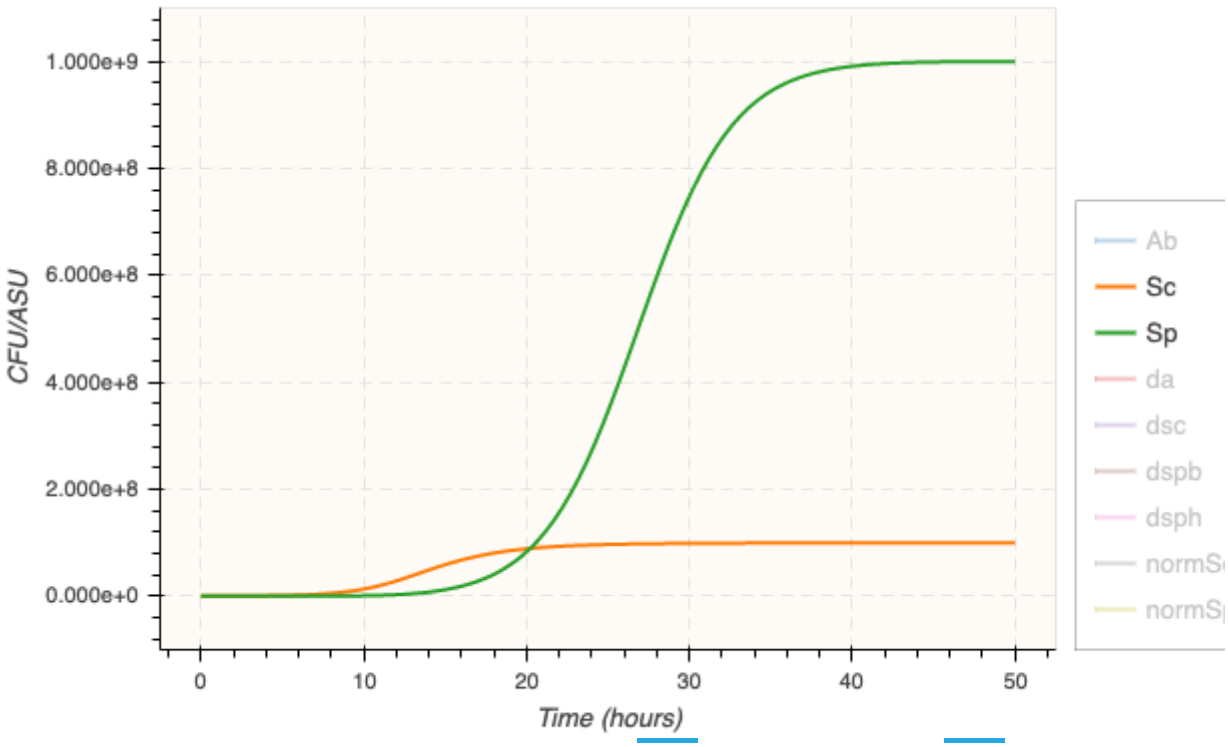

Out[9]:

```
2022-06-17 07:22:57.297 xcodebuild[2032:10721] Requested but did not find exte
nsion point with identifier Xcode.IDEKit.ExtensionSentinelHostApplications for
extension Xcode.DebuggerFoundation.AppExtensionHosts.watchOS of plug-in com.ap
ple.dt.IDEWatchSupportCore
2022-06-17 07:22:57.298 xcodebuild[2032:10721] Requested but did not find exte
nsion point with identifier Xcode.IDEKit.ExtensionPointIdentifierToBundleIdent
ifier for extension Xcode.DebuggerFoundation.AppExtensionToBundleIdentifierMa
p.watchOS of plug-in com.apple.dt.IDEWatchSupportCore
```

In [10]:
```
validity_domain(F(Time==40 /\ normSc = x1 /\ normSp = y1 /\ F(G(normSc = x2 /
```

Out[10]:
```
x1=0.996937/\y1=0.990333/\x2=0.999163/\y2=1.00058
```

In [11]:
```
satisfaction_degree(
    F(Time==40 /\ normSc = x1 /\ normSp = y1 /\ F(G(normSc = x2 /\ normSp = y
    [x1 -> 1, x2 -> 1, y1 -> 1, y2 -> 1]
).
```

Out[11]:
```
0.989911
```

Robustness of the result with respect to variations of rsc, kc, Ah parameter values

with coefficient of variation 0.1, 1, 10. (robustness as mean satisfaction degree of the behaviour specification).

In [12]:
```
validity_domain(F(Time==40 /\ normSc = x1 /\ normSp = y1 /\ F(G(normSc = x2 /
```

Out[12]:
```
x1=0.996937/\y1=0.990333/\x2=0.999163/\y2=1.00058
```

In [13]:
```
satisfaction_degree(
    F(Time==40 /\ normSc = x1 /\ normSp = y1 /\ F(G(normSc = x2 /\ normSp = y
    [x1 -> 1, x2 -> 1, y1 -> 1, y2 -> 1]
).
```

Out[13]:
```
0.989911
```

In [14]:
```
seed(1).
robustness(F(Time==40 /\ normSc = x1 /\ normSp = y1 /\ F(G(normSc = x2 /\ nor
    [rsc, kc, Ah],
    [x1 -> 1, x2 -> 1, y1 -> 1, y2 -> 1],
    robustness_coeff_var:0.1).
```

Out[14]:
```
Time: 7.62 s
Robustness degree: 0.873042
```

In [15]:
```
seed(1).
robustness(F(Time==40 /\ normSc = x1 /\ normSp = y1 /\ F(G(normSc = x2 /\ nor
    [rsc, kc, Ah],
    [x1 -> 1, x2 -> 1, y1 -> 1, y2 -> 1],
    robustness_coeff_var:1).
```

Out[15]:

```
Time: 6.14 s
Robustness degree: 0.416083
```

In [16]:
```
seed(1).
robustness(F(Time==40 /\ normSc = x1 /\ normSp = y1 /\ F(G(normSc = x2 /\ nor
    [rsc, kc, Ah],
    [x1 -> 1, x2 -> 1, y1 -> 1, y2 -> 1],
    robustness_coeff_var:10).
```

Out[16]:

```
Time: 5.728 s
Robustness degree: 0.771204
```

In [17]:
```
seed(1).
robustness(F(Time==40 /\ normSc = x1 /\ normSp = y1 /\ F(G(normSc = x2 /\ nor
    [rsc, kc, Ah],
    [x1 -> 1, x2 -> 1, y1 -> 1, y2 -> 1],
    robustness_coeff_var:100).
```

Out[17]:

```
Time: 6.674 s
Robustness degree: 0.327892
```

Conditions of healthy microbiome balance

Parameter values reproducing a healthy skin microbiome

- stabilizing at 40-50 hours with inverse balance with order of magnitude Sc=1e8, Sp=1e5
- starting from Sp(0)=1e3 and Sc(0)=1e5

In [18]:
```
parameter(sp0 =1e3, sc0=1e5).
function safeSc = Sc*1e-8.
function safeSp = Sp*1e-5.
```

Out[18]:

In [19]:
```
parameter(rsc=0.5,rsp=0.5,C1=2e8,kc=0.01,Ah=3).
```

Out[19]:

In [20]:
```
list_parameters.
```

Out[20]:
```
parameter(
  Ksc = 400000000.0,
  Ksp = 3000000000.0,
  Cab = 0.16,
  Cah = 8,
  sp0 = 1000.0,
  sc0 = 100000.0,
  rsc = 0.5,
  rsp = 0.5,
```

```
  C1 = 200000000.0,
  kc = 0.01,
  Ah = 3
).
```

In [21]:
```
numerical_simulation.
plot.
```

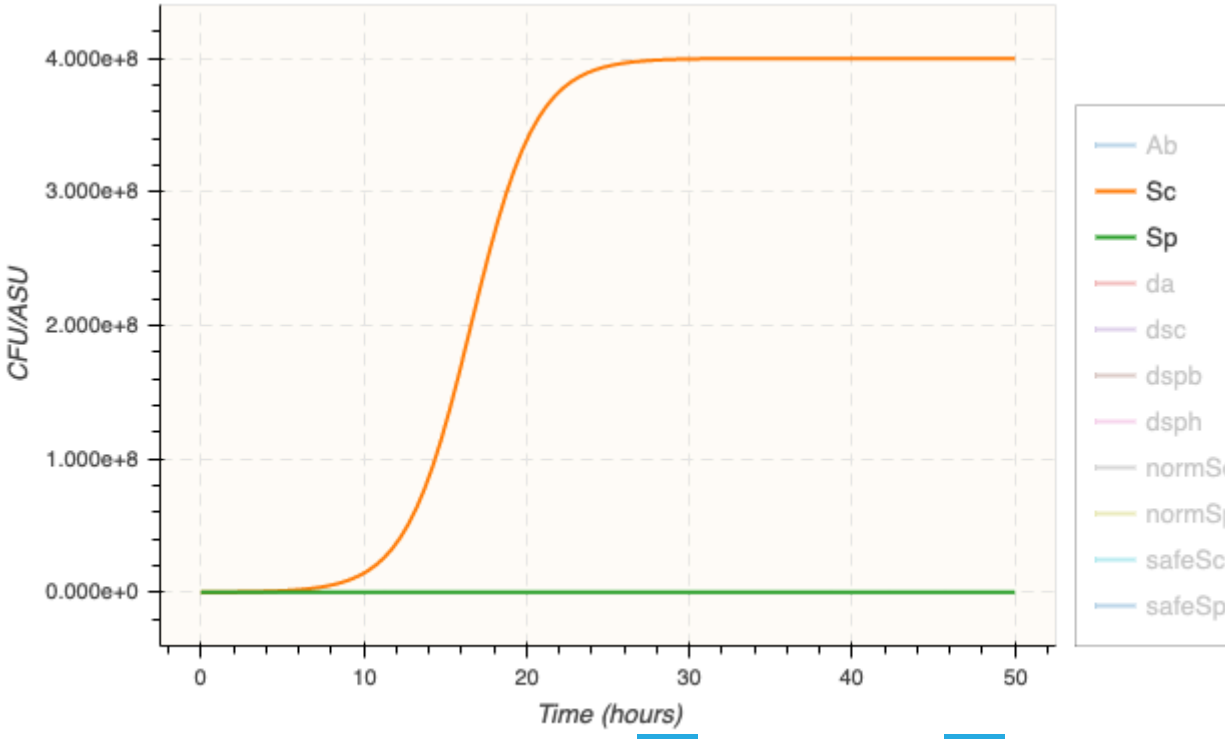

Out[21]:

In [22]:
```
validity_domain(F(Time==40 /\ safeSc = x1 /\ safeSp = y1 /\ F(G(safeSc = x2 /
```

Out[22]:
```
x1=3.99838/\y1=0.947149/\x2=3.99763/\y2=1.42024
```

In [23]:
```
satisfaction_degree(F(Time==40 /\ safeSc = x1 /\ safeSp = y1 /\ F(G(safeSc = 
[x1 -> 4, x2 -> 4, y1 -> 1, y2 -> 1.4]).
```

Out[23]:
```
0.946372
```

Sensitivity to parameter values

In [24]:
```
robustness(F(Time==40 /\ safeSc = x1 /\ safeSp = y1 /\ F(G(safeSc = x2 /\ saf
    [rsc],[x1 -> 4, x2 -> 4, y1 -> 1, y2 -> 1.4], robustness_coeff_var: 0.2).
```

Out[24]:
```
Time: 5.233 s
Robustness degree: 0.594962
```

In [25]:
```
robustness(F(Time==40 /\ safeSc = x1 /\ safeSp = y1 /\ F(G(safeSc = x2 /\ saf
    [rsp],[x1 -> 4, x2 -> 4, y1 -> 1, y2 -> 1.4], robustness_coeff_var: 0.2).
```

Out[25]:

```
Time: 5.45 s
Robustness degree: 0.524697
```

In [26]:
```
robustness(F(Time==40 /\ safeSc = x1 /\ safeSp = y1 /\ F(G(safeSc = x2 /\ saf
    [C1],[x1 -> 4, x2 -> 4, y1 -> 1, y2 -> 1.4], robustness_coeff_var: 10).
```

Out[26]:
```
Time: 5.117 s
Robustness degree: 0.946408
```

In [27]:
```
robustness(F(Time==40 /\ safeSc = x1 /\ safeSp = y1 /\ F(G(safeSc = x2 /\ saf
    [kc],[x1 -> 4, x2 -> 4, y1 -> 1, y2 -> 1.4], robustness_coeff_var: 1.0).
```

Out[27]:
```
Time: 5.284 s
Robustness degree: 0.946185
```

In [28]:
```
robustness(F(Time==40 /\ safeSc = x1 /\ safeSp = y1 /\ F(G(safeSc = x2 /\ saf
    [Ah],[x1 -> 4, x2 -> 4, y1 -> 1, y2 -> 1.4], robustness_coeff_var: 0.2).
```

Out[28]:
```
Time: 4.983 s
Robustness degree: 0.476586
```

In [29]:
```
robustness(F(Time==40 /\ safeSc = x1 /\ safeSp = y1 /\ F(G(safeSc = x2 /\ saf
    [sp0],[x1 -> 4, x2 -> 4, y1 -> 1, y2 -> 1.4], robustness_coeff_var: 10).
```

Out[29]:
```
Time: 5.516 s
Robustness degree: 0.161896
```

In [30]:
```
robustness(F(Time==40 /\ safeSc = x1 /\ safeSp = y1 /\ F(G(safeSc = x2 /\ saf
    [sc0],[x1 -> 4, x2 -> 4, y1 -> 1, y2 -> 1.4], robustness_coeff_var: 10).
```

Out[30]:
```
Time: 4.57 s
Robustness degree: 0.567383
```

Global sensitivity to some parameter pairs

In [31]:
```
robustness(F(Time==40 /\ safeSc = x1 /\ safeSp = y1 /\ F(G(safeSc = x2 /\ saf
    [rsc,rsp],[x1 -> 4, x2 -> 4, y1 -> 1, y2 -> 1.4], robustness_coeff_var: 0
```

Out[31]:
```
Time: 3.702 s
Robustness degree: 0.519691
```

In [32]:
```
robustness(F(Time==40 /\ safeSc = x1 /\ safeSp = y1 /\ F(G(safeSc = x2 /\ saf
    [sc0,sp0],[x1 -> 4, x2 -> 4, y1 -> 1, y2 -> 1.4], robustness_coeff_var: 1
```

Out[32]:
```
Time: 4.1 s
Robustness degree: 0.340808
```

Metastability Revealed on a Long Time Scale

The previous seemingly stable state on the 50 hours time scale of the experiments is in fact a metastable state which is reversed after 200 hours.

In [33]:
```
option(time:500).
```

Out[33]:

In [34]:
```
numerical_simulation.
plot.
```

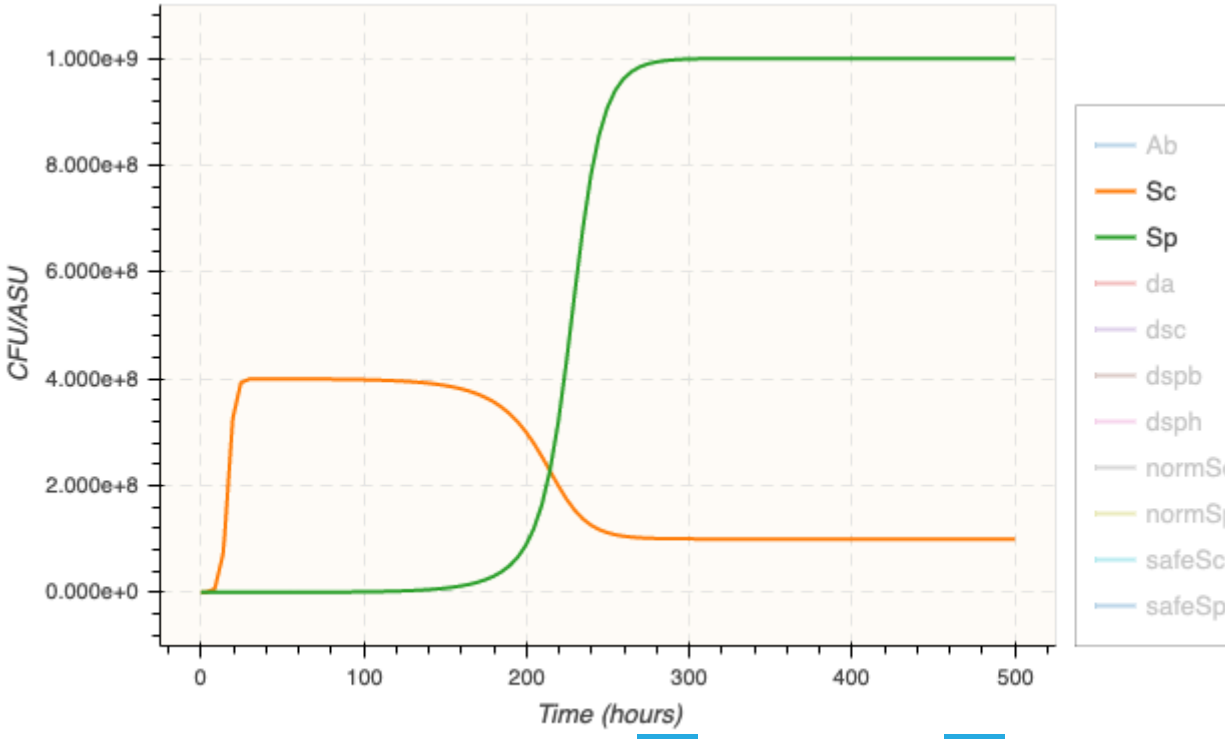

Out[34]:

In [35]:
```
validity_domain(F(Time=t /\ Sp==Sc)).
```

Out[35]:
```
t=209.522
```

This phenomenon appears above a threshold value for Ah>2.5 on a longer time scale

In [36]:
```
parameter(Ah=2.5).
numerical_simulation(time:1e5).
plot.
```

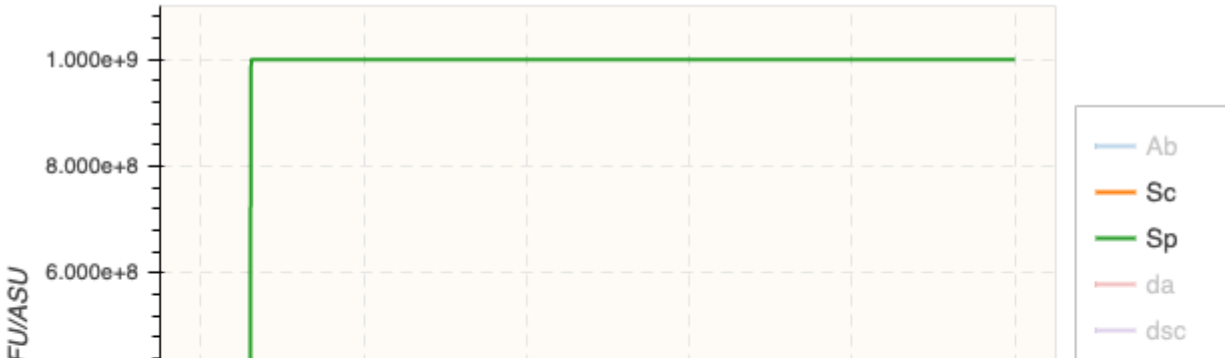

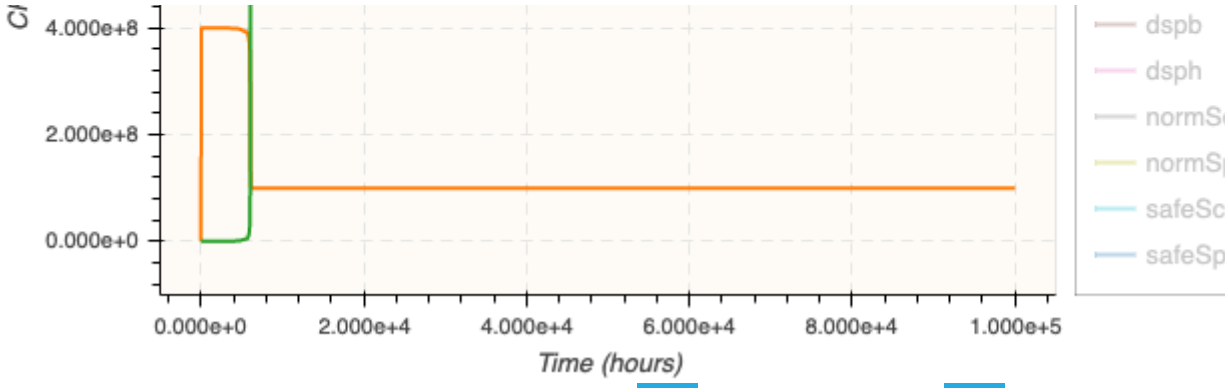

Out[36]:

In [37]:
```
validity_domain(F(Time=t /\ Sp==Sc)).
```

Out[37]: t=6067.17

In [38]:
```
parameter(Ah=2.49).
numerical_simulation(time:1e10).
plot.
```

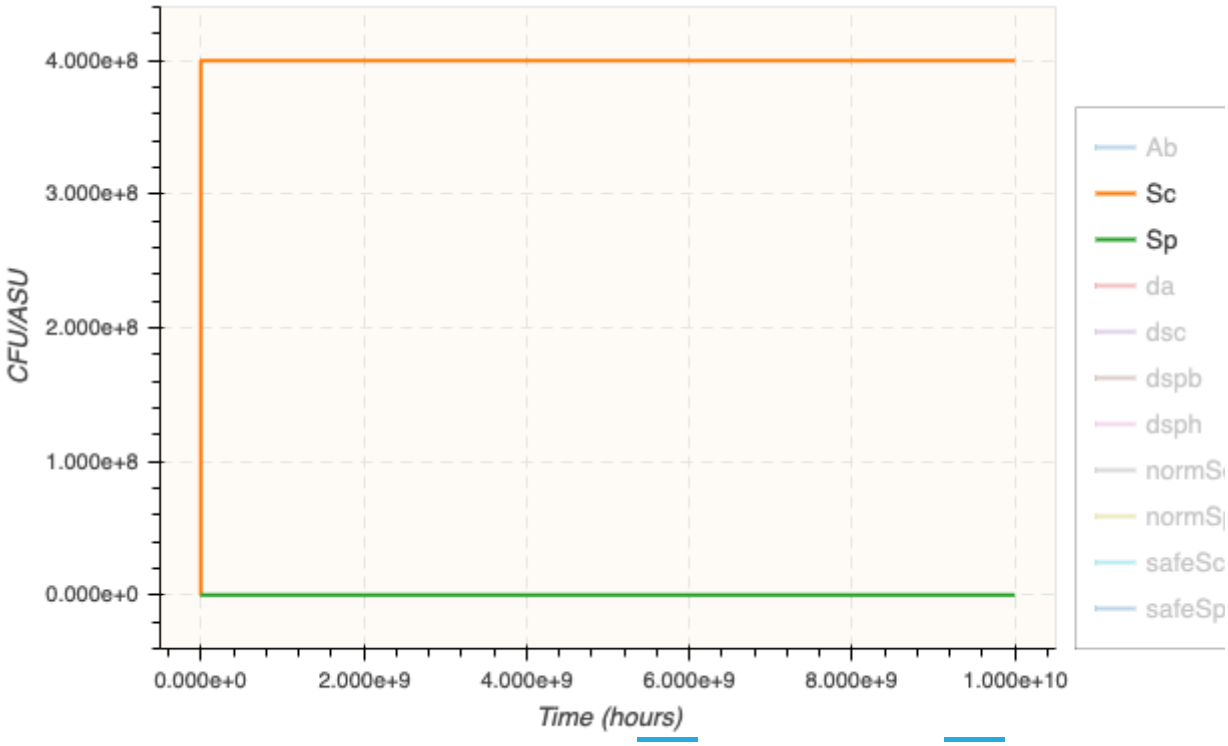

Out[38]:

Comparing 2 pH conditions on healthy condition

Low pH (around 5) - healthy skin

In [39]:
```
option(time:50).
parameter(rsc=0.5,rsp=0.3,C1=2e8,kc=0.01,Ah=3).
parameter(sc0=1e5, sp0=1e3).
```

Out[39]:

In [40]:
```
numerical_simulation.
plot.
satisfaction_degree(F(Time==40 /\ (Sc > u1*Sp) /\ F(G(Sc > u2*Sp))),[u1 -> 10
```

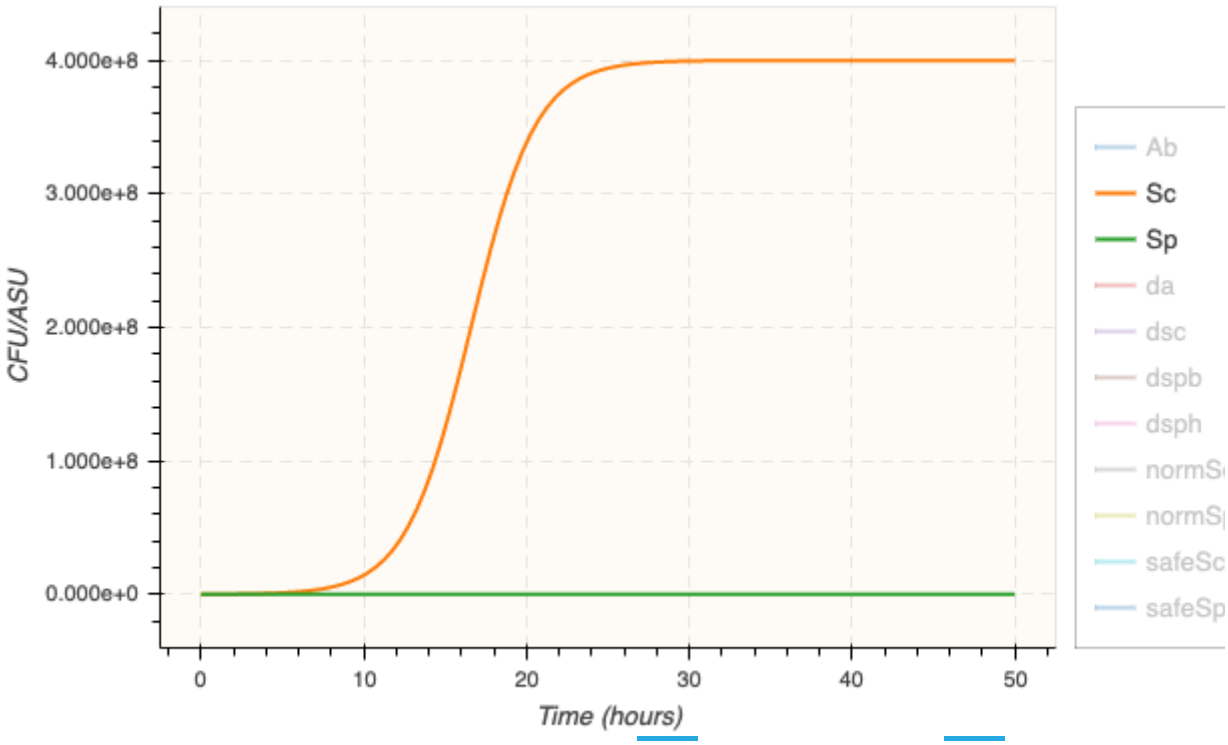

Out[40]:

```
20447.400000
```

In [10]:
```
%timeout 600000
```

Out[10]:
```
Timeout set to 600000
```

In [42]:
```
scan_parameters(F(Time==40 /\ (Sc > u1*Sp) /\ F(G(Sc > u2*Sp))),
    (1e5 <= sp0 <= 1e6), (1e3 <= sc0 <= 5e4), [u1 -> 10, u2 -> 10], resolutio
```

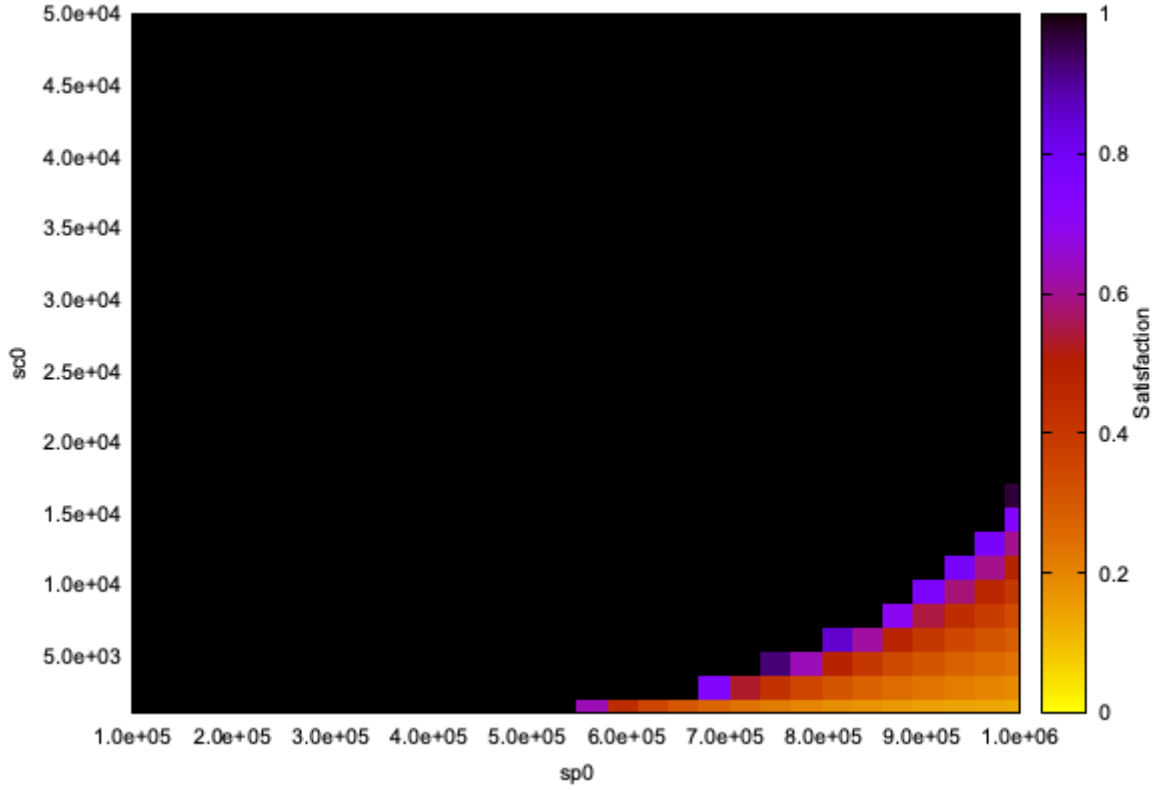

Out[42]:

```
Time: 3178.45 s
Mean satisfaction (robustness): 0.600085, standard deviation: 0.654062
Maximum satisfaction: 1.000000
Best solutions found with 100000.000000<=sp0<=1000000.000000, 1000.000000<=sc0
<=50000.000000
```

Higher pH (around 6.5) - compromised skin

In [43]:

```
parameter(rsc=0.9,rsp=1.3,C1=2e8,kc=0.01,Ah=3).
parameter(sc0=1e5, sp0=1e3).
```

Out[43]:

In [44]:

```
numerical_simulation.
plot.
satisfaction_degree(F(Time==40 /\ (Sc > u1*Sp) /\ F(G(Sc > u2*Sp))),[u1 -> 10
```

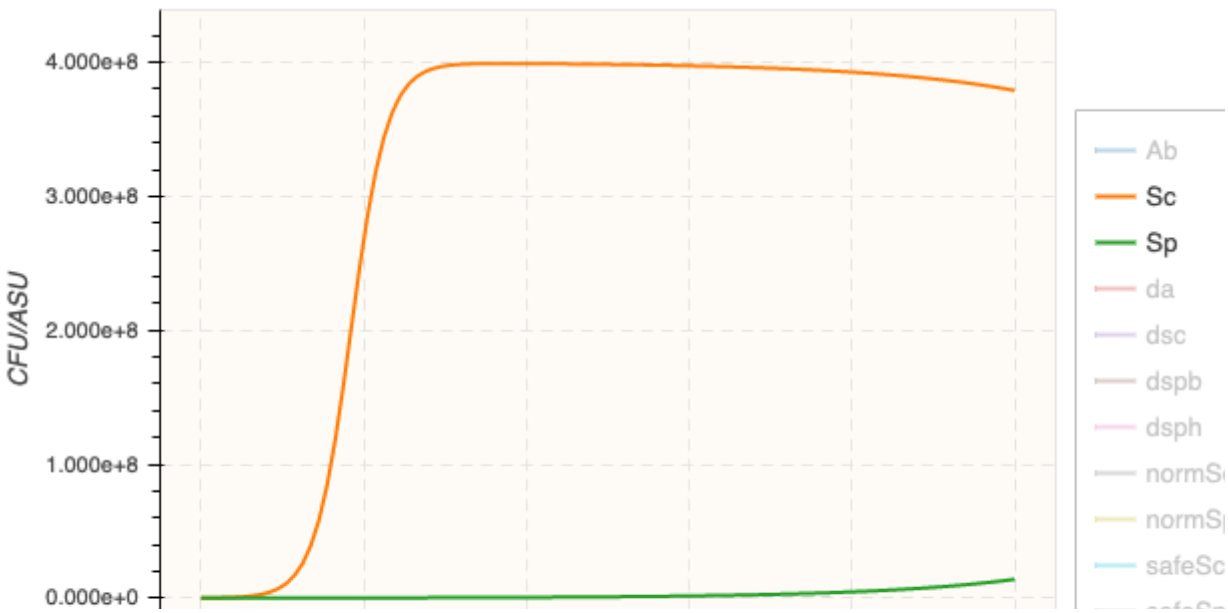

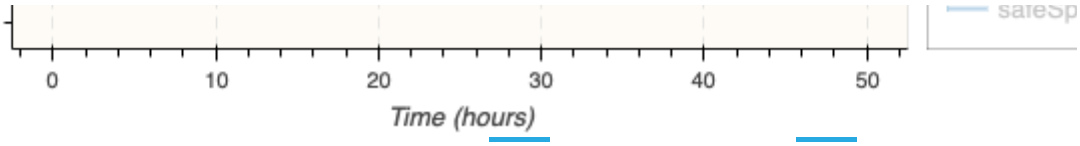

Out[44]:

```
17.876800
```

In [45]:

```
search_parameters(F(Time==40 /\ (Sc > u1*Sp) /\ F(G(Sc > u2*Sp))),
    [1e4 <= sp0 <= 1e6, 1e3 <= sc0 <= 1e8], [u1 -> 10, u2 -> 10], cmaes_log_n
    cmaes_init_center: yes).
```

Out[45]:

```
Time: 3.227 s
Stopping reason: Fitness: function value -9.38e-01 <= stopFitness (1.00e-04)
Best satisfaction degree: 16.005285
[0] parameter(sp0=22778.239766146624)
[1] parameter(sc0=29330926.381110094)
```

In [46]:

```
scan_parameters(F(Time==40 /\ (Sc > u1*Sp) /\ F(G(Sc > u2*Sp))),
    (1e4 <= sp0 <= 1e5), (1e7 <= sc0 <= 1e8), [u1 -> 10, u2 -> 10], resolutio
```

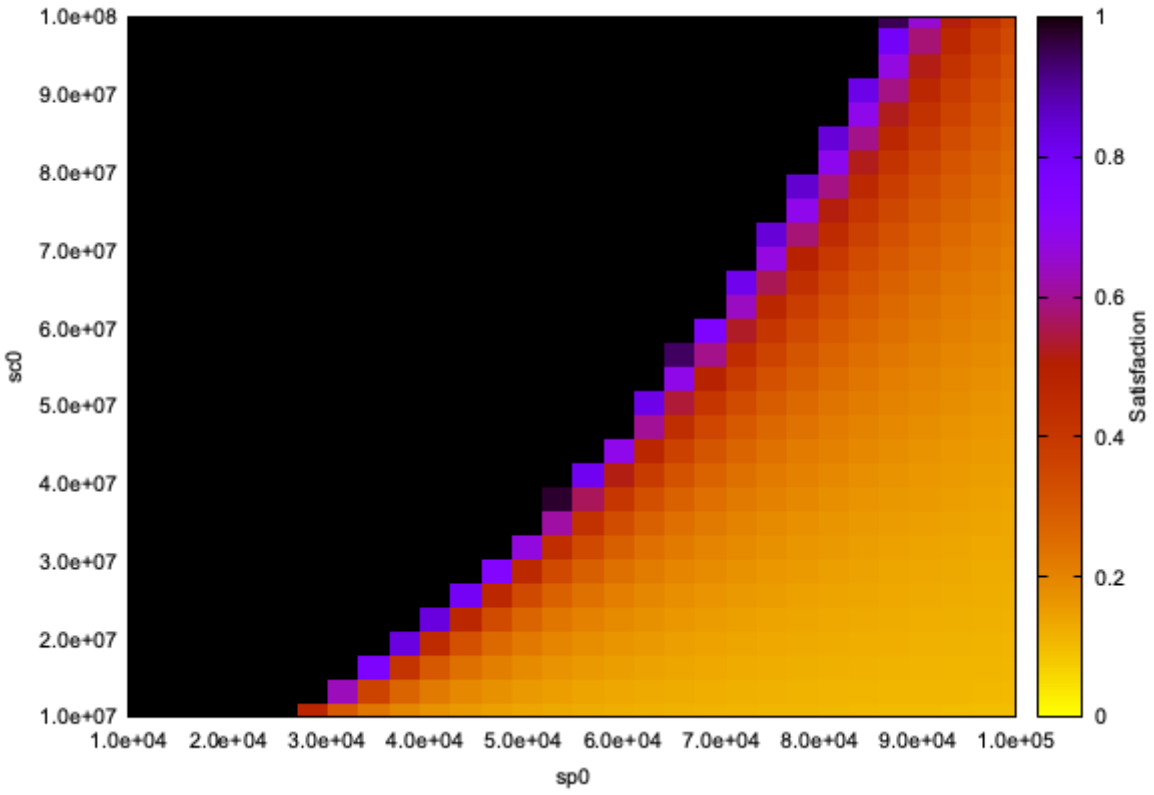

Out[46]:

```
Time: 2939.596 s
Mean satisfaction (robustness): 0.389989, standard deviation: 0.602861
Maximum satisfaction: 1.000000
Best solutions found with 10000.000000<=sp0<=84482.758621, 10000000.000000<=sc
0<=100000000.000000
```

Comparing AMP production level by the skin

Low production of AMPs (Ah = 0.5)

In [11]:

```
parameter(rsc=0.5,rsp=0.5,C1=2e8,kc=0.01,Ah=0.5).
parameter(sc0=1e5, sp0=1e3).
```

Out[11]:

In [12]:

```
numerical_simulation.
plot.
satisfaction_degree(F(Time==40 /\ (Sc > u1*Sp) /\ F(G(Sc > u2*Sp))),[u1 -> 10
```

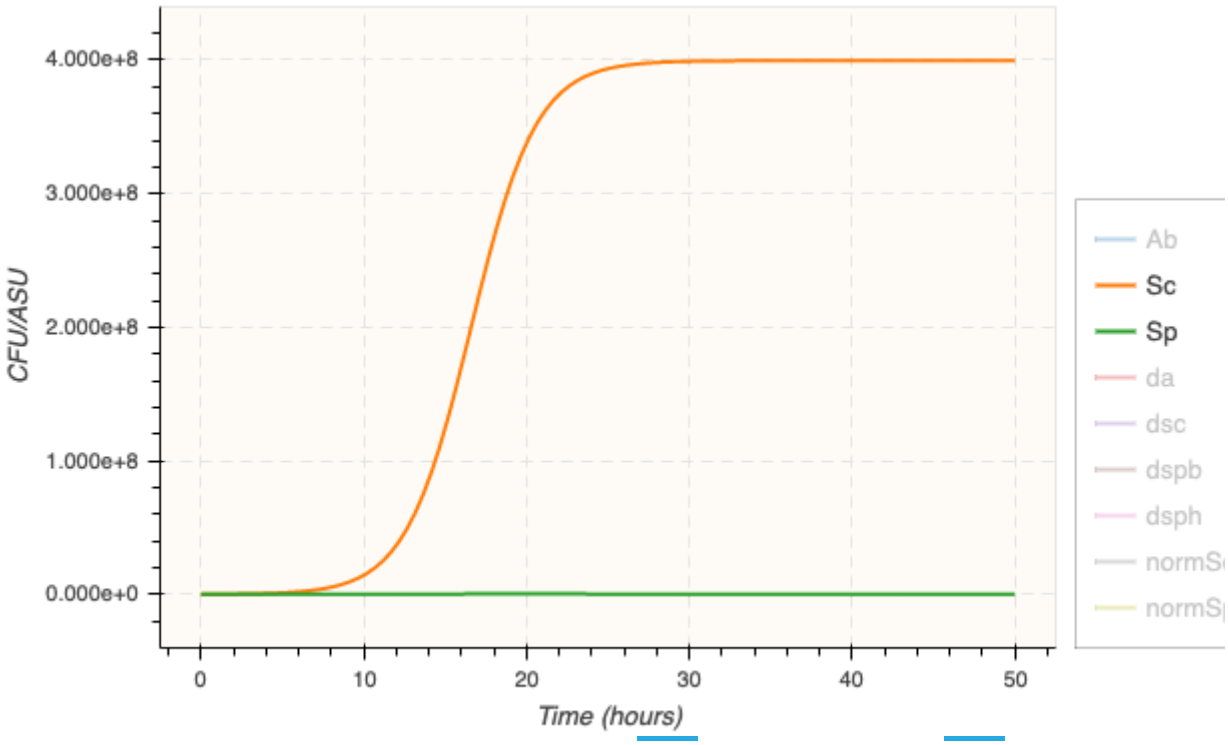

Out[12]:

2138.560000

In [13]:

```
scan_parameters(F(Time==40 /\ (Sc > u1*Sp) /\ F(G(Sc > u2*Sp))),
    (1e4 <= sp0 <= 5e5), (1e4 <= sc0 <= 1e6), [u1 -> 10, u2 -> 10], resolutio
```

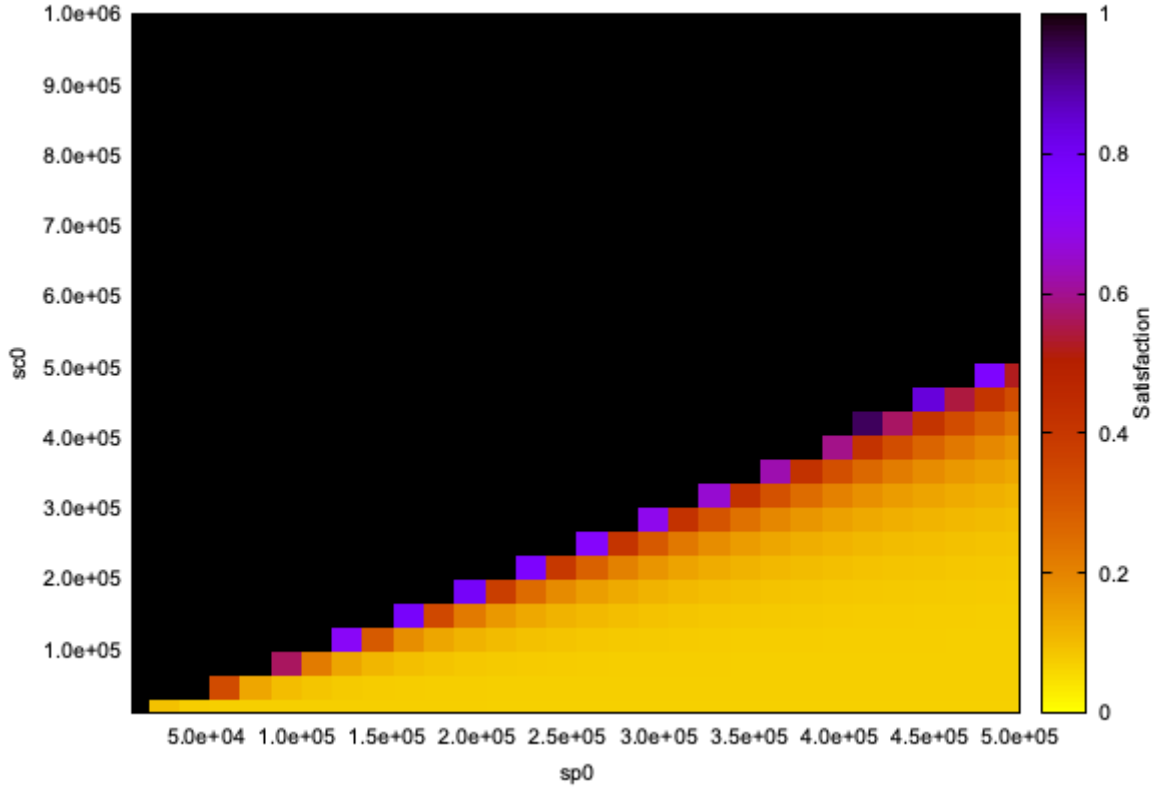

Out[13]:

```
Time: 3267.186 s
Mean satisfaction (robustness): 0.477428, standard deviation: 0.646201
Maximum satisfaction: 1.000000
Best solutions found with 10000.000000<=sp0<=500000.000000, 10000.000000<=sc0<
=1000000.000000
```

High production of AMPs (Ah = 3)

In [14]:

```
parameter(rsc=0.5,rsp=0.5,C1=2e8,kc=0.01,Ah=3).
parameter(sp0=1e3,sc0=1e5).
```

Out[14]:

In [15]:

```
numerical_simulation.
plot.
satisfaction_degree(F(Time==40 /\ (Sc > u1*Sp) /\ F(G(Sc > u2*Sp))),[u1 -> 10
```

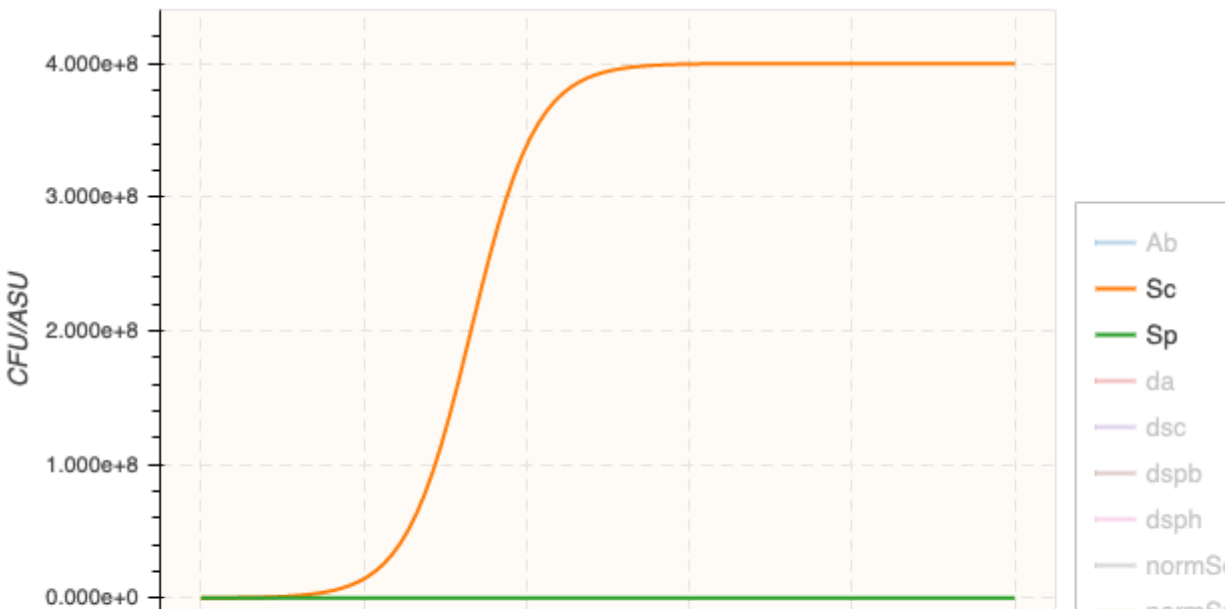

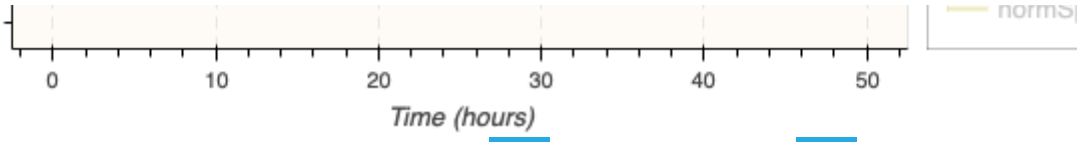

Out[15]:

```
2805.760000
```

In [16]:

```
scan_parameters(F(Time==40 /\ (Sc > u1*Sp) /\ F(G(Sc > u2*Sp))),
    (1e4 <= sp0 <= 5e5), (1e4 <= sc0 <= 1e6), [u1 -> 10, u2 -> 10], resolutio
```

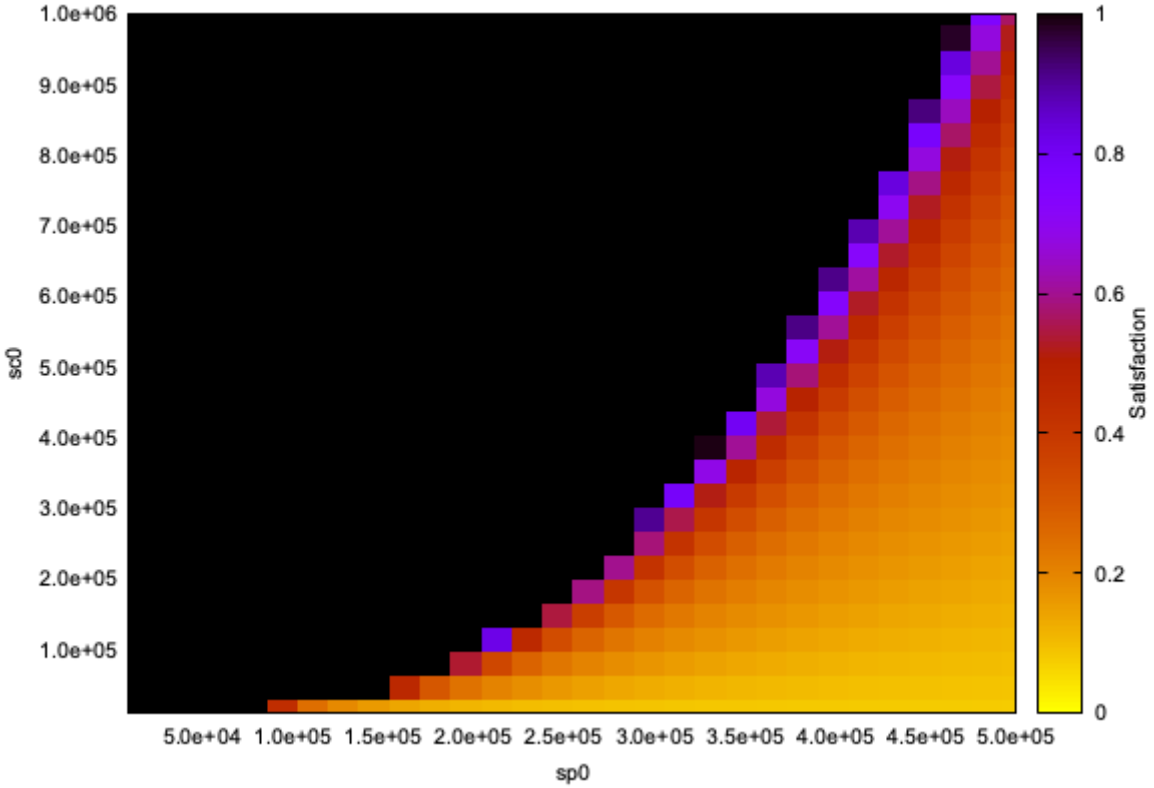

Out[16]:

```
Time: 3204.896 s
Mean satisfaction (robustness): 0.449891, standard deviation: 0.626255
Maximum satisfaction: 1.000000
Best solutions found with 10000.000000<=sp0<=466206.896552, 10000.000000<=sc0<
=1000000.000000
```

In [ ]:

ECOLE DOCTORALE

Titre : Approches de modélisation computationnelle des aspects multifactoriels de la dermatite atopique

Mots clés : bioinformatique, biomathématiques, dermatite atopique, modèle multi-agent, biologie des systèmes, épiderme

Résumé : La dermatite atopique (DA) est une maladie chronique affectant jusqu'à 20% des jeunes enfants, en fonction des pays, et environ 10% des adultes dans le monde. Elle se traduit par une sécheresse cutanée, d'intenses démangeaisons et la formation de lésions. Malgré des traitements efficaces à base d'anticorps monoclonaux pour les formes les plus sévères, les mécanismes complexes impliqués sont encore mal compris et des progrès restent à faire pour soulager les formes plus légères de cette maladie. Divers facteurs contribuent à la DA tels qu'une fonction barrière réduite, une inflammation cutanée exacerbée et un déséquilibre du microbiome. Cette multiplicité de facteurs et leur lien étroit rendent difficile le développement des malades in vitro.

L'approche computationnelle permet de rassembler les connaissances actuelles sur la maladie et de prédire le comportement du système sous certaines conditions, tout en facilitant la visualisation des phénomènes impliqués. Tout d'abord, nous introduisons un modèle à agent de l'épiderme capable de représenter certains aspects de la DA tels que le dysfonctionnement de la barrière cutanée, et le déséquilibre du microbiome. En intégrant les réactions enzymatiques contribuant au processus de desquamation dans un modèle à agent de l'épiderme existant, il est possible d'étudier l'impact du pH de la peau sur la structure et la fonction de l'épiderme.

Dans un deuxième temps, nous présenterons un modèle basé sur des équations différentielles ordinaires, décrivant les interactions de 2 types de populations bactériennes (les espèces commensales et les pathogènes opportunistes) afin d'étudier les mécanismes responsables de la prédominance d'une population sur l'autre. Sur une échelle de temps similaire à celle des expériences, le modèle prédit que certaines modifications de l'environnement, telles que l'augmentation du pH, créent des conditions favorables pour l'émergence et la colonisation de la peau par des pathogènes opportunistes. De façon surprenante, pour certaines valeurs de paramètres, un état méta-stable, atteint après l'équivalent de 2 jours suivant l'introduction des bactéries dans le modèle, est suivi par un état stable inverse après environ 300 heures.

Enfin, nous intégrons le modèle mathématique du microbiome dans le modèle à agents. Une attention particulière est portée sur l'échelle de temps des processus décrits ainsi que sur leur localisation dans l'épiderme. Le modèle ainsi obtenu est utilisé pour étudier l'impact du renouvellement constant des cellules de surface sur la dynamique du microbiome. Ce travail apporte des preuves supplémentaires de la pertinence de considérer le pH cutané, les protéases sérines et le microbiome comme de potentiels leviers pour le traitement de la DA.

Title: Computational modeling approaches to multifactorial aspects of atopic dermatitis

Keywords: bioinformatics, biomathematics, atopic dermatitis, agent-based model, systems biology, epidermis

Abstract: Atopic dermatitis (AD) is a common chronic disease affecting up to 20% of young children, depending on countries, and around 10% of adults globally. It manifests as dry, itchy and sometimes cracked skin lesions on the face and body. Despite efficient immunotherapy treatments for the most severe forms of the disease, the complex mechanisms involved are still incompletely understood and improvements can be made regarding management strategies for milder forms. AD involves diverse interacting factors such as impaired skin barrier function, exacerbated inflammation, and microbiome dysbiosis, making it challenging to develop adequate in vitro models.

A computational approach allows the aggregation of current pathophysiology knowledge, facilitates the visualization of the phenomena involved, and enables the prediction of certain behaviors of the system under specific conditions. First, we introduce an agent-based model of the epidermis, able to represent aspects of atopic skin such as skin barrier dysfunction and microbiome dysbiosis. By integrating enzymatic reactions contributing to the desquamation process, into an existing agent-based model of the epidermis at the cellular level, we can study the impact of skin surface pH on the epidermal structure and function. The model predicts that an elevation of skin surface pH above physiologic levels accelerates the desquamation process through its action on serine proteases. This results in a significant reduction of the skin's capacity to retain water, and increases its permeability to external penetration, including irritants. This skin barrier impairment further leads to a more intense inflammatory reaction under conditions of high skin surface pH, compared to physiologic pH levels.

Next, we introduce a mathematical model of the microbiome, based on ordinary differential equations, with 2 types of bacteria populations (skin commensals and opportunistic pathogens) to study the mechanisms driving the dominance of one population over the other. On the time scale of the experiments, the model predicts that certain changes of the environment, like the elevation of skin surface pH from physiologic levels, create favorable conditions for the emergence and colonization of the skin by opportunistic pathogens. Interestingly, for certain parameter values, a meta-stable state settled at around 2 days following the introduction of bacteria in the model, is followed by a reversed stable state after 300 hours.

Finally, we integrate the mathematical model of the microbiome into the agent-based model. Special consideration is taken regarding the timescales of the processes described and their location in the epidermis. The resulting model is used to study how the constant surface cells renewal impacts the microbiome kinetics. This work provides additional evidence that skin surface pH, serine proteases and skin microbiome could be interesting therapeutic targets for AD maintenance therapy.

Institut Polytechnique de Paris

91120 Palaiseau, France